

Advective Accretion Disks and Related Problems Including Magnetic Fields

G.S.Bisnovatyi-Kogan* and R.V.E. Lovelace[†]

November 3, 2018

Abstract

Accretion disk theory was first developed as a theory with the local heat balance, where the whole energy produced by a viscous heating was emitted to the sides of the disk. One of the most important new invention of this theory was the phenomenological treatment of the turbulent viscosity, known the “alpha” prescription, where the $(r\phi)$ component of the stress tensor was approximated by (αp) with a unknown constant α . This prescription played the role in the accretion disk theory as well important as the mixing-length theory of convection for stellar evolution. Sources of turbulence in the accretion disk are discussed, including hydrodynamical turbulence, convection and magnetic field role. In parallel to the optically thick geometrically thin accretion disk models, a new branch of the optically thin accretion disk models was discovered, with a larger thickness for the same total luminosity. The choice between these solutions should be done of the base of a stability analysis. The ideas underlying the necessity to include advection into the accretion disk theory are presented and first models with advection are reviewed. The present status of the solution for a low-luminous optically thin accretion disk model with advection is discussed and the limits for an advection dominated accretion flows (ADAF) imposed by the presence of magnetic field are analysed. Related problems of mass ejection from accretion disks and jet formation are discussed.

1 Introduction

Accretion is served as a source of energy in many astrophysical objects, including different types of binary stars, binary X-ray sources, most probably quasars and active galactic nuclei (AGN). While first development of accretion theory

*Space Research Institute, Profsoyuznaya 84/32, Moscow 117810, Russia; GKogan@mx.iki.rssi.ru

[†]Department of Astronomy, Cornell University, Ithaca, NY 14853; RVL1@cornell.edu

started long time ago (Bondi and Hoyle, 1944; Bondi, 1952), the intensive development of this theory began after discovery of first X ray sources (Giacconi et al, 1962) and quasars (Schmidt, 1963). Accretion onto stars, including neutron stars, terminates at an inner boundary. This may be the stellar surface, or the outer boundary of a magnetosphere for strongly magnetized stars. We may be sure in this case, that all gravitational energy of the falling matter will be transformed into heat and radiated outward.

The situation is quite different for sources containing black holes, which are discovered in some binary X-ray sources in the galaxy, as well as in many AGN. Here matter is falling to the horizon, from where no radiation arrives, so all luminosity is formed on the way to it. The efficiency of accretion is not known from the beginning, contrary to the accretion into a star, and depends strongly on such factors, like angular momentum of the falling matter, and magnetic field embedded into it. It was first shown by Schwarzman (1971), that during spherical accretion of nonmagnetized gas the efficiency may be as small as 10^{-8} for sufficiently low mass fluxes. He showed that presence of magnetic field in the accretion flux matter increase the efficiency up to about 10%, and account of heating of matter due to magnetic field annihilation in the flux rises the efficiency up to about 30% (Bisnovatyi-Kogan, Ruzmaikin, 1974; Meszáros, 1975). In the case of a thin disk accretion when matter has large angular momentum, the efficiency is about 1/2 of the efficiency of accretion into a star with a radius equal to the radius of the last stable orbit. Matter cannot emit all the gravitational energy, part of which is absorbed by the black hole. In the case of geometrically thick and optically thin accretion discs the situation is approaching the case of spherical symmetry, and a presence of a magnetic field plays also a critical role.

Here we consider a development of the theory of a disk accretion, starting from creation of a so called “standard model”, and discuss recent trends, connected with a presence of advection. The flow of papers (see e.g. references in Narayan, Barret, McClintock, 1996; Menon, Quataert, Narayan, 1999) considering advection dominated accretion flow (ADAF) as a solution for many astrophysical problems should be treated with some caution, because of its vague physical background. The suggestions underlying ADAF: ignorance of the magnetic field annihilation in heating of accretion plasma flow, and electron heating ONLY due to binary collisions with protons (ions) were critically analysed in several papers (Bisnovatyi-Kogan and Lovelace, 1997, 2000; Quataert, 1997, Blackman, 1999), and the above mentioned suggestions have been strongly doubted.

Competition between rapid accumulation of observational data, mainly from Hubble Space Telescope, X-ray satellites, and rapid as well construction of theoretilal models for their explanation creates sometimes a situation when the model dyes during the time of its publication. Some ADAF models give a good examples of this situation. One is connected with an explanation of the unusual spectra of the galaxy NGC 4258, with a nonmonotoneous curve. It was claimed

(Lasota et al., 1996), that such spectrum may be explained only by ADAF model. Observations (Herrnstein et al., 1998; Cannizzo et al., 1998) gave data in radio, in optical/UV region showing existence of spectral maximum on the place where suspected minimum had been explained by ADAF, and posing constraints on ADAF model. Restrictions on ADAF model had been obtained from radio observations of elliptical galaxies (Wrobal and Herrnstein, 2000).

Another example is connected with an attempt to prove the existence of the event horizon in black holes by ADAF model. The figure 7 from the work of Menon, Quataert and Narayan (1997) (fig.2 from Narayan, Garcia and McClintock, 1997) was considered as a proof of the existence of the event horizon of black holes and at the same time as a triumph of the ADAF model. Regretfully, the data on this figures occurs to be incomplete and a full set of observational data altered this picture (Chen et al., 1998).

It is, of course, dangerous to justify any physical model by astronomical observations without a firm physical ground. Here we analyse physical processes in an optically thin accretion flow at low accretion rates, connected with a presence of a small-scale magnetic field. We show, that accurate account of these processes strongly restrict the boundaries of the ADAF solution. Namely, the efficiency of the accretion flow cannot become less than about 1/3 of the standard accretion disk value. It makes senseless the attempts to connect ADAF models with existence of the event horizon of a black hole, or to explain why we do not see a large luminosity from supermassive black holes in the nearby galactic nuclei.

It seems now, that explanation of unusual observational features, in particular, of "underluminous galactic nuclei" is connected with more complicated processes than a simple ADAF solution. Energy losses connected with magnetohydrodynamical acceleration of matter from accretion disk, formation of jets may be very important. These problems are considered in the last section of the review.

2 Foundation of accretion disk theory

2.1 Development of the standard model of the disk accretion

Matter falling into a compact object tends to form a disk when its angular momentum is sufficiently high. It happens when the matter falling into a black hole comes from the neighboring ordinary star companion in the binary, or when the matter appears as a result of a tidal disruption of the star which trajectory of motion approaches sufficiently close to the black hole, so that forces of selfgravity could be overcome. The first situation is observed in many galactic X-ray sources containing a stellar mass black hole (Cherepashchuk, 1996, 2000). A tidal disruption happens in quasars and active galactic nuclei

(AGN), if the model of supermassive black hole surrounded by a dense stellar cluster of Lynden-Bell (1969) is true for these objects.

The models of the accretion disk structure around a black hole had been investigated by Lynden-Bell (1969), Pringle and Rees (1972). The modern "standard" theory of the disk accretion was formulated in the papers of Shakura (1972), Novikov and Thorne (1973) and Shakura and Sunyaev (1973). It is important to note, that all authors of the accretion disk theory from USSR were students (N.I.Shakura) or collaborators (I.D.Novikov and R.A.Sunyaev) of academician Ya.B.Zeldovich, who was not among the authors, but whose influence on them hardly could be overestimated.

The equations of the standard disk accretion theory were first formulated by Shakura (1972); some corrections and generalization to general relativity (GR) were done by Novikov and Thorne (1973), see also correction to their equations in GR made by Riffert & Herold (1995). The main idea of this theory is to describe a geometrically thin non-self-gravitating disk of the mass M_d , which is much smaller than the mass of the black hole M , by hydrodynamic equations averaged over the disk thickness $2h$ Fig.1 shows the disk geometry.

2.2 Basic Equations

Let us start with Navier-Stokes equations in Cartesian coordinates, describing the motion of the viscid compressible fluid with variable viscosity η and bulk viscosity η_B coefficients (Chapman and Cowling 1939)

$$\rho \left(\frac{\partial u_i}{\partial t} + u_k \frac{\partial u_i}{\partial x_k} \right) = -\frac{\partial p}{\partial x_i} + \rho g_i + \frac{\partial}{\partial x_k} \left[\eta \left(\frac{\partial u_i}{\partial x_k} + \frac{\partial u_k}{\partial x_i} - \frac{2}{3} \frac{\partial u_l}{\partial x_l} \delta_{ik} \right) + \eta_B \frac{\partial u_l}{\partial x_l} \delta_{ik} \right], \quad (1)$$

or in vector notation,

$$\rho \left(\frac{\partial \mathbf{u}}{\partial t} + (\mathbf{u} \cdot \nabla) \mathbf{u} \right) = -\nabla p + \rho \mathbf{g} + \nabla_k \left[\eta \left(\nabla_k \mathbf{u} + \nabla \mathbf{u}_k - \frac{2}{3} (\nabla \cdot \mathbf{u}) \underline{\delta} \right) + \eta_B (\nabla \cdot \mathbf{u}) \underline{\delta} \right]. \quad (2)$$

Here, the usual tensor definitions are used with δ_{ik} and $\underline{\delta}$ the unit tensor and g_i the gravitational acceleration. Summation over repeated indices is assumed. The last term in (1) is the divergence of the viscosity stress tensor σ_{ik} , which is related to the symmetric and divergentless deformation tensor τ_{ik} by the relation

$$\sigma_{ik} = 2\eta\tau_{ik} + \eta_B \frac{\partial u_l}{\partial x_l} \delta_{ik}, \quad \tau_{ik} = \frac{1}{2} \left(\frac{\partial u_i}{\partial x_k} + \frac{\partial u_k}{\partial x_i} - \frac{2}{3} \frac{\partial u_l}{\partial x_l} \delta_{ik} \right). \quad (3)$$

The bulk viscosity η_B is connected with finite rate of relaxation processes (ionization, chemical or nuclear reactions, etc). It is important only for rapid processes (e.g., shocks) which are not considered here. Thus we take $\eta_B = 0$ everywhere below.

For accretion flows, it is natural to express equation (1) in cylindrical coordinates (r, ϕ, z) . For making transformation to cylindrical coordinates we need to write in these coordinates some differential operators on the scalar a , vector $\mathbf{a} = (a_r, a_\phi, a_z)$ and tensor

$$\underline{\mathbf{a}} = \begin{pmatrix} a_{rr} & a_{r\phi} & a_{rz} \\ a_{\phi r} & a_{\phi\phi} & a_{\phi z} \\ a_{zr} & a_{z\phi} & a_{zz} \end{pmatrix}. \quad (4)$$

a) gradient of the scalar:

$$\nabla a = \left(\frac{\partial a}{\partial r}, \quad \frac{1}{r} \frac{\partial a}{\partial \phi}, \quad \frac{\partial a}{\partial z} \right). \quad (5)$$

b) divergence of vector:

$$\nabla \cdot \mathbf{a} = \frac{1}{r} \frac{\partial (ra_r)}{\partial r} + \frac{1}{r} \frac{\partial a_\phi}{\partial \phi} + \frac{\partial a_z}{\partial z}. \quad (6)$$

c) curl of vector:

$$\nabla \times \mathbf{a} = \left(\frac{1}{r} \frac{\partial a_z}{\partial \phi} - \frac{\partial a_\phi}{\partial z}, \quad \frac{\partial a_r}{\partial z} - \frac{\partial a_z}{\partial r}, \quad \frac{\partial a_\phi}{\partial r} + \frac{a_\phi}{r} - \frac{1}{r} \frac{\partial a_r}{\partial \phi} \right). \quad (7)$$

d) gradient of vector:

$$\nabla \mathbf{a} = \begin{pmatrix} \frac{\partial a_r}{\partial r} & \frac{\partial a_\phi}{\partial r} & \frac{\partial a_z}{\partial r} \\ \frac{1}{r} \frac{\partial a_r}{\partial \phi} - \frac{a_\phi}{r} & \frac{1}{r} \frac{\partial a_\phi}{\partial \phi} + \frac{a_r}{r} & \frac{1}{r} \frac{\partial a_z}{\partial \phi} \\ \frac{\partial a_r}{\partial z} & \frac{\partial a_\phi}{\partial z} & \frac{\partial a_z}{\partial z} \end{pmatrix}. \quad (8)$$

e) divergence of the tensor:

$$\nabla \cdot \underline{\mathbf{a}} = \begin{pmatrix} \frac{\partial a_{rr}}{\partial r} + \frac{1}{r} \frac{\partial a_{\phi r}}{\partial \phi} + \frac{\partial a_{zr}}{\partial z} + \frac{a_{rr} - a_{\phi\phi}}{r} \\ \frac{\partial a_{r\phi}}{\partial r} + \frac{1}{r} \frac{\partial a_{\phi\phi}}{\partial \phi} + \frac{\partial a_{z\phi}}{\partial z} + \frac{a_{r\phi} + a_{\phi r}}{r} \\ \frac{\partial a_{rz}}{\partial r} + \frac{1}{r} \frac{\partial a_{\phi z}}{\partial \phi} + \frac{\partial a_{zz}}{\partial z} + \frac{a_{rz}}{r} \end{pmatrix}. \quad (9)$$

f) Laplacian of the scalar:

$$\nabla^2 a \equiv (\nabla \cdot \nabla) a = \frac{\partial^2 a}{\partial r^2} + \frac{1}{r} \frac{\partial a}{\partial r} + \frac{1}{r^2} \frac{\partial^2 a}{\partial \phi^2} + \frac{\partial^2 a}{\partial z^2}. \quad (10)$$

g) Laplacian of the vector:

$$\nabla^2 \mathbf{a} \equiv (\nabla \cdot \nabla) \mathbf{a} = \begin{pmatrix} \frac{\partial^2 a_r}{\partial r^2} + \frac{1}{r} \frac{\partial a_r}{\partial r} - \frac{a_r}{r^2} + \frac{1}{r^2} \frac{\partial^2 a_r}{\partial \phi^2} - \frac{2}{r^2} \frac{\partial a_\phi}{\partial \phi} + \frac{\partial^2 a_r}{\partial z^2} \\ \frac{\partial^2 a_\phi}{\partial r^2} + \frac{1}{r} \frac{\partial a_\phi}{\partial r} - \frac{a_\phi}{r^2} + \frac{1}{r^2} \frac{\partial^2 a_\phi}{\partial \phi^2} + \frac{2}{r^2} \frac{\partial a_r}{\partial \phi} + \frac{\partial^2 a_\phi}{\partial z^2} \\ \frac{\partial^2 a_z}{\partial r^2} + \frac{1}{r} \frac{\partial a_z}{\partial r} + \frac{1}{r^2} \frac{\partial^2 a_z}{\partial \phi^2} + \frac{\partial^2 a_z}{\partial z^2} \end{pmatrix}. \quad (11)$$

For the transformation of equation (3) to cylindrical coordinates we have

$$\tau_{ik} = \frac{1}{2} (\nabla_k \mathbf{u} + \nabla \mathbf{u}_k) - \frac{1}{3} (\nabla \cdot \mathbf{u}) \underline{\delta}, \quad (12)$$

with

$$2\tau_{ik} = \begin{pmatrix} \frac{4}{3} \frac{\partial u_r}{\partial r} - \frac{2}{3} \left(\frac{u_r}{r} + \frac{1}{r} \frac{\partial u_\phi}{\partial \phi} + \frac{\partial u_z}{\partial z} \right) & \frac{\partial u_\phi}{\partial r} + \frac{1}{r} \frac{\partial u_r}{\partial \phi} - \frac{u_\phi}{r} \\ \frac{\partial u_\phi}{\partial r} + \frac{1}{r} \frac{\partial u_r}{\partial \phi} - \frac{u_\phi}{r} & \frac{4}{3} \left(\frac{1}{r} \frac{\partial u_\phi}{\partial \phi} + \frac{u_r}{r} \right) - \frac{2}{3} \left(\frac{\partial u_r}{\partial r} + \frac{\partial u_z}{\partial z} \right) \\ \frac{\partial u_z}{\partial r} + \frac{\partial u_r}{\partial z} & \frac{1}{r} \frac{\partial u_z}{\partial \phi} + \frac{\partial u_\phi}{\partial z} \\ \frac{\partial u_z}{\partial r} + \frac{\partial u_r}{\partial z} & \frac{1}{r} \frac{\partial u_z}{\partial \phi} + \frac{\partial u_\phi}{\partial z} \\ \frac{4}{3} \frac{\partial u_z}{\partial z} - \frac{2}{3} \left(\frac{\partial u_r}{\partial r} + \frac{1}{r} \frac{\partial u_\phi}{\partial \phi} + \frac{u_r}{r} \right) \end{pmatrix} \quad (13)$$

The second term in the brackets on the left-hand side of equation (2) is a scalar product of the vector \mathbf{u} and tensor $\nabla \mathbf{u}$, which is the same in Cartesian and curvilinear coordinates. The last term on the right-hand side of equation (2) is the divergence of the tensor $2\eta\tau_{ik}$, which is calculated using equations (9) and (13). As a result we get the components of equation (2) in cylindrical coordinates:

$$\begin{aligned} & \rho \left(\frac{\partial u_r}{\partial t} + u_r \frac{\partial u_r}{\partial r} + \frac{u_\phi}{r} \frac{\partial u_r}{\partial \phi} + u_z \frac{\partial u_r}{\partial z} - \frac{u_\phi^2}{r} \right) = -\frac{\partial p}{\partial r} + \rho g_r \\ & + \frac{2}{3} \frac{\partial}{\partial r} \left\{ \eta \left[\frac{2}{r} \frac{\partial (ru_r)}{\partial r} - \frac{1}{r} \frac{\partial u_\phi}{\partial \phi} - \frac{\partial u_z}{\partial z} \right] \right\} - 2 \frac{u_r}{r} \frac{\partial \eta}{\partial r} + \frac{1}{r} \frac{\partial}{\partial \phi} \left[\eta \left(\frac{\partial u_\phi}{\partial r} + \frac{1}{r} \frac{\partial u_r}{\partial \phi} - \frac{u_\phi}{r} \right) \right] \\ & - 2 \frac{\eta}{r^2} \frac{\partial u_\phi}{\partial \phi} + \frac{\partial}{\partial z} \left[\eta \left(\frac{\partial u_z}{\partial r} + \frac{\partial u_r}{\partial z} \right) \right]. \quad (14) \end{aligned}$$

$$\begin{aligned} & \rho \left(\frac{\partial u_\phi}{\partial t} + u_r \frac{\partial u_\phi}{\partial r} + \frac{u_\phi}{r} \frac{\partial u_\phi}{\partial \phi} + u_z \frac{\partial u_\phi}{\partial z} + \frac{u_r u_\phi}{r} \right) = -\frac{1}{r} \frac{\partial p}{\partial \phi} + \rho g_\phi \\ & + \frac{1}{r^2} \frac{\partial}{\partial r} \left[\eta r^3 \frac{\partial}{\partial r} \left(\frac{u_\phi}{r} \right) \right] + \frac{\partial}{\partial r} \left(\frac{\eta}{r} \frac{\partial u_r}{\partial \phi} \right) + \frac{2}{3r} \frac{\partial}{\partial \phi} \left\{ \eta \left[2 \left(\frac{1}{r} \frac{\partial u_\phi}{\partial \phi} + \frac{u_r}{r} \right) \right] \right\} \end{aligned}$$

$$-\frac{\partial u_r}{\partial r} - \frac{\partial u_z}{\partial z} \Big] \Big\} + \frac{\partial}{\partial z} + \left[\eta \left(\frac{1}{r} \frac{\partial u_z}{\partial \phi} + \frac{\partial u_\phi}{\partial z} \right) \right] + \frac{2\eta}{r^2} \frac{\partial u_r}{\partial \phi} . \quad (15)$$

$$\begin{aligned} \rho \left(\frac{\partial u_z}{\partial t} + u_r \frac{\partial u_z}{\partial r} + \frac{u_\phi}{r} \frac{\partial u_z}{\partial \phi} + u_z \frac{\partial u_z}{\partial z} \right) &= -\frac{\partial P}{\partial z} + \rho g_z \\ + \frac{1}{r} \frac{\partial}{\partial r} \left[\eta r \left(\frac{\partial u_z}{\partial r} + \frac{\partial u_r}{\partial z} \right) \right] + \frac{1}{r} \frac{\partial}{\partial \phi} \left[\eta \left(\frac{1}{r} \frac{\partial u_z}{\partial \phi} + \frac{\partial u_\phi}{\partial z} \right) \right] \\ + \frac{2}{3} \frac{\partial}{\partial z} \left[\eta \left(2 \frac{\partial u_z}{\partial z} - \frac{\partial u_r}{\partial r} - \frac{1}{r} \frac{\partial u_\phi}{\partial \phi} - \frac{u_r}{r} \right) \right] . \end{aligned} \quad (16)$$

The continuity equation for the disk flow is

$$\frac{\partial \rho}{\partial t} + \frac{\partial(\rho u_i)}{\partial x_i} = 0 , \quad \text{or} \quad \frac{\partial \rho}{\partial t} + \nabla \cdot (\rho \mathbf{u}) = 0 . \quad (17)$$

In cylindrical coordinates this equation becomes

$$\frac{\partial \rho}{\partial t} + \frac{\partial(r\rho u_r)}{r\partial r} + \frac{\partial(\rho u_\phi)}{r\partial \phi} + \frac{\partial(\rho u_z)}{\partial z} = 0 . \quad (18)$$

2.3 Derivation of Thin disk Equations

For axisymmetric disk flows the ϕ -partial derivatives of the different scalar quantities vanish so that equations (14)-(16) become

$$\begin{aligned} \rho \left(\frac{\partial u_r}{\partial t} + u_r \frac{\partial u_r}{\partial r} + u_z \frac{\partial u_r}{\partial z} - \frac{u_\phi^2}{r} \right) &= -\frac{\partial p}{\partial r} + \rho g_r \\ + \frac{2}{3} \frac{\partial}{\partial r} \left\{ \eta \left[\frac{2}{r} \frac{\partial(ru_r)}{\partial r} - \frac{\partial u_z}{\partial z} \right] \right\} - 2 \frac{u_r}{r} \frac{\partial \eta}{\partial r} + \frac{\partial}{\partial z} \left[\eta \left(\frac{\partial u_z}{\partial r} + \frac{\partial u_r}{\partial z} \right) \right] , \end{aligned} \quad (19)$$

$$\begin{aligned} \rho \left(\frac{\partial u_\phi}{\partial t} + u_r \frac{\partial u_\phi}{\partial r} + u_z \frac{\partial u_\phi}{\partial z} + \frac{u_r u_\phi}{r} \right) \\ = \frac{1}{r^2} \frac{\partial}{\partial r} \left[\eta r^3 \frac{\partial}{\partial r} \left(\frac{u_\phi}{r} \right) \right] + \frac{\partial}{\partial z} \left(\eta \frac{\partial u_\phi}{\partial z} \right) , \end{aligned} \quad (20)$$

$$\begin{aligned} \rho \left(\frac{\partial u_z}{\partial t} + u_r \frac{\partial u_z}{\partial r} + u_z \frac{\partial u_z}{\partial z} \right) &= -\frac{\partial p}{\partial z} + \rho g_z \\ + \frac{1}{r} \frac{\partial}{\partial r} \left[\eta r \left(\frac{\partial u_z}{\partial r} + \frac{\partial u_r}{\partial z} \right) \right] + \frac{2}{3} \frac{\partial}{\partial z} \left[\eta \left(2 \frac{\partial u_z}{\partial z} - \frac{\partial u_r}{\partial r} - \frac{u_r}{r} \right) \right] . \end{aligned} \quad (21)$$

The continuity equation (18) takes the form

$$\frac{\partial \rho}{\partial t} + \frac{1}{r} \frac{\partial(r\rho u_r)}{\partial r} + \frac{\partial(\rho u_z)}{\partial z} = 0 . \quad (22)$$

Many problems concerning thin accretion disks can be solved using the above equations in the equatorial plane or averaged over the thickness of the disk. The vertical structure of the disk is determined by the equilibrium of the pressure gradient and the vertical gravitational force g_z , which may include self-gravitation for sufficiently massive disks.

Problems connected with convective and meridional motion in disks need more detailed description with the full set of equations (18)-(18). A complete description requires including the magnetic force in the Navier-Stokes equations and the Maxwell equations for the field evolution.

In the equatorial plane of a thin disk, we have

$$u_z = 0, \quad g_z = \frac{\partial \rho}{\partial z} = \frac{\partial p}{\partial z} = \frac{\partial u_r}{\partial z} = \frac{\partial u_\phi}{\partial z} = 0, \quad (23)$$

where mirror symmetry about the equatorial plane is assumed. However, note that $\partial u_z / \partial z \neq 0$ even in this case. Neglecting u_z , g_ϕ and all z derivatives, we obtain the approximate equations

$$\rho \left(\frac{\partial u_r}{\partial t} + u_r \frac{\partial u_r}{\partial r} - \frac{u_\phi^2}{r} \right) = -\frac{\partial p}{\partial r} + \rho g_r + \frac{4}{3} \frac{\partial}{\partial r} \left[\frac{\eta}{r} \frac{\partial (r u_r)}{\partial r} \right] - 2 \frac{u_r}{r} \frac{\partial \eta}{\partial r}, \quad (24)$$

$$\rho r \left(\frac{\partial r u_\phi}{\partial t} + u_r \frac{\partial r u_\phi}{\partial r} \right) = \frac{\partial}{\partial r} \left[\eta r^3 \frac{\partial}{\partial r} \left(\frac{u_\phi}{r} \right) \right], \quad (25)$$

$$\rho g_z = \frac{\partial p}{\partial z}, \quad (26)$$

$$\frac{\partial \rho}{\partial t} + \frac{1}{r} \frac{\partial (r \rho u_r)}{\partial r} = 0. \quad (27)$$

Combining equations (24) and (27) we get the radial equation in the form

$$\frac{\partial \rho r u_r}{\partial t} + \frac{\partial \rho r u_r^2}{\partial r} - \rho r \left(\frac{u_\phi^2}{r} + g_r \right) = -r \frac{\partial p}{\partial r} + \frac{4}{3} r \frac{\partial}{\partial r} \left[\frac{\eta}{r} \frac{\partial (r u_r)}{\partial r} \right] - 2 u_r \frac{\partial \eta}{\partial r}. \quad (28)$$

Following Shakura (1972), we write the viscosity coefficient η using the α -prescription,

$$\eta = \frac{2}{3} \alpha \rho_0 u_{s0} z_0, \quad (29)$$

where u_{s0} is a sound velocity in the equatorial plane ($z = 0$), and z_0 is half-thickness of the disk. Integrating the equations (25) and (27) over the thickness of the disk, we get an approximate set of equations describing the thin disk behaviour, neglecting viscosity in the radial equation (24) which is taken in the symmetry plane of the disk

$$\frac{\partial u_r}{\partial t} + u_r \frac{\partial (u_r)}{\partial r} - \rho_0 (\Omega^2 r + g_r) + \frac{\partial P_0}{\partial r} = 0 \quad (30)$$

$$r\Sigma\frac{\partial j}{\partial t} + \frac{\dot{M}}{2\pi}\frac{\partial j}{\partial r} = \frac{2}{3}\alpha\frac{\partial}{\partial r}\left(\Sigma u_{s0}z_0r^3\frac{\partial\Omega}{\partial r}\right) \quad (31)$$

$$\frac{\partial\Sigma}{\partial t} + \frac{1}{2\pi r}\frac{\partial\dot{M}}{\partial r} = 0 \quad (32)$$

The average values, surface density Σ , mass flux over the disk \dot{M} , and the values of angular velocity Ω and specific angular momentum j are determined as follows

$$\Sigma = \int_{-z_0}^{z_0} \rho dz, \quad \dot{M} = 2\pi r \int_{-z_0}^{z_0} \rho u_r dz = 2\pi r \Sigma u_r, \quad (33)$$

$$\Omega = \frac{u_\phi}{r}, \quad j = r u_\phi$$

The equations (30)-(32) determine the variables (Σ, \dot{M}, j) , where (u_r, Ω) are expressed from (33) with

$$u_r, \dot{M} < 0 \quad (34)$$

The solution of the equation of vertical balance (26) permits to obtain the variables

$$u_{z0} = \left(\frac{\partial P_0}{\partial \rho_0}\right)_S^{1/2}, \quad z_0, \quad P_0 \quad (35)$$

as a functions of (r, Σ) , when the equation of state is given in the form $P(\rho)$ (e.g. a polytropic). Here ρ_0, P_0 are the density and the pressure in the equatorial plane.

When pressure P and velocity u_r derivatives are neglected in (30), the boundary conditions consist of the value of the mass flux and Keplerian angular velocity at infinity; and of a condition on the angular velocity derivative near the accreting body (black hole, neutron star or other), determining the total angular momentum flux through the disk and zero density and pressure on the outer boundary of the disk.

$$\dot{M}(\infty) = \dot{M}_\infty, \quad \Omega(r \rightarrow \infty) = \left(\frac{GM}{r^3}\right)^{1/2}, \quad \rho(\pm z_0) = 0$$

$$\Omega(r_{in}) = \Omega_{in}, \quad \text{or} \quad \left(\frac{\partial\Omega}{\partial r}\right)(r_{in}) = \left(\frac{\partial\Omega}{\partial r}\right)_{in} \quad (36)$$

where M is the mass of the star-disk body. If all terms remain in the equation (30) then an additional boundary condition is necessary. It follows from the demand, that the solution must go smoothly through the sonic (singular) point in the radial motion of the accretion disk to the black hole, or be adjusted

continuously to the conditions at the outer boundary on the stellar equator. The stellar angular velocity may be much less than the Keplerian velocity of the accretion disk. In that case a boundary layer is established between the disk and the star, which needs to be treated separately.

In the case of general equation of state $P(\rho, T)$ a new variable the temperature T appears, which is connected with a heat flux F (ergs/cm²/s), radiative or convective. Two additional equations of the energy balance over the disk and heat transfer to its outer boundary must be added together with boundary conditions for obtaining the full solution. These equations will be considered in later sections.

For solution of nonstationary accretion problems initial distributions are needed

$$\Sigma(r), j(r), \dot{M}(r) \quad (37)$$

in addition to the boundary conditions. In most cases the external force is represented by the gravity of the star, which may be treated as a point mass with a potential

$$\phi_g = -\frac{GM}{(r^2 + z^2)^{1/2}} \quad (38)$$

The components of the gravitational acceleration g_i are written as

$$g_i = -\frac{\partial\phi_g}{\partial x_i} = \left(-\frac{GMr}{(r^2 + z^2)^{3/2}}, 0, \frac{GMz}{(r^2 + z^2)^{3/2}} \right) \quad (39)$$

For a thin disk we can use the expansion

$$g_i = \left\{ -\frac{GM}{r^2} \left(1 - \frac{3z^2}{2r^2} \right), 0, -\frac{GMz}{r^3} \left(1 - \frac{3z^2}{2r^2} \right) \right\} \quad (40)$$

2.4 Structure of Polytropic Accretion Disks

For a polytropic equation of state

$$P = K\rho^{1+\frac{1}{n}}, \quad (41)$$

taking the main term in the gravitational force g_z from (40) we get the solution of the equation (26) (Hōshi, 1977)

$$\rho = \rho_0 \left(1 - \frac{z^2}{z_0^2} \right)^n, \quad (42)$$

where the density in the equatorial plane ρ_0 is connected with r and z_0 by the relation

$$\rho_0 = \left[\frac{GM}{2K(n+1)} \right]^n \frac{z_0^{2n}}{r^{3n}}. \quad (43)$$

Some physical quantities from (33) - (35) can be expressed in terms of r and ρ_0 .

$$z_0 = \left[\frac{2K(n+1)}{GM} \right]^{\frac{1}{2}} \rho_0^{\frac{1}{2n}} r^{\frac{3}{2}} = \beta_{z0} \rho_0^{\frac{1}{2n}} r^{\frac{3}{2}}, \quad (44)$$

$$\Sigma = \sqrt{\pi} \frac{\Gamma(n+1)}{\Gamma(n+\frac{3}{2})} \rho_0 z_0 = \beta_{\Sigma} \rho_0^{\frac{2n+1}{2n}} r^{\frac{3}{2}}, \quad (45)$$

$$P_0 = K \rho_0^{1+\frac{1}{n}}, \quad u_{s0} = \left(\frac{n+1}{n} K \right)^{1/2} \rho_0^{\frac{1}{2n}} = \beta_{s0} \rho_0^{\frac{1}{2n}}, \quad (46)$$

where

$$\beta_{\Sigma} = \sqrt{\pi} \frac{\Gamma(n+1)}{\Gamma(n+\frac{3}{2})} \left[\frac{2K(n+1)}{GM} \right]^{\frac{1}{2}}. \quad (47)$$

For the isothermal case, corresponding to $n = \infty$,

$$P = K\rho \quad (48)$$

we have instead of (42)

$$\rho = \rho_0 \exp\left(-\frac{GMz^2}{2Kr^3}\right) = \rho_0 \exp\left(-\frac{z^2}{z_i^2}\right), \quad z_i = \left(\frac{2Kr^3}{GM}\right)^{1/2}. \quad (49)$$

Formally an isothermal disk has infinite thickness z_0 , but the density falls exponentially with the characteristic height z_i from (49). Instead of (45)-(46) we have

$$\Sigma = \left(\frac{2\pi K}{GM}\right)^{\frac{1}{2}} \rho_0 r^{3/2}, \quad (50)$$

$$P_0 = K\rho_0, \quad u_{s0} = \sqrt{K}. \quad (51)$$

Restrict ourself by stationary accretion disks with $\frac{\partial}{\partial t} = 0$. Then we have from (32)

$$\dot{M} = \text{const} \quad (52)$$

and (31) is integrated, giving (Shakura, 1972)

$$\frac{\dot{M}}{2\pi}(j - j_0) = \frac{2}{3} \alpha \Sigma u_{s0} z_0 r^3 \frac{d\Omega}{dr}. \quad (53)$$

The integration constant j_0 after multiplication by \dot{M} gives the total (advective plus viscous) flux of angular momentum within the accretion disk. A positive value of j_0 corresponds to a negative total flux (due to a negative \dot{M}), which means that the central body accretes its angular momentum. When j_0 is negative the central body decreases its total angular momentum, while increasing its mass.

For a thin disk neglecting u_r and \mathcal{P} and taking only the main term for g_r from (40) we get from (30)

$$\Omega^{(0)} = \left(\frac{GM}{r^3}\right)^{1/2} = \Omega_K, \quad j^{(0)} = j_K = (GMr)^{1/2}. \quad (54)$$

The solution (54) is used up to the inner boundary of the accretion disk at $r = r_{in}$. The integration constant j_0 can be scaled by the Keplerian angular momentum $j_K(r_{in})$, so that

$$j_0 = \xi j_K(r_{in}) = \xi \sqrt{GM r_{in}} \quad (55)$$

Substituting (55) into (53) we get with account of (44)-(47) the relation for the density in the equatorial plane

$$\rho_0^{(0)} = b_{\rho 0} \left[-\frac{\dot{M}}{r^3} \left(1 - \xi \sqrt{\frac{r_{in}}{r}} \right) \right]^{\frac{2n}{2n+3}}, \quad (56)$$

$$b_{\rho 0} = \left[\frac{1}{4\pi^{3/2}\alpha} \frac{\sqrt{n}}{(n+1)^{3/2}} \frac{\Gamma(n + \frac{3}{2})}{\Gamma(n+1)} \frac{GM}{K^{3/2}} \right]^{\frac{2n}{2n+3}}. \quad (57)$$

Using (47), in (44)-(46) we get

$$z_0^{(0)} = b_{z 0} \left[-\dot{M} \left(1 - \xi \sqrt{\frac{r_{in}}{r}} \right) \right]^{\frac{1}{2n+3}} r^{\frac{3}{2} \frac{2n+1}{2n+3}}, \quad (58)$$

$$\Sigma^{(0)} = b_{\Sigma} \left[-\dot{M} \left(1 - \xi \sqrt{\frac{r_{in}}{r}} \right) \right]^{\frac{2n+1}{2n+3}} r^{-\frac{3}{2} \frac{2n-1}{2n+3}}, \quad (59)$$

$$P_0^{(0)} = b_{P 0} \left[-\frac{\dot{M}}{r^3} \left(1 - \xi \sqrt{\frac{r_{in}}{r}} \right) \right]^{\frac{2(n+1)}{2n+3}}, \quad (60)$$

$$u_{s 0}^{(0)} = b_{s 0} \left[-\frac{\dot{M}}{r^3} \left(1 - \xi \sqrt{\frac{r_{in}}{r}} \right) \right]^{\frac{1}{2n+3}}, \quad (61)$$

where

$$b_{z 0} = [2(n+1)]^{1/2} \left[\frac{1}{4\pi^{3/2}\alpha} \frac{\sqrt{n}}{(n+1)^{3/2}} \frac{\Gamma(n + \frac{3}{2})}{\Gamma(n+1)} \right]^{\frac{1}{2n+3}} K^{\frac{n}{2n+3}} (GM)^{-\frac{2n+1}{2(2n+3)}} \quad (62)$$

$$b_{\Sigma} = [2\pi(n+1)]^{\frac{1}{2}} \frac{\Gamma(n+1)}{\Gamma(n+\frac{3}{2})} \left[\frac{1}{4\pi^{3/2}\alpha} \frac{\sqrt{n}}{(n+1)^{3/2}} \frac{\Gamma(n+\frac{3}{2})}{\Gamma(n+1)} \right]^{\frac{2n+1}{2n+3}} K^{-\frac{2n}{2n+3}} (GM)^{\frac{2n-1}{2(2n+3)}} \quad (63)$$

$$b_{P0} = K b_{\rho 0}^{1+\frac{1}{n}}, \quad b_{s0} = b_{\rho 0}^{\frac{1}{2n}} \left(K \frac{n+1}{n} \right)^{1/2}. \quad (64)$$

In the formula for viscosity coefficient (29) z_0 must be replaced by z_i from (49) in the isothermal case,

$$\eta = \frac{2}{3} \alpha \rho u_{s0} z_i \quad (65)$$

Then instead of (55)-(64) we get a solution

$$P_0^{(0)} = K \rho_0^{(0)} = \frac{GM}{4\pi^{3/2}\alpha K^{3/2}} \left(-\frac{\dot{M}}{r^3} \right) \left(1 - \xi \sqrt{\frac{r_{in}}{r}} \right), \quad (66)$$

$$\Sigma^{(0)} = \frac{\sqrt{GM}}{\alpha 2\pi K \sqrt{2}} \left(-\frac{\dot{M}}{r^{3/2}} \right) \left(1 - \xi \sqrt{\frac{r_{in}}{r}} \right). \quad (67)$$

The formulas for the values of z_i in (49) and u_{s0} in (51) remain the same in all approximations for isothermal case.

For accretion into a black hole in presence of a free inner boundary with $\xi = 1$ the zero order approximation is not valid in the vicinity of r_{in} , where other terms in (30) must be taken into account. For accretion onto the slowly rotating star with angular velocity smaller than the Keplerian velocity on the equator, the drop of the angular velocity from Keplerian in the disk to stellar equatorial happens in a thin boundary layer, which must be considered separately with proper account of the pressure term in (30).

2.5 Standard Accretion Disk Model

2.5.1 Equilibrium equations

The small thickness of the disk in comparison with its radius $h \ll r$ indicate to small importance of the pressure gradient ∇P in comparison with gravity and inertia forces. That leads to a simple radial equilibrium equation denoting the balance between the last two forces occurring when the angular velocity of the disk Ω is equal to the Keplerian one Ω_K ,

$$\Omega = \Omega_K = \left(\frac{GM}{r^3} \right)^{1/2}. \quad (68)$$

Note, just before a last stable orbit around a black hole, and of course inside it, this suggestion fails, but in the “standard” accretion disk model the relation (68) is suggested to be fulfilled all over the disk, with an inner boundary at the last stable orbit.

The equilibrium equation in the vertical z -direction is determined by a balance between the gravitational force and pressure gradient

$$\frac{dP}{dz} = -\rho \frac{GMz}{r^3} \quad (69)$$

For a thin disk this differential equation is substituted by an algebraic one, determining the half-thickness of the disk in the form

$$h \approx \frac{1}{\Omega_K} \left(2 \frac{P}{\rho} \right)^{1/2}. \quad (70)$$

The balance of angular momentum, related to the ϕ component of the Euler equation has an integral in a stationary case written as

$$\dot{M}(j - j_{in}) = -2\pi r^2 2ht_{r\phi}, \quad t_{r\phi} = \eta r \frac{d\Omega}{dr}. \quad (71)$$

Here $j = v_\phi r = \Omega r^2$ is the specific angular momentum, $t_{r\phi}$ is a component of the viscous stress tensor, $\dot{M} > 0$ is a mass flux per unit time into a black hole, j_0 is an integration constant having, after multiplication by \dot{M} , a physical sense of difference between viscous and advective flux of the angular momentum, when j_{in} itself is equal to the specific angular momentum of matter falling into a black hole. In the standard theory the value of j_{in} is determined separately, from physical considerations. For the accretion into a black hole it is suggested, that on the last stable orbit the gradient of the angular velocity is zero, corresponding to zero viscous momentum flux. In that case

$$j_{in} = \Omega_K r_{in}^2, \quad (72)$$

corresponding to the Keplerian angular momentum of the matter on the last stable orbit. During accretion into a slowly rotating star which angular velocity is smaller than a Keplerian velocity on the inner edge of the disk, there is a maximum of the angular velocity close to its surface, where viscous flux is zero, and there is a boundary layer between this point and stellar surface. In that case (72) remains to be valid. The situation is different for accretion discs around rapidly rotating stars with a critical Keplerian speed on the equator (see Section 3). Note, that in the pioneering paper of Shakura (1972) the integration constant j_{in} was found as in (72), but was taken zero in his subsequent formulae. Importance of using j_{in} in the form (72) was noticed by Novikov and Thorne (1973), and became a feature of the standard model.

2.5.2 Turbulent Viscosity and Instabilities

The choice of the viscosity coefficient is the most difficult and speculative problem of the accretion disk theory. In the laminar case of microscopic (atomic or plasma) viscosity, which is very low, the stationary accretion disk must be very massive and very thick, and before its formation the matter is collected by disk leading to a small flux inside. It contradicts to observations of X-ray binaries, where a considerable matter flux along the accretion disk may be explained only when viscosity coefficient is much larger than the microscopic one. In the paper of Shakura (1972) it was suggested, that matter in the disk is turbulent, what determines a turbulent viscous stress tensor, parametrized by a pressure

$$t_{r\phi} = -\alpha\rho v_s^2 = -\alpha P, \quad (73)$$

where v_s is a sound speed in the matter. This simple presentation comes out from a relation for a turbulent viscosity coefficient $\eta_t \approx \rho v_t l$ with an average turbulent velocity v_t and mean free path of the turbulent element l . It follows from the definition of $t_{r\phi}$ in (71), when we take $l \approx h$ from (70)

$$t_{r\phi} = \rho v_t h r \frac{d\Omega}{dr} \approx \rho v_t v_s = -\alpha\rho v_s^2, \quad (74)$$

where a coefficient $\alpha < 1$ is connecting the turbulent and sound speeds $v_t = \alpha v_s$. Presentations of $t_{r\phi}$ in (73) and (74) are equivalent, and only when the angular velocity differs considerably from the Keplerian one the first relation to the right in (74) is preferable. That does not appear (by definition) in the standard theory, but may happen when advective terms are included.

Development of a turbulence in the accretion disk cannot be justified simply, because a Keplerian disk is stable in linear approximation to the development of axially symmetric perturbations, conserving the angular momentum, and against the Reyleigh-Taylor effect. It was suggested by Ya.B.Zeldovich, that in presence of very large Reynolds number $Re = \frac{\rho v l}{\eta}$ the amplitude of perturbations at which nonlinear effects become important is very low, so in this situation turbulence may develop due to nonlinear instability even when the disk is stable in linear approximation. Another source of viscous stresses may arise from a magnetic field, but it was suggested by Shakura (1972), that magnetic stresses cannot exceed the turbulent ones.

Magnetic plasma instability as a source of the turbulence in the accretion discs has been studied extensively in last years (see review of Balbus and Hawley, 1998). They used an instability of the uniform magnetic field parallel to the axis in differentially rotating disk, discovered by Velikhov (1959). It could be really important in absence of any other source of the turbulence, but it is hard to believe that there is no radial or azimuthal component of the magnetic field in matter flowing into the accretion disk from the companion star. In that case the field amplification due to twisting by a differential rotation take place without necessity of any kind of instability. Explanation of viscosity in accretion disks,

based on development of plasma instabilities, have been considered by Coppi (2000).

It was shown by Bisnovatyi-Kogan and Blinnikov (1976, 1977), that inner regions of a highly luminous accretion discs where pressure is dominated by radiation, are unstable to vertical convection. Development of this convection produce a turbulence, needed for a high viscosity. Other regions of a standard accretion disk should be stable to development of a vertical convection, so other ways of a turbulence excitation are needed there.

For Keplerian angular velocity the angular momentum per unit mass $j = \omega r^2 \sim r^{1/2}$ is growing outside. In this respect it is similar to the viscid flow between two rotating cylinders (Taylor experiment), when the inner cylinder is at rest. There are however important differences between these two problems. There are two boundaries on cylinder surfaces with adhesion conditions, and free boundaries in the case of accretion disk. The radial equilibrium in the fluid between cylinders is supported by the balance between centrifugal, and pressure gradient forces, while the last is substituted by the gravity in the accretion disks. Finally, the fluid between cylinders in the laboratory experiments is usually strongly subsonic, determining a non-compressible medium, while the Keplerian motion in the thin accretion disk is highly supersonic. Nevertheless, it is hoped that the fundamental theory checked in the laboratory will answer the astrophysical questions.

Phenomenological analysis of the Taylor experiment, and the onset of turbulence in the "stable" case of the inner cylinder at rest had been done by Zeldovich (1981). There are two characteristic specific energies in the problem. One is the energy, necessary for performing the ring exchange with conservation of the angular momentum of each ring $E_s = 2\frac{\omega}{r}\frac{d(\omega r^2)}{dr}(\Delta r)^2$; here the exchange is supposed to happen for rings with small distance Δr between them. This energy is positive in the "stable", and negative in the case unstable to Reyleigh-Taylor effect. Another energy E_t produced after merging of these two rings with conservation of the total angular momentum $E_t = \frac{1}{4}r\left(\frac{d\omega}{dr}\right)^2(\Delta r)^2$ is always positive. The ratio of these two energies is defined by Zeldovich (1981) as Taylor number

$$Ty = \frac{E_s}{E_t} = 4\frac{d[(\omega r^2)^2]/dr}{r^5(d\omega/dr)^2}. \quad (75)$$

The boundary $Ty = 0$ separate regions stable and unstable to Reyleigh-Taylor effect. In the case of close cylinder radiuses $R_{out} - R_{in} \ll R = \frac{1}{2}(R_{out} + R_{in})$ we get with account of (75)

$$\omega_{out} \approx \omega_{in} \approx \omega, R_{out} \approx R_{in} \approx R, R_{out} - R_{in} = t, \frac{d}{dr} = \frac{1}{t}, Ty \approx 8\frac{t}{R}. \quad (76)$$

This case at $t \rightarrow 0$ corresponds to the flat Couette flow, which is formally stable at all Re numbers (Schlichting, 1964) when $\frac{dv}{dr}$, is constant (v is the fluid

velocity), in contradiction with the experiment. Account of the curvature of the curve $v(r)$, even small, is very important here, and gives the instability, similar to the case with the free outer boundary, also corresponding to $Ty = 0$, when the instability starts at $Re = \frac{\rho \omega t}{\eta} \approx 2000$. Note, that account of a compressibility leads to the instability even in the case of the flat Couette flow Glatzel (1989). The maximum of instability region corresponds to Mach number $Ma \approx 4.9$, when unstable mode appears at $Re \approx 84$.

Taylor experiments with rotating cylinders has shown that at $Ty > 0$ the flow is becoming turbulent, but the Reynolds number Re , corresponding to the boundary of stability is increasing with increasing Ty . For the case of the Keplerian disk $\omega \sim r^{-3/2}$ we have $Ty = \frac{16}{9}$, formally corresponding to $\frac{t}{R} = \frac{2}{9} = 0.222$, for which the experimental number of the critical $Re \approx 2 \times 10^5$ (Zeldovich, 1981). Experimental dependence of the critical value $Re = f(Ty)$ is characterized by the Couette-flow critical value $Re(0) = 2000$, and can be approximated by the dependence $Re \approx 10^4 Ty^2$ for $Ty > 0.6$, $\frac{t}{R} > 0.075$. The last dependence was interpreted theoretically by Zeldovich (1981) by introduction of the *split* regime of the turbulence between cylinders.

In the laminar viscid flow between cylinders the exact solution (Schlichting, 1964) gives for $\omega_{in} = 0$ the rotational velocity distribution as

$$v(r) = \frac{R_{out}^2 \omega_{out}}{R_{out}^2 - R_{in}^2} \left(r - \frac{R_{in}^2}{r} \right) \approx \omega_{out} \frac{R}{t} (r - R_{in}) = \omega_{out} \frac{q}{t} = \omega_{out} x \quad (77)$$

$$q = r - R_{in}, \quad x = \frac{q}{t}$$

The local values of Re' and Ty' numbers, defined by fluid parameters near the inner cylinder, have been introduced by Zeldovich (1981) as

$$Re' = \frac{\rho v x}{\eta} = x^2 Re \quad Ty' = 8 \frac{x}{R} = x Ty. \quad (78)$$

It was suggested by Zeldovich (1981) that turbulence between rotating cylinders is installed, when one of the inequalities is fulfilled

$$\mathbf{a.} \quad Re = f(Ty) \quad \text{or} \quad \mathbf{b.} \quad Re' = (Ty'). \quad (79)$$

If the relation (79b) is fulfilled first the global condition of instability is not reached, and the turbulence is started in the local region near the inner cylinder, and was called as a split regime. Assuming that (79b) is fulfilled first we get

$$Re = \frac{Re'}{x^2} = \frac{f(Ty')}{x^2} = Ty'^2 \frac{f(y)}{y^2}, \quad y = x Ty. \quad (80)$$

Suppose now, that the function $\phi(y) = \frac{f(y)}{y^2}$ has a minimum at

$$y = y_m, \quad \phi_m = \frac{f(y_m)}{y_m^2}. \quad (81)$$

Then, taking into account (77) we get the relation $Ty > y_m$, so

$$\phi(Ty) > \phi(y_m), \quad Re = Ty^2 \phi(y_m) < f(Ty), \quad (82)$$

the global criterion of the turbulence is not fulfilled, and the split regime is realized. The turbulence is started in the region $x < x_m = y_m/Ty$. So, the criterion of the beginning of the split regime of the convection has a quadratic dependence on Ty in accordance with the experimental results.

It is noticed by Zeldovich (1981) that a boundary of the split regime of turbulence does not necessary mean the beginning of the turbulence in the accretion disk, where the condition (79a) is probably needed. Two examples of different functions are considered by Zeldovich (1981). For the function

$$f(y) = A \left(1 - \frac{y}{y_0}\right)^{-1} \quad (83)$$

the absolute instability (79a) exist only at $Ty < y_0$, and the minimum is reached at

$$y = \frac{2}{3}y_0, \quad \phi_m = \frac{f(y_m)}{y_m^2} = \frac{27}{4} \frac{A}{y_0^2}. \quad (84)$$

From the condition of the plane Couette flow it follows $A = 2000$, and from Taylor experiments, assuming there the split regime turbulence and assuming (82), we get $\phi_m = 10^4$, $y_0 = 1.16$. Note, that for the Keplerian accretion disk we have $Ty = \frac{16}{9} > 1.16$.

Another function from Zeldovich (1981) is

$$f(y) = A \exp\left(\frac{y}{y_0}\right), \quad (85)$$

where $A = 2000$, similar to (83), and $y_0 = 0.3$ from the Taylor experiment. Here $Re = f(16/9) = 2000 \exp(1.78/0.3) \approx 8 \times 10^5$ for the beginning of the absolute instability to the turbulence development.

The evaluations above show, that the problem of the hydrodynamic instability of the Keplerian accretion disk is far from a full understanding, and there are arguments, both experimental and theoretical, supporting the hydrodynamic origin of the accretion disk turbulence. The certain answer could be obtained from the full stability analysis of the Keplerian disk, similar to the one made for the viscous accretion tori in cylindrical approximation, made by Kleiber and Glatzel (1999) for a constant specific angular momentum distribution.

With alpha- prescription of viscosity the equation of angular momentum conservation is written in the plane of the disk as

$$\dot{M}(j - j_{in}) = 4\pi r^2 \alpha P_0 h. \quad (86)$$

When angular velocity is far from Keplerian the relation (71) is valid with a coefficient of a turbulent viscosity

$$\eta = \frac{2}{3} \alpha \rho_0 v_{s0} h, \quad (87)$$

where values with the index “0” denotes the plane of the disk.

2.5.3 Heat Balance

In the standard theory a heat balance is local, what means that all heat produced by viscosity in the ring between r and $r + dr$ is radiated through the sides of disk at the same r . The heat production rate Q_+ related to the surface unit of the disk is written as

$$Q_+ = h t_{r\phi} r \frac{d\Omega}{dr} = \frac{3}{8\pi} \dot{M} \frac{GM}{r^3} \left(1 - \frac{j_{in}}{j}\right). \quad (88)$$

Heat losses by a disk depend on its optical depth. The first standard disk model of Shakura (1972) considered a geometrically thin disk as an optically thick in a vertical direction. That implies energy losses Q_- from the disk due to a radiative conductivity, after a substitution of the differential equation of a heat transfer by an algebraic relation

$$Q_- \approx \frac{4}{3} \frac{acT^4}{\kappa\Sigma}. \quad (89)$$

Here a is the usual radiation energy-density constant, c is a speed of light, T is a temperature in the disk plane, κ is a matter opacity, and a surface density

$$\Sigma = 2\rho h, \quad (90)$$

here and below ρ , T , P without the index “0” are related to the disk plane. The heat balance equation is represented by a relation

$$Q_+ = Q_-, \quad (91)$$

A continuity equation in the standard model of the stationary accretion flow is used for finding of a radial velocity v_r

$$v_r = \frac{\dot{M}}{4\pi r h \rho} = \frac{\dot{M}}{2\pi r \Sigma}. \quad (92)$$

Equations (68),(70), (86),(90), (91), completed by an equation of state $P(\rho, T)$ and relation for the opacity $\kappa = \kappa(\rho, T)$ represent a full set of equations for a standard disk model. For power law equations of state of an ideal gas $P = P_g =$

$\rho \mathcal{R} T$ (\mathcal{R} is a gas constant), or radiation pressure $P = P_r = \frac{aT^4}{3}$, and opacity in the form of electron scattering κ_e , or Karammer's formula κ_k , the solution of a standard disk accretion theory is obtained analytically (Shakura, 1972; Novikov, Thorne, 1973; Shakura, Sunyaev, 1973). Checking the suggestion of a large optical thickness confirms a self-consistency of the model. One of the shortcomings of the analytical solutions of the standard model lay in the fact, that solutions for different regions of the disk with different equation of states and opacities are not matched to each other.

2.5.4 Optically thin solution

Few years after appearance of the standard model it was found that in addition to the optically thick disk solution there is another branch of the solution for the disk structure with the same input parameters M , \dot{M} , α which is also self-consistent and has a small optical thickness (Shapiro, Lightman, Eardley, 1976). Suggestion of the small optical thickness implies another equation of energy losses, determined by a volume emission

$$Q_- \approx q \rho h, \quad (93)$$

where due to the Kirchoff law the emissivity of the unit of a volume q is connected with a Plankian averaged opacity κ_p by an approximate relation $q \approx acT_0^4 \kappa_p$. Note, that Krammers formulae for opacity are obtained after Rosseland averaging of the frequency dependent absorption coefficient. In the optically thin limit the pressure is determined by a gas $P = P_g$. Analytical solutions are obtained here as well, from the same equations with volume losses and gas pressure. In the optically thin solution the thickness of the disk is larger then in the optically thick one, and density is lower.

While heating by viscosity is determined mainly by ions, and cooling is determined by electrons, the rate of the energy exchange between them is important for a thermal structure of the disk. The energy balance equations are written separately for ions and electrons. For small accretion rates and lower matter density the rate of energy exchange due to binary collisions is so slow, that in the thermal balance the ions are much hotter then the electrons. That also implies a high disk thickness and brings the standard accretion theory to the border of its applicability. Nevertheless, in the highly turbulent plasma the energy exchange between ions and electrons may be strongly enhanced due to presence of fluctuating electrical fields, where electrons and ions gain the same energy. In such conditions difference of temperatures between ions and electrons may be negligible. Regretfully, the theory of relaxation in the turbulent plasma is not completed, but there are indications to a large exhanacement of the relaxation in presence of plasma turbulence, in comparison with the binary collisions (Quataert, 1997).

2.6 Accretion disk structure from equations describing continuously optically thin and optically thick disk regions

In order to find equations of the disk structure valid in both limiting cases of optically thick and optically thin disk, and smoothly describing transition between them, use Eddington approximation for obtaining formulae for a heat flux and for a radiation pressure (Artemoma et al., 1996). Suppose that disk is geometrically thin and has a constant density along z -axis. Defining S_r as the energy density of the radiation, F_{rad} as radiation flux in z -direction, P_{rad} as radiation pressure we write momentum equations for averaged κ_p in the form (Bisnovatyi-Kogan, 1989)

$$\frac{dF_{rad}}{dz} = -\rho c \kappa_p a T^4 \left(\frac{S_r}{a T^4} - 1 \right), \quad (94)$$

$$c \frac{dP_{rad}}{dz} = -\kappa_e \rho F_{rad}. \quad (95)$$

Consider the case when scattering opacity κ_e is much larger than absorption opacity κ_p , and suggest that heat production rate is proportional to the mass density ρ . Then, neglecting the flux in the radial direction we get

$$F_{rad} = 2 \frac{F_0}{\Sigma_0} \rho z, \quad (96)$$

where F_0 is the flux from the unit surface of the disk at $z = h$. Substituting (96) into (94) we get

$$S_r = 3P_{rad} = a T^4 \left(1 - \frac{2F_0}{c \kappa_p a T^4 \Sigma_0} \right). \quad (97)$$

Using (96) in (95) we get

$$c \frac{dP_{rad}}{dz} = -2\kappa_e \frac{F_0}{\Sigma_0} \rho^2 z. \quad (98)$$

Introducing the scattering optical depth

$$\begin{aligned} \tau &= \int_z^\infty \kappa_e \rho dz = \kappa_e \rho (h - z) = \tau_0 - \kappa_e \rho z, \\ \tau_0 &= \kappa_e \rho h = \frac{1}{2} \kappa_e \Sigma_0, \end{aligned} \quad (99)$$

we rewrite (98) in the form

$$c \frac{dP_{rad}}{d\tau} = 2 \frac{F_0}{\Sigma_0} \frac{\tau_0 - \tau}{\kappa_e}. \quad (100)$$

Solve (100) with the following boundary condition

$$F_{rad}|_{\tau=0} = F_0 = \frac{cS_r|_{\tau=0}}{2} = \frac{3cP_{rad}|_{\tau=0}}{2}, \quad (101)$$

resulting in

$$cP_{rad} = F_0 \left(\frac{2}{3} + \tau - \frac{\tau^2}{2\tau_0} \right). \quad (102)$$

In the symmetry plane of the disk at $\tau = \tau_0$ we have

$$cP_{rad,0} = F_0 \left(\frac{2}{3} + \frac{\tau_0}{2} \right). \quad (103)$$

Using (103) in (97) we get in the symmetry plane, where $T = T_0$

$$F_0 = caT_0^4 \left(2 + \frac{3\tau_0}{2} + \frac{1}{\tau_{\alpha 0}} \right)^{-1}, \quad (104)$$

where absorption optical depth

$$\begin{aligned} \tau_\alpha &= \int_z^\infty \kappa_p \rho dz = \kappa_p \rho (h - z) = \tau_{\alpha 0} - \kappa_p \rho z, \\ \tau_{\alpha 0} &= \kappa_p \rho h = \frac{1}{2} \kappa_p \Sigma_0. \end{aligned} \quad (105)$$

Introducing effective optical depth

$$\tau_* = (\tau_0 \tau_{\alpha 0})^{1/2}, \quad (106)$$

we get finally the expressions for the vertical energy flux from the disk F_0 and the radiation pressure in the symmetry plane as

$$F_0 = \frac{2acT_0^4}{3\tau_0} \left(1 + \frac{4}{3\tau_0} + \frac{2}{3\tau_*^2} \right)^{-1}, \quad (107)$$

$$P_{rad,0} = \frac{aT_0^4}{3} \frac{1 + \frac{4}{3\tau_0}}{1 + \frac{4}{3\tau_0} + \frac{2}{3\tau_*^2}}. \quad (108)$$

At $\tau_0 \gg \tau_* \gg 1$ we have (89) from (107). In the optically thin limit $\tau_* \ll \tau_0 \ll 1$ we get

$$F_0 = acT_0^4 \tau_{\alpha 0}, \quad P_{rad,0} = \frac{2}{3} acT_0^4 \tau_{\alpha 0}. \quad (109)$$

Using F_0 instead of Q_- and equation of state $P = \rho \mathcal{R}T + P_{rad,0}$, the equations of accretion disk structure together with equation

$$Q_+ = F_0 \quad (110)$$

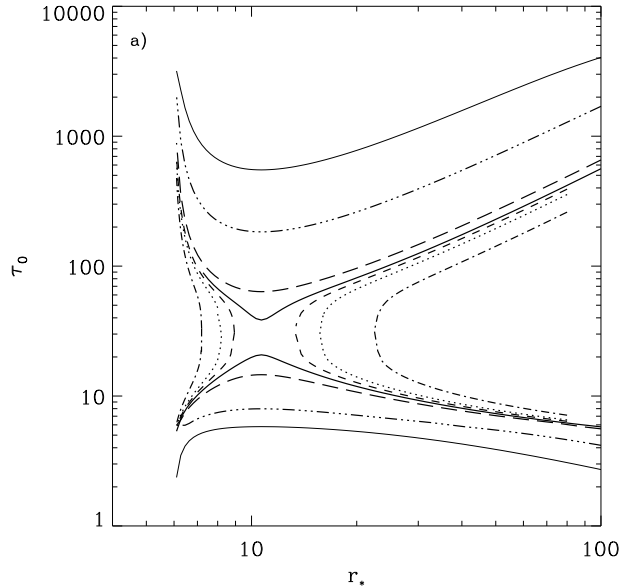


Figure 1: The dependences of the optical depth τ_0 on radius, $r_* = r/r_g$, for the case $M_{BH} = 10^8 M_{\odot}$, $\alpha = 1.0$ and different values of \dot{m} . The thin solid, dot-triple dash, long dashed, heavy solid, short dashed, dotted and dot-dashed curves correspond to $\dot{m} = 1.0, 3.0, 8.0, 9.35, 10.0, 11.0, 15.0$, respectively. The upper curves correspond to the optically thick family, lower curves correspond to the optically thin family.

with Q_+ from (88), have been solved numerically by Artemova et al. (1996). It occurs that two solutions, optically thick and optically thin, exist separately when luminosity is not very large. Two solutions intersect at $\dot{m} = \dot{m}_b$, where

$$\dot{m} = \frac{\dot{M}c^2}{L_{\text{Edd}}}, \quad L_{\text{Edd}} = \frac{4\pi cGM}{\kappa_e}, \quad (111)$$

and there is no global solution for accretion disk at $\dot{m} > \dot{m}_b$ (see Figure 1). It was concluded by Artemova et al (1996), that in order to obtain a global physically meaningful solution at $\dot{m} > \dot{m}_b$, account for an advective term in (110) is needed.

2.7 Accretion discs with advection

Standard model gives somewhat nonphysical behaviour near the inner edge of the accretion disk around a black hole. For high mass fluxes when central regions are radiation-dominated ($P \approx P_r$, $\kappa \approx \kappa_e$), the radial dependence follows

relations (Shakura, Sunyaev, 1973, Bisnovatyi-Kogan, 1999)

$$\begin{aligned} \rho &\sim r^{3/2} \mathcal{J}^{-2} \rightarrow \infty, & T &\sim r^{-3/8}, \\ h &\sim \mathcal{J} \rightarrow 0, & \Sigma &\sim r^{3/2} \mathcal{J}^{-1} \rightarrow \infty, & v_r &\sim r^{-5/2} \mathcal{J} \rightarrow 0, \end{aligned} \quad (112)$$

where limits relate to the inner edge of the disk with $r = r_{in}$,

$$\mathcal{J} = 1 - \frac{j_{in}}{j} = 1 - \sqrt{\frac{r_{in}}{r}}. \quad (113)$$

At smaller \dot{M} , when near the inner edge $P \approx P_g$, $\kappa \approx \kappa_e$, there are different type of singularities

$$\begin{aligned} \rho &\sim r^{-33/20} \mathcal{J}^{2/5} \rightarrow 0, & T &\sim r^{-9/10} \mathcal{J}^{2/5} \rightarrow 0, \\ h &\sim r^{21/20} \mathcal{J}^{1/5} \rightarrow 0, & \Sigma &\sim r^{-3/5} \mathcal{J}^{3/5} \rightarrow 0, & v_r &\sim r^{-2/5} \mathcal{J}^{-3/5} \rightarrow \infty. \end{aligned} \quad (114)$$

This results from the local form of the equation of the thermal balance (91). It is clear from physical ground, that when a local heat production due to viscosity goes to zero, the heat brought by radial motion of matter along the accretion disk becomes more important. In the presence of this advective heating (or cooling term, depending on the radial entropy S gradient) written as

$$Q_{adv} = -\frac{\dot{M}}{2\pi r} T \frac{dS}{dr}, \quad (115)$$

the equation of a heat balance is modified to

$$Q_+ - Q_{adv} = Q_-. \quad (116)$$

In order to describe self-consistently the structure of the accretion disk we should also modify the radial disk equilibrium equation, including pressure and inertia terms

$$r(\Omega^2 - \Omega_K^2) = \frac{1}{\rho} \frac{dP}{dr} - v_r \frac{dv_r}{dr}. \quad (117)$$

Appearance of inertia term leads to transonic radial flow with a singular point. Conditions of a continuous passing of the solution through a critical point choose a unique value of the integration constant j_{in} .

Simplified solutions with inclusion of the advective terms into the vertically averaged equations describing accretion disks was obtained by Paczyński & Bisnovatyi-Kogan (1981). This approach with some modifications have been used by many researchers to study transonic accretion flows around black holes (Muchotrzeb & Paczyński 1982; Matsumoto et al. 1984; Abramowicz et al. 1988; Beloborodov 1998). The importance of transonic nature of accretion flows on the disk structure has been emphasized by Hōshi & Shibazaki (1977),

Liang & Thompson (1980) and Abramowicz & Zurek (1981), and later studied in more details by Abramowicz & Kato (1989), see also Kato et al. (1998).

The problems at finding the numerical solution of advective disk structure are connected with the possible non-uniqueness of global solutions at $\alpha > 0.01$ and the non-standard behavior of a type of a singular point. It was reported by Matsumoto et al. (1984), Abramowicz et al. (1988) that in the case of viscosity prescription (68) the singular point changes its type from a saddle to node when increasing α . The presence of the nodal-type singular point leads to creating of possibility of multiple solutions as the authors have claimed.

In the paper of Artemova et al. (2001) it was shown that the mentioned problems have been created by several inconsistencies in the preceding studies. Some problems are connected with an inaccurate averaging of the equations over the disk thickness, another ones appear due to incomplete investigation of the singular points (Abramowicz et al. 1988). It was found that in the case of viscosity prescription (73) a set of equations describing the vertically averaged advective accretion disks has *two* singular points, depending on α and accretion rate. Calculations of the advective disk structure are performed in Paczyński-Wiita potential (Paczyński & Wiita 1980)

$$\Phi(r) = -\frac{GM}{r - 2r_g}, \quad (118)$$

where M is the black hole mass and $2r_g = 2GM/c^2$ is the gravitational radius. The disk self-gravity is neglected. Note, that the multiplicity of singular points in solutions for accretion flows in Paczyński-Wiita potential (118) was revealed by Fukue (1987), Chakrabarti & Molteni (1993) and Chakrabarti (1996) in somewhat different context. Another type of accretion flows with multiple singular points was found by Dullemond & Turolla (1998) and Turolla & Dullemond (2000), who considered accretion disks experienced a phase transition. It was shown by Artemova et al. (2001), that at $\alpha < 0.01$ the inner and outer (with respect to the black hole location) singular points are of a saddle type, and only one integral curve ('separatrix') which crosses the inner point simultaneously crosses the outer one. This separatrix corresponds to the unique global solution which is determined by two parameters, α and $\dot{m} = \dot{M}c^2/L_{Edd}$, for the given black hole mass. At larger $\alpha > 0.1$ the inner singular point changes its type to a node, while the outer point remains of a saddle-type. There is still one integral curve which goes continuously through both the singular points providing the unique global solution.

In the case of viscosity prescription in the first relation of (74)

$$t_{r\phi} = \eta r \frac{d\Omega}{dr} = \rho \nu r \frac{d\Omega}{dr} \quad (119)$$

it was found that there is only one singular point which is always a saddle, and only one physical solution which passes through this point exists. Solu-

tions which correspond to both forms of viscosity (73) and (119) are very close quantitatively at low α limit, $\alpha < 0.1$.

A numerical method was developed by Artemova et al. (2001) to solve a set of equations describing the vertically averaged advective accretion disks. The method is based on the standard relaxation technique and explicitly uses conditions at the inner singular point and its vicinity. These conditions had been obtained by expanding the solution into power series around the singular point. Such a modification of the method allowd to construct solutions which smoothly pass the singular points and satisfy the regularity conditions at these points with high computer precision in wide range of parameters α and \dot{m} .

The equations describing the radial disk structure are written for the mid-plane density ρ , pressure P , radial velocity v and angular velocity Ω . They consist of the mass conservation equation taken the form,

$$\dot{M} = 4\pi r h \rho v, \quad (120)$$

$\dot{M} > 0$, and h is the disk half-thickness, which is expressed in terms of the isothermal sound speed $c_s = \sqrt{P/\rho}$ of gas,

$$h = \frac{c_s}{\Omega_K}. \quad (121)$$

The equations of motion in the radial (117) and azimuthal direction

$$\frac{\dot{M}}{4\pi} \frac{dj}{dr} + \frac{d}{dr}(r^2 h t_{r\phi}) = 0, \quad (122)$$

where Ω_K is the Keplerian angular velocity, $\Omega_K^2 = GM/r(r - 2r_g)^2$, $j = \Omega r^2$ is the specific angular momentum and $t_{r\phi}$ is the (r, ϕ) -component of the viscous stress tensor. Other components of the stress tensor are assumed to be negligibly small. The vertically averaged energy conservation equation is written in (115),(116) ¹, with the advective term in the form

$$Q_{\text{adv}} = -\frac{\dot{M}}{2\pi r} \left[\frac{dE}{dr} + P \frac{d}{dr} \left(\frac{1}{\rho} \right) \right], \quad (123)$$

and

$$Q_+ = h t_{r\phi} r \frac{d\Omega}{dr}, \quad Q_- = \frac{2aT^4 c}{3\kappa \rho h}, \quad (124)$$

are the viscous dissipation rate and the cooling rate per unit surface, respectively, T is the midplane temperature. The equation of state for accretion matter consisted of a gas-radiation mixture is

¹The vertical averaging in equation (116) have been made differently by different authors (compare e.g. Shakura & Sunyaev 1973, and Abramowicz et al. 1988). Our choice of the coefficients in (123),(124), may be not the optimal one. Aposteriori analysis had shown that using the factor 4 instead of 2 in the denominator of (123) would be more consistent choice, but this change has a little influence on our numerical results.

$$c_s^2 = \mathcal{R}T + \frac{1}{3} \frac{aT^4}{\rho}, \quad (125)$$

where \mathcal{R} is the gas constant. The specific energy of the mixture is

$$E = \frac{3}{2} \mathcal{R}T + \frac{aT^4}{\rho}. \quad (126)$$

Both prescriptions of viscosity (73) and (119) have been used in calculations with ν in the form

$$\nu = \frac{2}{3} \alpha c_s h. \quad (127)$$

Note that in the limit $\Omega \rightarrow \Omega_K$ both the prescriptions (73) and (119) coincide. Integration of equation (122) gives

$$r^2 h t_{r\phi} = -\frac{\dot{M}}{4\pi} (j - j_{\text{in}}), \quad (128)$$

where the integration constant j_{in} has meaning of the specific angular momentum of accreting matter near the black hole horizon. The value of j_{in} is chosen to obtain the global transonic solution with the subsonic part at large radii and the supersonic part in vicinity of the black hole horizon. In the case of viscosity prescription (73) the expression (128) results in an algebraical equation, and the radial structure of the accretion disks is described by two first order differential equations (117) and (116). In general formulation, these two equations require to fix two parameters as boundary conditions to determine the solution. In the case of viscosity prescription (119) expression (128) results in additional first order differential equation, so we have to fix three parameters as boundary conditions.

We show here two examples of numerical results obtained by Artemova et al. (2001). Each calculated model is characterized by the unique value of j_{in} . Figures 3 and 4 show the dependences of j_{in} on the accretion rate $\dot{m} = \dot{M} c^2 / L_{\text{Edd}}$ for three values of $\alpha = 0.01, 0.1$ and 0.5 in the case of viscosity prescription (73) and (119) respectively. At low $\dot{m} < 1$ the value of j_{in} is independent of \dot{m} and weakly varies with α . In the low α case, $\alpha = 0.01$ and 0.1 , the values of j_{in} are close to the minimum value of the Keplerian angular momentum, $(j_K)_{\text{min}} = 3.6742$. At high $\dot{m} > 0.1$ the values of j_{in} deviate from $(j_K)_{\text{min}}$ to larger or smaller values depending on α . In the case of $\alpha = 0.01$ and 0.1 one can see only minor differences between models with different forms of viscosity. But, for large $\alpha = 0.5$ the difference in values of j_{in} increases.

Figures 5 and 6 show locations of the inner singular points $(r_s)_{\text{in}}$ as a function of \dot{m} for different values of α and both viscosity prescriptions. Similar to the case of j_{in} discussed above the models at low \dot{m} show a weak dependence of $(r_s)_{\text{in}}$ on \dot{m} . In the low α models (squares and circles in Figures 3-6) the values

of $(r_s)_{\text{in}}$ are close to the location of the black hole last stable orbit at $r = 6r_g$. At high $\dot{m} > 0.1$ the values of $(r_s)_{\text{in}}$ are decreasing functions of \dot{m} in the case of low $\alpha = 0.01$ and 0.1 , and non-monotonically behave in the case of $\alpha = 0.5$ (triangles in Figures 3-6).

In the case of viscosity prescription (73) the solutions have the outer singular point in addition to the inner one. The change of value of $\beta = \frac{R\dot{J}}{c_s^2}$ from 1 to 0 corresponds to the change of a state from the gas pressure to radiative pressure dominated one. The thin disks with $\beta \simeq 1$ are locally stable, whereas parts of the disk in which $\beta \simeq 0$ are thermally and viscously unstable (Pringle, Rees, & Pacholczyk 1973). At large $\dot{m} > 100$ the instability can be suppressed by the advection effect (Abramowicz et al. 1988). It was shown by Artemova et al. (2001), that significant deviations of j_{in} and $(r_s)_{\text{in}}$ in Figures 3-6 from the constant happens when β begins to deviate from the unity. The analysis of the critical points had shown that they are either saddle or nodal-type. In Figures 3-6 the saddle-type points are indicated by the solid squares, circles and triangles. The nodal-type points are represented by the corresponding empty dots in the same figures. In the case of viscosity prescription (73) the inner singular points can be saddles or nodes depending on values of α and \dot{m} . Note that the change of type from a saddle to nodal one does not introduce any features in the solutions. The outer singular points are always of a saddle-type. In the case of viscosity prescription (119) the solutions have only one (inner) singular point which is always of a saddle-type.

The models with $\dot{m} < 16$ and low $\alpha < 0.1$ have values of r_s and j_{in} which are very close to the location of the last stable orbit, $r_{\text{in}} = 6r_g$, and value of $j_{\text{in}} = (j_K)_{\text{min}}$ assumed in the standard model (Shakura & Sunyaev 1973). The radial structures of the models are also very close to the ones for the standard model in the same range of \dot{m} and α . Such a good coincidence means that the advective terms in equations (116) and (117) are negligibly small in the considered models. However, the high α models show quite significant deviation from the standard model for all \dot{m} (see Figures 3-6).

At high accretion rates, $\dot{m} > 16$, the effect of advection becomes significant, and at $\dot{m} = 100$ the advective part of the energy flux is ~ 2 times larger than the luminosity.

2.8 Convection in accretion discs

2.8.1 Vertical structure and convective instability in the radiation-dominated disk region

Let us consider in more details the vertical structure of the accretion disk. Following Shakura(1972), Shakura and Sunyaev(1973) let us suggest that viscous heat production per unit mass in the accretion disk is constant, what is used

also in section 1.6. For variable vertical density the equation of vertical heat flux is different from (96), and has a differential form with $F_0 \equiv Q_+$ from (88):

$$\frac{dF_{rad}}{dz} = 2F_0 \frac{\rho}{\Sigma_0} = \frac{3}{4\pi} \dot{M} \frac{GM}{r^3} \left(1 - \frac{j_{in}}{j}\right) \frac{\rho}{\Sigma_0}, \quad (129)$$

what gives after integration

$$F_{rad} = 2F_0 \frac{\Sigma}{\Sigma_0}. \quad (130)$$

Here Σ is the mass in the layer $(0, z)$, so that $\Sigma(h) = \Sigma_0/2$, $d\Sigma = \rho dz$. The equation of a heat conductivity in the optically thick disk in vertical direction is written as

$$F_{rad} = -\frac{ac}{3\kappa\rho} \frac{dT^4}{dz} = -\frac{ac}{3\kappa} \frac{dT^4}{d\Sigma}. \quad (131)$$

We consider here only regions where electron scattering dominates, so $\kappa = \kappa_e$. Solving (131) together with (130) we obtain

$$T^4 = T_0^4 \left(1 - \frac{3\kappa F_0 \Sigma^2}{ac \Sigma_0 T_0^4}\right). \quad (132)$$

At the surface of the disk

$$\Sigma = \Sigma_0/2, \quad T = T_s, \quad F_0 = \frac{acT_s^4}{4}, \quad (133)$$

like in black-body radiation, so we obtain from (132)

$$T_0^4 = T_s^4 \left(1 + \frac{3\kappa \Sigma_0}{16}\right). \quad (134)$$

Assuming high optical depth $\Sigma_0 \kappa \gg 1$, and using (134) in (132) we obtain the temperature distribution over the thickness of the disk in the form

$$T^4 = T_0^4 \left[1 - \left(\frac{2\Sigma}{\Sigma_0}\right)^2\right]. \quad (135)$$

Note, that equation (89) follows from (134) at high optical depth, after using black-body connection between T_s and F_0 .

Consider now a vertical density dependence in the accretion disk. In the radiation-dominated region with $P \approx P_r = \frac{aT^4}{3}$ we obtain from the vertical equilibrium equation (69)

$$\frac{a}{3\rho} \frac{dT^4}{dz} = -\frac{GMz}{r^3}. \quad (136)$$

Using (130),(131),(136), we obtain

$$\Sigma = \frac{GMc\Sigma_0}{2r^3\kappa F_0} z. \quad (137)$$

After differentiating, we obtain that in the radiation-dominated disk the density does not depend on the vertical coordinate z

$$\rho = \frac{GMc\Sigma_0}{2r^3\kappa F_0}. \quad (138)$$

In the constant density layer with falling temperature the entropy

$$S = \frac{4}{3} \frac{aT^3}{\rho} \quad (139)$$

is falling outside in the direction of the gravitation force. It corresponds to convectively unstable situation, what was noticed first by Bisnovatyi-Kogan and Blinnikov (1976, 1977).

For outer region of the accretion disk with $P_g \gg P_r$, $\kappa = \kappa_e$, there is no analytic solution for a vertical disk structure. We may however to check the convective instability in another way. In the gas-pressure dominated region the entropy

$$\frac{S}{\mathcal{R}} = \log\left(\frac{T^{3/2}}{\rho}\right) + \text{const}, \quad \frac{dS}{\mathcal{R}} = \frac{3}{2} \frac{dT}{T} - \frac{d\rho}{\rho}, \quad (140)$$

and with $P = P_g = \mathcal{R}\rho T$ it follows from the vertical equilibrium equation (69)

$$\frac{dT}{T} + \frac{d\rho}{\rho} = -\frac{GMz}{r^3 P} d\Sigma. \quad (141)$$

We obtain from (135)

$$\frac{dT}{T} = -\frac{1}{2} \frac{T_0^4 - T^4}{T^4} \frac{d\Sigma}{\Sigma}. \quad (142)$$

Using (141),(142) in (140) we obtain

$$\frac{dS}{\mathcal{R}} = -\frac{5}{2} \frac{dT}{T} + \frac{GMz}{r^3 P} d\Sigma = \left(\frac{GMz}{r^3 P} \Sigma - \frac{5}{4} \frac{T_0^4 - T^4}{T^4} \right) \frac{d\Sigma}{\Sigma} \quad (143)$$

It is easy to prove that entropy is growing with height in the region near the equatorial plane $z \ll h$. Here we have $\Sigma \approx \rho_0 z \ll \Sigma_0$, and it follows from (135),(142),(143)

$$\frac{dS}{\mathcal{R}} \approx \left(\frac{GM\Sigma_0^2}{r^3 P_0 \rho_0} - 5 \right) \frac{\Sigma d\Sigma}{\Sigma_0^2}. \quad (144)$$

Calculating the last expression in brackets, using the accretion disk solution (see e.g. Shakura & Sunyaev (1973)), we obtain

$$\frac{dS}{\mathcal{R}} = (8 - 5) \frac{\Sigma d\Sigma}{\Sigma_0^2} > 0,$$

what means stability relative to convection. Similarly we prove a stability relative to convection in the region close to the surface of accretion disk, where $\Sigma = \frac{\Sigma_0}{2}$, $T = T_s$, $z = h$, $P = P_s$. From the theory of stellar atmospheres (see e.g. Bisnovatyi-Kogan (2001)) we have a condition at the photosphere, corresponding to the optical depth $\tau = 2/3$, in the form $P_s = \frac{2}{3} \frac{g}{\kappa}$, where

$$g = \frac{GMh}{r^3} \quad (145)$$

is the gravitational acceleration at the disk surface. Using these relations and (134) in (143) we get

$$\begin{aligned} \frac{dS}{\mathcal{R}} &\approx \left(\frac{GM\Sigma_0 h}{2r^3 P_s} - \frac{5 T_0^4}{4 T_s^4} \right) \frac{d\Sigma}{\Sigma} \\ &= \left(\frac{GMh}{r^3 P_s \kappa} - \frac{15}{32} \right) \kappa d\Sigma = \left(\frac{3}{2} - \frac{15}{32} \right) \kappa d\Sigma > 0 \end{aligned}$$

So, the accretion disk in a standard model is convectively unstable in the radiation dominated region, which is the nearest to the black hole, and is stable in the adjusting region. The most outer gas-pressure dominated regions with $\kappa_p \gg \kappa_e$ are also stable relative to convection until the gas is fully ionized. In the colder regions with incomplete ionization a behaviour of the accretion disk becomes more complicated, with a non-unique solution, and convective instability (Cannizzo, Ghosh & Wheeler, 1982).

2.8.2 Structure of convective accretion disk region

In a standard model with a radiative heat conductivity in vertical direction the radiation-dominated region exist only when (Shakura and Sunyaev, 1973)

$$\frac{L}{L_{\text{Edd}}} \geq \frac{1}{50} \left(\frac{\alpha M}{M_\odot} \right)^{-1/8}. \quad (146)$$

Existence of convection changes the structure of the radiation-dominated region, and condition (146). Let us estimate a part of the energy flux carried out by convection, using a mixing length model of the convection (Bisnovatyi-Kogan and Blinnikov, 1976).

The convective heat flow Q_{conv} (ergs/cm²/s), the convection velocity v , and the excess $\Delta\nabla T$ of the temperature gradient above the adiabatic gradient (we shall take the mixing length l to be the half-thickness z_0 of the disk) are given by the equations

$$Q_{conv} = c_p \rho v (z_0/2) \Delta\nabla T, \quad (147)$$

where

$$c_p = \mathcal{R} \left[\frac{5}{2} + 20 \frac{P_r}{P_g} + \left(\frac{4P_r}{P_g} \right)^2 \right],$$

$$v = \left[\frac{Q_{conv}(1 + 4P_r/P_g) GM}{2\rho c_p T r^3} \right]^{1/3} z_0^{2/3}, \quad (148)$$

$$\Delta \nabla T = \left(\frac{4Q_{conv}}{\rho c_p} \right)^{2/3} \left[\frac{T}{(1 + 4P_r/P_g) GM} \right]^{1/3} r z_0^{-5/3}. \quad (149)$$

Hence we find that the excess $\Delta \nabla T$ in the temperature gradient does not exceed 20% of ∇T , while the convection velocity is $v = 3 \cdot 10^8$ cm/sec for $r = 10r_g$, what is close to the velocity v_s of the sound in this region. The heat flow is carried mainly by convection ($Q \approx Q_{conv}$), because of a high matter density, and the radiative flux is $\sim 20\%$ of the total flux. Convection is smoothing out the entropy in vertical direction, so with a precision $\sim 20\%$ we may consider the entropy as a constant in the vertical direction.

Bisnovatyi-Kogan and Blinnikov (1977) had obtained an analytic solution for the isentropic convective accretion disk in the radiation-dominated region. When $P_r \gg P_g$ the surface pressure at the photosphere with $\tau = 2/3$ is equal to

$$P_s = \frac{4g}{3\kappa} = \frac{4GMh}{3\kappa r^3}. \quad (150)$$

The effective temperature at the disk surface is connected with the surface radiative pressure in (150), and with the surface radiative flux in (88) as

$$\frac{aT_s^4}{3} = P_s = \frac{4GMh}{3\kappa r^3}; \quad \frac{acT_s^4}{4} = Q_+ = \frac{3}{8\pi} \dot{M} \frac{GM}{r^3} \left(1 - \frac{j_{in}}{j} \right). \quad (151)$$

The disk thickness is obtained from comparison of two expressions in (151) as

$$h = \frac{3\kappa}{8\pi c} \dot{M} \left(1 - \frac{j_{in}}{j} \right). \quad (152)$$

In the radiative-dominated region the equation of state at constant entropy, using (139), is writetn as

$$P = \frac{aT^4}{3} = \left(\frac{3S^4}{256a} \right)^{1/3} \rho^{4/3} \equiv K_r \rho^{4/3}. \quad (153)$$

Integration of the equation of vertical equilibrium (69) gives

$$\rho^{1/3} = \rho_0^{1/3} - \frac{GMz^2}{8K_r r^3}. \quad (154)$$

Using the surface boundary condition

$$\rho_s \equiv \rho(h) = \left(\frac{P_s}{K_r} \right)^{3/4} = \left(\frac{4GMh}{3\kappa r^3 K_r} \right)^{3/4}$$

we determine the equatorial density ρ_0 from (154). Assuming $P_0 \gg P_s$ and $\rho_0 \gg \rho_s$, we obtain

$$\begin{aligned} \rho_0^{1/3} &= \frac{GMh^2}{8K_r r^3}, & P &= K_r \left(\frac{GMh^2}{8K_r r^3} \right)^4 \left(1 - \frac{z^2}{h^2} \right)^4 \\ & & &= P_0 \left(1 - \frac{z^2}{h^2} \right)^4, & \rho &= \rho_0 \left(1 - \frac{z^2}{h^2} \right)^3. \end{aligned} \quad (155)$$

The equatorial pressure is obtained from the angular momentum equation (71) and (152) as

$$P_0 = \frac{2c\Omega_K}{3\kappa\alpha}, \quad T_0^4 = \frac{2c\Omega_K}{a\kappa\alpha}, \quad (156)$$

and from the boundary condition (133) we obtain

$$P_s = \frac{4F_0}{3c}, \quad \frac{P_s}{P_0} = 2\alpha \frac{\Omega_K h}{c} \ll 1, \quad (157)$$

what justifies the previous assumption. We used here the relation following from (88) and (152)

$$F_0 = \frac{c\Omega_K}{\kappa} h. \quad (158)$$

Note, that we used here the exact angular momentum equation (71) in the plane of the disk, instead of the approximate equation obtained by averaging over the thickness, used by Bisnovatyi-Kogan and Blinnikov (1977). In this approach the equations (156)-(158) are valid always in the radiation-dominated region, both radiative and convective. The convection does not change the pressure and temperature distribution over the thickness of the disk, and the thickness itself, changing only its density distribution. The temperature distribution in the radiative disk (135) at constant density, and corresponding pressure distribution are identical to their distribution in the convective disk (155).

The density and surface density in the radiative disk are found from (133), (134), (156) and (158) as

$$\rho_0 = \frac{4c}{3\kappa\alpha} \frac{1}{\Omega_K h^2}, \quad \Sigma_0 = 2\rho_0 h = \frac{8c}{3\alpha} \frac{1}{\kappa\Omega_K h}. \quad (159)$$

In the isentropic convective disk the density distribution is given in (155), the equatorial density ρ_0 , surface density Σ_0 , constant K and entropy S are found from (155),(156) as

$$\rho_0 = \frac{16c}{3\kappa\alpha} \frac{1}{\Omega_K h^2}, \quad \Sigma = \frac{32}{35} \rho_0 h = \frac{512c}{105\kappa\alpha} \frac{1}{\Omega_K h}, \quad (160)$$

$$K = \left(\frac{3\alpha\kappa}{2c\Omega_K} \right)^{1/3} \frac{(\Omega_K h)^{8/3}}{16}, \quad S = \left(\frac{a\alpha\kappa}{2c\Omega_K} \right)^{1/4} \frac{\Omega_K^2 h^2}{2}.$$

It follows from (159),(160), that in the equatorial plane the density of the convective disk is 4 times larger, than in the radiative one, and in the surface density the difference is only 64/35 times. Increase of the convective disk density at the same temperature narrows the radiative-dominated region, which may exist now at luminosities ~ 2 times larger than in the radiative one (146).

2.8.3 Numerical simulations of convection in accretion disks

2-D numerical simulations had confirmed in general the conclusion about the isentropic vertical structure of the disk in convectively unstable regions. Fujita and Okuda (1998) had obtained that the excess $\Delta\nabla T$ in the temperature gradient does not exceed $\sim 1\%$, what is even closer to the adiabatic structure, than followed from estimations of Bisnovatyi-Kogan and Blinnikov (1976). It probably happend, because in the computations convective cells generally stretch from the disk mid-plane to the disk surface, increasing the efficiency of the convective mixing in vertical direction, relative to the model of isotropic convection used in estimations. 2-D calculations made by Agol et al. (2000) also had shown a satisfactory correspondence with the analytical solution of the isentropic convective disk structure of Bisnovatyi-Kogan and Blinnikov (1977).

2-D numerical simulations of accretion of highly viscous nonradiating gas had been performed by Igumenshchev (2000), and Igumenshchev and Abramowicz (1999,2000). Ideal gas with an adiabatic index γ was considered, so that pressure was connected with the density and specific internal energy ε in the form

$$P = (\gamma - 1)\rho\varepsilon. \quad (161)$$

Calculations have been done in a range of viscous parameters $\alpha = 0.01 - 1$, and $\gamma = 4/3, 3/2, 5/3$. Convective instability or large scale circulation occured at smaller α and γ . At $\gamma = 4/3$ all models with $\alpha \leq 0.3$ are unstable; at $\gamma = 3/2$ and $5/3$ the instability takes place at $\alpha \leq 0.1$, and $\alpha \leq 0.03$ respectively. The calculations have been performed also with account of a turbulent heat conductivity, characterized by non-dimensional Prandtl number

$$Pr = \frac{\nu}{\chi}, \quad (162)$$

where $\chi = \lambda/\rho$ is the thermometric conductivity, and kinematic turbulent viscosity coefficient ν is given in (127). Stabilization of the flow had been obtained at $Pr = 1$ for all γ with $\alpha \geq 0.1$, and for $\alpha = 0.03$ at $\gamma = 5/3$.

The high-viscosity models at $\alpha = 1$ form powerful bipolar outflows. The pure inflow and large-scale circulation patterns occur in the moderate viscosity models $\alpha = 0.1 - 0.3$. All models with bipolar outflows and pure inflows are steady. The models with large scale circulation could be either steady or unsteady, depending on values of α and γ . All convective models are unsteady. The self-similar solution for accretion flows with bipolar outflows (advection-dominated inflows-outflows ADIOS) proposed by Blandford and Begelman (1999) have not been confirmed in the numerical simulations of Igumenshchev and Abramowicz (2000).

3-D numerical simulations of viscous non-radiating accretion flows made by Igumenshchev et al. (2000) have confirmed qualitatively and quantitatively those obtained in 2-D simulations. It was shown that convective eddies are nearly axisymmetric and transport angular momentum inward, tending to smooth out the angular momentum distribution. This is in contrast with a small scale turbulence, acting as a viscosity, transporting angular momentum outside, and tending to smooth out the angular velocity distribution.

2.8.4 Hot corona and Cyg X-1 variability

In the convective disk the flow Q_{ac} of acoustic energy in the vertical direction is given by Bierman and Lüst (1960) as

$$Q_{ac} \simeq \rho v^3 (v/v_s)^5 \simeq 10^{21-22} \text{erg} \cdot \text{sec}^{-1} \cdot \text{cm}^2, \quad (163)$$

and is a quantity of the same order as the total energy flux for characteristic parameters of Cyg X-1 (Bisnovatyi-Kogan and Blinnikov, 1976).

Acoustic waves generated in the convection zone escape into optically thin layers, induce variable soft X rays in the photosphere, and also are responsible for variable heating of the corona. Comptonization of the photospheric radiation by hot electrons under conditions where both temperature and density are variable should lead to flux variations in the hard range, $h\nu \geq 5$ keV. This X-ray fluctuation mechanism, involving the emergence of waves into transparent layers, evidently is of the same wave nature as the variability of the ultraviolet excess in stars experiencing intensive convection, such as T Tauri and UV Ceti.

The waves escaping into the transparent layers and producing variable radiation in the photosphere and corona occupy a rather narrow frequency band. Physically, the reason for this circumstance is the following. A media with a high radiation pressure and a non-uniform distribution of plasma along the z coordinate (across the disk) serve as efficient filters, picking out a characteristic frequency range from the broader spectrum generated by convection and turbulence. Waves of low frequency and a wavelength exceeding the scale height of the atmosphere will not escape outside but will induce oscillations of the coronal atmosphere as a whole. On the other hand, under conditions where radiation pressure predominates, high-frequency waves experience a se-

vere damping because of radiative friction, and their role in heating the corona will be insignificant.

The propagation of acoustic waves through a medium with strong radiation pressure, followed by their escape into the atmosphere had been investigated in details by Bisnovaty-Kogan and Blinnikov (1978a,b; 1979), and by Agol and Krolik (1998) for MHD waves. Waves emerging into the transparent layers will have a phase and group velocity equal to the velocity of sound in gas, $v_g = (\gamma P_g / \rho)^{1/2} = (\gamma \mathcal{R} T)^{1/2}$, where $\gamma = 5/3$ or $\gamma = 1$ according as scattering or absorption predominates, \mathcal{R} is the gas constant, and the temperature T of the equilibrium atmosphere is approximately equal to the temperature T_s of the photosphere. The characteristic frequency ω_c of waves emerging into the atmosphere is given by the expression

$$\omega_c = \left(\frac{\gamma}{\mathcal{R} T} \right)^{1/2} g \left(1 - \frac{F}{F_c} \right) \text{sec}^{-1}. \quad (164)$$

For the accretion disk model, the gravitational acceleration g at radius r is given by (145), and characteristic thickness h is given by (152). The quantity $F/F_c = \kappa F/gc$ represents the ratio of the radiation pressure force to the gravity; κ is the opacity, including both absorption and scattering. In a spherically symmetric star of luminosity L and radius R we have $g = GM/R^2$, $F = L/4\pi R^2$, and $F/F_c = L/L_c$, where $L_c = 4\pi cGM/\kappa$ is the Eddington limiting luminosity.

Characteristic frequencies ω_c from (164) of fluctuations of Cyg X-1 in the convective accretion-disk model of Bisnovaty-Kogan and Blinnikov (1977), with a black hole mass $M = 10 M_\odot$, luminosity between $0.1 L_c$ and $0.3 L_c$, corresponding to the photospheric temperature T_s , lay in the range 5-40 msec. If a corona with $T_{cor} \approx 10^2 T_s$ is present, waves whose frequency is $\omega = \omega_c$ or even little lower will be able to escape. This frequency range is in a good accord with the observed time-scales of variability (Bolt, 1977).

Due to strong radiative damping of the sound waves, only small part of acoustic energy flux of order

$$Q_{cor} \sim (P_g/P_r) Q_{ac} \quad (165)$$

is expended in heating the outer layers with an optical depth $\tau < 1$. Another mechanism is acting to heat these layers (Bisnovaty-Kogan and Blinnikov, 1977). A particle in a region near the surface of the disk that is transparent to radiation will be subject to the influence of radiation from the whole disk, and not only to the local radiation pressure gradient. The force of the radiation pressures will accelerate particles in the transparent region above the disk. Calculations of the equations of motion for particles subject to radiative, centrifugal, and gravitational forces show that in the region with $\tau < 1$ the particles (protons and electrons) will acquire vertical velocities corresponding to the temperatures $(1 - 8) \cdot 10^8$ K of protons for $L \approx 0.1 L_c$. Turbulent relaxation of the particle motions in the corona will tend to equalize the mean energies

of the ions and electrons and to form a quasi-Maxwellian particle velocity distribution. Thus the combined action of the two heating mechanisms we have described will produce around the accretion disk a hot corona with $T_e \approx 10^9$ K for $L \approx 0.1L_c$. The existence of an analogous corona has been postulated phenomenologically by Price and Liang (1977).

Let us estimate the density ρ_{cor} of the corona and the amount of material it contains. Since the gas pressure varies continuously with transition from the photosphere to the corona, we readily find that at the base of the corona

$$\rho_{cor} \simeq \rho_s T_s / T_{cor} \simeq 10^{-2} \rho_s \approx 10^{-5} \text{ g/cm}^3, \quad (166)$$

where ρ_s, T_s are the density and temperature in the photosphere of the disk for the parameters of the source Cyg X-1 in the region of maximum energy release. The surface density of the corona is determined by the condition $\tau_{es} \approx 1$ and is $\approx 2 \text{ g/cm}^2$, which is more than an order of magnitude lower than the density of the opaque disk.

The existence of a hot corona can easily explain the peculiarities of the Cyg X-1 spectrum during its variations (Bisnovatyi-Kogan and Blinnikov, 1976). The soft X-rays at $h\nu \leq 7$ keV, which comprise $\approx 70\%$ of the total flux, are formed in the photosphere of the opaque disk. Some of the radiation ($\approx 10\%$) passing through the hot corona, experience comptonization and transforms into a hard radiation up to $h\nu \approx 3kT_e \approx 200$ keV, which amounts up to $\approx 30\%$ of the total flux. In Cyg X-1 the total luminosity varies around $L = 0.1L_c$.

The changes in the spectrum as the luminosity of Cyg X-1 varies (Holt et al., 1975) exhibit the following characteristic behavior. As the total energy flux rises, the radiation in the soft part of the spectrum ($h\nu \leq 7$ keV) increases, but in the hard range ($h\nu \geq 10$ keV) it remains almost constant, or perhaps may even decrease slightly. We shall assume that the variations in the luminosity are associated with variations in the power of accretion. As the mass flow \dot{M} rises in the region with $P_r \gg P_g$ the fraction of the acoustic flow (165) used for heating of the corona decreases:

$$Q_{cor} = (P_g/P_r)Q_{ac} \sim \dot{M}^{-1}. \quad (167)$$

For $L \approx 0.1L_c$, when acoustic heating predominates, the rise in \dot{M} may cause some decrease in the heating of the corona and in the amount of hard radiation. At the same time the flux in the soft range is determined by the radiation of the disk photosphere and increases $\sim \dot{M}$. In strong bursts of luminosity, when L reaches about $0.3L_c$, the heating begins to be governed by radiation-pressure forces, so the temperature of the corona and thereby also the power of the hard radiation should increase along with the rise of \dot{M} and total energy flux. Similar explanation of spectral transitions in Cyg X-1 was considered by Poutanen et al. (1997).

Even if a corona with $T \approx 10^9$ K is present in the disk accretion model, radiation at $E_\gamma \geq 200$ keV cannot be produced, and more energetic electrons

are needed. Radiation with energies E_γ up to 5 MeV was observed by CRGO from Cyg X-1 (McConnell et al., 2000). It was noted by Bisnovatyi-Kogan and Blinnikov (1976), that explanation of hard X-ray and gamma radiation from Cyg X-1 would need a presence of a magnetic field in the accretion disk. Two ways to form very energetic electrons had been considered. Both required the presence of a magnetic field in the disk. A magnetic field could exist in the disk either through twisting of the lines of force by differential rotation (Shakura and Sunyaev, 1973), or through infall onto the black hole of magnetized material having a small angular momentum (Bisnovatyi-Kogan and Ruzmaikin, 1976). In the latter case a poloidal magnetic field would be generated.

In the binary system containing the source Cyg X-1, some of the material flowing from the giant star is dispersed in space near the system. The attraction of the black hole will not only produce an accretion disk. A small proportion of material having a low angular momentum will fall into the black hole and be decelerated in the disk. If this deceleration takes place at radii of $(10-30)r_g$ and if a thin collisionless shock wave is formed (as is very likely in the presence of an azimuthal magnetic field) wherein the kinetic energy is transformed into thermal energy and $T_e \approx T_i$, then hot electrons with $T = 10^{10} - 10^{12}$ K will appear. The inverse Compton mechanism of interaction of the disk radiation with these electrons can lead to the generation of hard radiation with $h\nu \approx 200 - 2000$ keV or even higher energies.

Another mechanism for producing fast particles is analogous to the pulsar process. If magnetized matter with low angular momentum falls into the black hole (in addition to the disk accretion), a strong poloidal magnetic field will arise (Bisnovatyi-Kogan and Ruzmaikin, 1976). By analogy to pulsars (Goldreich and Julian, 1969), rotation will generate an electric field of strength $E \approx -(v/c)B$ in which electrons are accelerated to energies $\varepsilon \approx R(v/c)Be \approx 3 \cdot 10^4 [B/(10^7 \text{ gauss})]$ Mev where $v/c \approx 0.1$ and $R \approx 10^7$ cm is the characteristic scale. In a field $B \approx 10^7$ gauss, such electrons will generate synchrotron radiation with energies up to $\approx 10^5$ keV. Just as in pulsars, it would be possible here for e^+e^- pairs to be formed and to participate in the synchrotron radiation.

3 Boundary layers between disks and rotating Stars

3.1 Boundary Layers

3.1.1 Structure of the boundary layer. Fitting with the disk solution

Inside the boundary layer (BL) variables change considerably over the small thickness of the layer $H_b \ll r_{in}$. Matter has no room to accelerate in radial direction, so the radial velocity term in (30) is negligible, but the pressure term is comparable with the gravitational and centrifugal forces (Regev, 1983;

Papaloizou and Stanley, 1986; Regev and Hougerat, 1988). The thickness H_b of the BL is smaller than its vertical size z_0 , which also remains small. The adopted inequalities for the boundary layer parameters

$$H_b \ll z_0 \ll r_* \quad (168)$$

will be confirmed by the results. The radius of the star r_* differs from the radius, at which $\frac{\partial\Omega}{\partial r} = 0$, by the very small value H_b . In the asymptotic consideration of the BL we use r_* as an inner boundary for the disk solution

$$r_{in} = r_* \quad (169)$$

The variable x

$$r = r_* + \delta x, \quad \delta = \frac{H_b}{r_*} \ll 1 \quad (170)$$

is used inside BL instead of r . The inner solution within BL is looked for in the region $0 < x < \infty$, while the outer solution (55)-(60) is valid in $r_* < r < \infty$. According to the method of matched asymptotic expansion (MAE) (see Nayfeh, 1973) the inner and outer solutions are fitted so that values for the outer solution at $r = r_*$ are equal to the corresponding values of the inner solution at $x = \infty$. This condition is valid asymptotically at $\delta \rightarrow 0$.

Consider a stationary accretion disk BL where equations (30), (52),(53) are valid with the integration constant ξ_b for ξ in (55). The thickness of the disk remains small in the boundary layer, so relations (41) -(47) for the polytropic case and (48)-(51) for the isothermal case are valid. Accounting only for the main terms in the asymptotic expansion inside BL, we get the equations from (30), (53) (Regev,1983)

$$\frac{dP_0}{dx} = -\Omega_{K*}^2 H_b \rho_0 (1 - \omega^2), \quad (171)$$

$$\frac{d\omega}{dx} = -\frac{\dot{M} H_b}{2\pi \Sigma \nu_b r_*^2} (\xi_b - \omega), \quad (172)$$

where

$$\omega = \frac{\Omega}{\Omega_{K*}}, \quad \Omega_{K*}^2 = \frac{GM}{r_*^3}. \quad (173)$$

The equation (171) was obtained from the exact equation of radial equilibrium (30), instead of the approximate equation averaged over the disk thickness, used originally by Regev (1983). In the MEA approximation these two equations are identical (Shorokhov, 2000), in the case of an advective disk the difference is essential, and the exact equation (30) should be used. The viscosity coefficient η is expressed in BL through the coefficient of kinematical viscosity ν_b

$$\eta = \rho_0 \nu_b. \quad (174)$$

While the radial extend of the BL H_b is much less then its vertical size z_0 the formula (29) cannot be used for a viscosity coefficient approximation. Inside BL we thus use the α approximation in the form

$$\nu_b = \alpha_b u_{s0} H_b. \quad (175)$$

3.1.2 Polytropic case

This case was investigated by Bisnovatyi-Kogan (1994). It is convenient to use the variables (Σ, ω) in the equations (171), (172). We get from (45) - (46)

$$\rho_0 = d_{\rho 0} \Sigma^{\frac{2n}{2n+1}}, \quad P_0 = d_{P0} \Sigma^{\frac{2(n+1)}{2n+1}}, \quad (176)$$

$$u_{s0} = d_{s0} \Sigma^{\frac{1}{2n+1}}, \quad (177)$$

$$d_{\rho 0} = \left[\frac{1}{\sqrt{2\pi}} \frac{\Gamma(n + \frac{3}{2})}{\Gamma(n+1)} \right]^{\frac{2n}{2n+1}} \left[\frac{GM}{r_*^3 K(n+1)} \right]^{\frac{n}{2n+1}}, \quad d_{P0} = K d_{\rho 0}^{\frac{n+1}{n}}, \quad (178)$$

$$d_{s0} = \left[\frac{n+1}{n} K \right]^{\frac{1}{2}} d_{\rho 0}^{\frac{1}{2n}} = \quad (179)$$

$$\left(\frac{n+1}{n} K \right)^{1/2} \left[\frac{1}{\sqrt{2\pi}} \frac{\Gamma(n + \frac{3}{2})}{\Gamma(n+1)} \right]^{\frac{1}{2n+1}} \left[\frac{GM}{r_*^3 K(n+1)} \right]^{\frac{1}{2(2n+1)}}.$$

Write for convenience the dimension of d_{s0}

$$[d_{s0}] = [v][\rho r]^{-\frac{1}{2n+1}}. \quad (180)$$

From the matching conditions in MAE we need to get Keplerian angular velocity $\Omega = \Omega_{K*}$, $\omega = 1$ from the inner solution at $x \rightarrow \infty$ in order to fit the outer solution (54) at the inner boundary $r = r_*$. This implies $\xi_b = 1$ for the constant in (172). We get after transition to the variable Σ in (171), (172)

$$\frac{d\Sigma}{dx} = -\frac{d_{\rho 0}}{d_{P0}} \frac{2n+1}{2(n+1)} \Omega_{K*}^2 H_b (1 - \omega^2) \Sigma^{\frac{2n-1}{2n+1}}, \quad (181)$$

$$\frac{d\omega}{dx} = -\frac{\dot{M}}{2\pi \alpha_b r_*^2 d_{s0}} (1 - \omega) \Sigma^{-2\frac{n+1}{2n+1}}. \quad (182)$$

Dividing (181) on (182) we get

$$D_b \frac{d\Sigma}{d\omega} = -(1 + \omega) \Sigma^{\frac{4n+1}{2n+1}} \quad (183)$$

with

$$D_b = -\frac{2(n+1)}{2n+1} \frac{d_{P0}}{d_{\rho 0} d_{s0}} \frac{\dot{M}}{2\pi\alpha_b H_b} \frac{1}{r_*^2 \Omega_{K*}^2}. \quad (184)$$

The solution of (183) which fit the boundary condition on the stellar surface $\Sigma = \Sigma_*$ at $\omega = \omega_*$. Taking into account, that the surface density rapidly grows inter the star we may put with sufficient accuracy $\Sigma_* = \infty$ and obtain the solution, using (179), (178) and (184) in the form

$$\Sigma = d_\Sigma \frac{\sqrt{K\Omega_{K*}^{\frac{1}{n}}}}{(\Omega_{K*} r_*)^{\frac{2n+1}{n}}} \left(-\frac{\dot{M}}{\alpha_b H_b} \right)^{\frac{2n+1}{2n}} \left[(\omega - \omega_*) \left(1 + \frac{\omega + \omega_*}{2} \right) \right]^{-\frac{2n+1}{2n}}, \quad (185)$$

where

$$d_\Sigma = \sqrt{n+1} n^{-\frac{2n+1}{4n}} (2\pi)^{-\frac{4n+3}{4n}} \left[\frac{\Gamma(n + \frac{3}{2})}{\Gamma(n+1)} \right]^{\frac{1}{2n}}. \quad (186)$$

For fitting the inner BL solution and the outer solution for the accretion disk we must make the surface densities (185) at $\omega = 1$ and (58) at $r = r_{in}$ equal. This fitting uniquely determines the outer integration constant ξ . After some algebraic calculations with account of (62),(186), we get

$$1 - \xi = d_n \alpha \alpha_b^{-\frac{2n+3}{2n}} \left(\frac{r_*}{H_b} \right)^{\frac{2n+3}{2n}} \left[-\frac{\dot{M} K^n}{r_*^2 (\Omega_{K*} r_*)^{2n+1}} \right]^{\frac{3}{2n}} [(1 - \omega_*)(3 + \omega_*)]^{-\frac{2n+3}{2n}}, \quad (187)$$

where

$$d_n = 2^{\frac{4n+3}{2n}} \sqrt{\pi} (2\pi)^{-\frac{2n+9}{4n}} n^{-\frac{4n+3}{4n}} (n+1)^{\frac{3}{2}} \left[\frac{\Gamma(n + \frac{3}{2})}{\Gamma(n+1)} \right]^{\frac{3}{2n}}. \quad (188)$$

The value of H_b is still not determined. It must be found from equation (182), where Σ is substituted from the solution (185). Before doing this we estimate by order of magnitude the values of $\frac{u_{s0}}{u_K}$ from (43) and $\frac{u_r}{u_K}$ from (53)

$$u_K = \Omega_K r, \quad \frac{u_{s0}}{u_K} \sim \frac{z_0}{r}, \quad \frac{u_r}{u_K} \sim \alpha \left(\frac{z_0}{r} \right)^2 \left(1 - \xi \sqrt{\frac{r_{in}}{r}} \right)^{-1}. \quad (189)$$

The equation (182) contains a nonphysical logarithmic divergency because of using the MAE method. For an approximate estimation of the value of H_b we use a characteristic thickness over which the ω variation happens, and for this, using the definition (170), the following relation may be written

$$-\frac{2\pi\alpha_b r_* d_{s0}}{\dot{M}} \Sigma^{2\frac{n+1}{2n+1}} |_{\omega=1} = 1. \quad (190)$$

With the help of (179),(185),(186) we get from (190)

$$\frac{H_b}{r_*} \approx d_H \alpha_b^{-\frac{1}{n+1}} \left[-\frac{\dot{M} K^n}{r_*^2 (\Omega_{K^*} r_*)^{2n+1}} \right]^{\frac{1}{n+1}} [(1 - \omega_*)(3 + \omega_*)]^{-1}, \quad (191)$$

$$d_H = 2(2\pi)^{-\frac{3}{2(n+1)}} n^{-\frac{2n+1}{2(n+1)}} (n+1)^{\frac{n}{n+1}} \left[\frac{\Gamma(n + \frac{3}{2})}{\Gamma(n+1)} \right]^{\frac{1}{n+1}}. \quad (192)$$

Using (191),(192) in (187) we finally get the expression for $(1 - \xi)$

$$1 - \xi \approx d_\xi \alpha_b^{-\frac{2n+3}{2(n+1)}} \left[-\frac{\dot{M} K^n}{r_*^2 (\Omega_{K^*} r_*)^{2n+1}} \right]^{\frac{1}{2(n+1)}}, \quad (193)$$

$$d_\xi = d_n d_H^{-\frac{2n+3}{2n}} = 2\sqrt{\pi} (2\pi)^{-\frac{2n+5}{4(n+1)}} n^{\frac{1}{4(n+1)}} (n+1)^{\frac{n}{2(n+1)}} \left[\frac{\Gamma(n + \frac{3}{2})}{\Gamma(n+1)} \right]^{\frac{1}{2(n+1)}}. \quad (194)$$

Estimating the values by order of magnitude, with account of (189) we get, combining (191) and (193)

$$(1 - \xi) \sim \frac{\alpha}{\alpha_b} \frac{z_0}{r}, \quad (195)$$

$$\frac{H_b}{r_*} \sim \frac{1}{1 - \omega_*} \left(\frac{z_0}{r} \right)^2. \quad (196)$$

Thus we get a complete analytical solution for the accretion disk structure with the boundary layer near the star for a viscosity inside the layer from (175) and a polytropic equation of state everywhere. Analytical solutions for an accretion disk with boundary layer for some simplifying assumptions about the viscosity coefficient and temperature distribution were obtained directly without expansions by Colpi et al.(1991) and Glatzel (1992). The MAE method, used by Regev (1983) for the solution of the accretion disk BL problem permits to obtain a self-consistent analytical solution for a disk with boundary layer for a viscosity coefficient in the usual α representation.

3.1.3 Isothermal case

For an isothermal disk with the same viscosity (175) we get, using (48) -(50), (171) and (172)

$$\frac{d\rho_0}{dP_0} = \frac{1}{K}, \quad \frac{d\Sigma}{dx} = -\frac{\Omega_{K^*}^2}{K} H_b \Sigma (1 - \omega^2), \quad (197)$$

$$\frac{d\omega}{dx} = -\frac{\dot{M}(1 - \omega)}{2\pi \alpha_b \sqrt{K} \Sigma r_*^2}. \quad (198)$$

Dividing the last two equations, and using the approximate boundary condition $\Sigma_* = \infty$, we get the solution (Shakura and Sunyaev, 1988)

$$\Sigma = \left(-\frac{\dot{M}\sqrt{K}}{2\pi\alpha_b H_p} \right) \frac{1}{r_*^2 \Omega_{K*}^2} \left[(\omega - \omega_*) \left(1 + \frac{\omega + \omega_*}{2} \right) \right]^{-1}. \quad (199)$$

From (190),(199),(198) we obtain the characteristic scale, which we identify with H_b

$$\frac{H_b}{r_*} \approx \frac{2K}{r_*^2 \Omega_{K*}^2} [(1 - \omega_*)(3 + \omega_*)]^{-1}. \quad (200)$$

Matching (66) and (199) with account of (200) like for plynrope, we get the expression for the integration constant

$$1 - \xi = \frac{\sqrt{2K}}{r_* \Omega_{K*}} \frac{\alpha}{\alpha_b}. \quad (201)$$

Comparing (200),(201) with (195), (196) we see that the order of magnitude estimates for the polytropic case become exact the for isothermal case apart a numerical coefficients close to unity.

In the isothermal case there is a simple solution of equation (198) when (199) is substituted for Σ ,

$$(1 - \omega)^{-2} (\omega - \omega_*)^{\frac{3+\omega_*}{1+\omega_*}} (2 + \omega + \omega_*)^{-\frac{1-\omega_*}{1+\omega_*}} = \exp \left[2 \frac{H_b}{K} \Omega_{K*}^2 x (1 - \omega_*) (3 + \omega_*) \right]. \quad (202)$$

We can see from (202) that the scale (200) is naturally appears under the exponent. It is clear that this solution makes physical sence only over this characteristic scale (thickness of BL) where $0 < x < r_*$. It is proved (Nayfet, 1973), that the region of applicability of the inner and outer solutions, obtained by MAE method, do overlap and the formula, constructed from the inner (i) and outer (e) solutions, gives a good interpolation also for the intermediate region. The formula, describing the function f in the whole region, has a structure

$$f = f_i + f_e - (f_i)_e. \quad (203)$$

Here $(f_i)_e$ is the value of the inner solution on the outer edge [equal to the value of the outer solution on the inner edge $(f_e)_i$]. The solution for $\Sigma(r)$ is constructed using $\Sigma^{(0)}(r)$ from the relation (45) for the outer solution, and the solution of the equation (181) with account of (170),(185),(186) for $\Sigma_i(r)$. The choice of ξ from (193) gives the equality $(\Sigma_i)_e = (\Sigma_e)_i$. The solution for $\Omega(r)$ is constructed using $\Omega_K(r)$ from (54) for the external, and the solution of (182), with account of (170), (173), (185), for the internal solution $\Omega_i(r)$. It is clear from the above consideration that $(\Omega_i)_e = (\Omega_e)_i = \Omega_{K*}$.

The existence of the overlapping regions, where both solutions (external and internal) are valid was first proved by Prandtl (1905, cited by Nayfet, 1973) for the problem of the boundary layer near the body in the flow of the rapidly moving viscous fluid, for which he had invented the MAE method. The interpolation formulae of the type (203) had been introduced by Vasil'eva (1959, cited by Nayfet, 1973), and is considered as a uniformly valid approximation in the whole region, due to existence of the overlapping regions. The direct proof of the validity of (203), for the cases where general analytic solutions exist, can be found in the books of Nayfet (1981) and Zwillinger (1992). These books, as well as Nayfet (1973), contain examples of the application of MAE method, including quasi-linear equations of the type (52), (53), and also references to many other applications of the MAE method and its detailed mathematical investigation.

Using the relation $\dot{M} = 2\pi r_* \Sigma u_r$ for the estimation of the radial velocity u_r in the boundary layer, we get, from (176)-(178), (185), (191) for polytropic [or from (199), (200) for isothermal] cases, the estimation

$$u_r/u_{s0} \sim \alpha_b. \quad (204)$$

This means that the solution obtained, where radial velocity was neglected, is valid only for sufficiently small viscosity, with $\alpha_b \ll 1$.

3.1.4 Boundary layers with account of thermal processes. Heat production in the boundary layer

Rapid braking of rotational velocity in the boundary layer during accretion into a slowly rotating star leads to strong heating and large energy release. It is expected, that matter in the boundary layer is hotter than in the disk, and is emitting radiation with a larger effective temperature. The equations of a heat balance in the boundary layer are different from the similar equations in the accretion disk (115), (116), (124). The component of the stress tensor should be written on the form (119) only, because in the boundary layer Ω deviates strongly from the keplerian value. The turbulent viscosity coefficient should be scaled by a smaller value of boundary layer thickness H_b , instead of the disk thickness h , like in (174), (175). Due to thinness of the boundary layer the radial heat flux inside it should be taken into account, and is usually more important than the losses through the sides of the disk Q_- in (124). From (124), (119), and using the momentum conservation equation (128), we obtain the expression for the viscous heat production rate in the half-thickness of the boundary layer per unit disk surface in the form

$$Q_+ = ht_{r\phi} r \frac{d\Omega}{dr} = h\eta \left(r \frac{d\Omega}{dr} \right)^2 \approx \frac{GM\dot{M}}{4\pi r_*^2} (\omega - 1) \frac{d\omega}{dr}. \quad (205)$$

Here, like in the previous section, we take in the boundary layer $\xi_b = 1$, $r = r_*$, $\omega = \Omega/\Omega_{K*}$. It is convenient in the boundary layer to define the value

$$Q_t = 4\pi r Q_+ \approx 4\pi r_* Q_+ = \frac{GM\dot{M}}{r_*}(\omega - 1)\frac{d\omega}{dr}, \quad (206)$$

determining the heat production by the viscosity in the whole ring of the boundary layer per unit of its radial thickness in the accretion disk. Let us consider the radiative heat conductivity along the radius as the main term in the heat balance of the boundary layer. Defining the radial heat flux through the optically thick boundary layer Φ as

$$\Phi = -\frac{4acT^3}{3\kappa\rho}\frac{dT}{dr}4\pi rh, \quad (207)$$

we write the heat balance equation as

$$\frac{d\Phi}{dr} = Q_t = \frac{GM\dot{M}}{r_*}(\omega - 1)\frac{d\omega}{dr}. \quad (208)$$

Integrating this equation, we obtain

$$\Phi = \frac{GM\dot{M}}{r_*} \left(\omega - \frac{\omega^2}{2} - \omega_A + \frac{\omega_A^2}{2} \right) = \frac{GM\dot{M}}{r_*}(\omega - \omega_A) \times \left(1 - \frac{\omega}{2} - \frac{\omega_A}{2} \right). \quad (209)$$

We consider here the layer at $\omega = \omega_A$, where the temperature has a maximum, so the radial flux is zero in this point, and had opposite direction at both sides of this layer. A position of this layer should be found from time-dependent evolutionary calculation of the boundary layer structure. If, for example, accretion is started into the cold neutron star, that the heating wave is started from the boundary layer, outside in the accretion disk, and inside the neutron star, heating it. In this case the level with $\omega = \omega_A$ is moving with time to the boundary of the star, and for larger times when the whole star becomes almost isothermal, this level coincides with the star boundary. If accretion is going on into the hot neutron star, the heat production in the boundary layer may be comparable with the heat flux from the star, which is equal to Φ_* on the star surface with $\omega = \omega_*$. Then we obtain instead of (209), the solution

$$\Phi = \Phi_* + \frac{GM\dot{M}}{r_*}(\omega - \omega_*) \times \left(1 - \frac{\omega}{2} - \frac{\omega_*}{2} \right). \quad (210)$$

It follows from (210), taking into account that the angular velocity is keplerian at the outer boundary of the boundary layer $\omega_{out} = 1$, that the total energy flux from the boundary layer due to heating by viscosity Q_{bl} is equal to (Popham and Narayan, 1995)

$$Q_{bl} = \frac{GM\dot{M}}{2r_*}(1 - \omega_*)^2. \quad (211)$$

The relation (211) may be obtained also from the conservation laws. When a mass dm crosses the boundary layer the change of its energy is

$$dE_m = \frac{1}{2}dm\Omega_{K*}^2 r_*^2 (1 - \omega_*^2). \quad (212)$$

From the angular momentum conservation law the angular momentum lost by the accreting matter

$$dJ_m = dm\Omega_{K*} r_*^2 (1 - \omega_*) \quad (213)$$

is absorbed by the star, so that

$$dJ_* = I_* \Omega_{K*} d\omega_* = dJ_m. \quad (214)$$

Obtaining from two last equations $I_* d\omega_* = dm r_*^2 (1 - \omega_*)$, we obtain the kinetic energy absorbed by the star in the form

$$dE_* = I_* \Omega_{K*}^2 \omega_* d\omega_* = dm \Omega_{K*}^2 r_*^2 \omega_* (1 - \omega_*). \quad (215)$$

The heat produced in the boundary layer is defined as

$$dE_{bl} = dE_m - dE_* = \frac{1}{2}dm\Omega_{K*}^2 r_*^2 (1 - \omega_*)^2, \quad (216)$$

what gives (211) with account of

$$Q_{bl} = \frac{dE_{bl}}{dt}, \quad \dot{M} = \frac{dm}{dt}, \quad \Omega_{K*}^2 = \frac{GM}{r_*^3}. \quad (217)$$

3.1.5 Explicit models of the accretion disk with a boundary layer

Set of equations, describing stationary accretion disk together with a boundary layer was solved numerically by several authors. The equations of radial and azimuthal motion, and continuity equation coincide with the corresponding equations of the advective disk structure (117), (71) with Ω - derivative description of the viscosity, and a continuity equation (120). Contrary to the advective disk structure at accretion into a black hole with a transonic radial motion, the accretion disk around a star with a boundary layer has always a subsonic radial velocity (204), with a Mach number $\sim \alpha_b$, where α_b is characterizing the viscosity in the boundary layer (174),(175). The viscosity coefficient describing continuously the disk and boundary layer should include a transition from the thickness scale h in the disk to the smaller value of the boundary layer thickness H_b in the layer itself. The expression having these properties was used by Popham and Narayan (1995)

$$\nu = \frac{2}{3} \left[\frac{1}{(\alpha h)^2} + \frac{(2 dP_0/dr)^2}{(3\alpha_b P_0)^2} \right]^{-1/2}. \quad (218)$$

The coefficient $(\frac{2}{3})$ is included 2 times into (218) to make a continuous transition to the (127) in the disk where $h \ll H_b = \frac{P_0}{dP_0/dr}$, and to (175) in the boundary layer where $h \gg H_b$. The equation of a thermal balance should include the radiative heat transfer Φ in radial direction from (207), which exceeds all other cooling sources inside the boundary layer. Taking Q_+ and Q_- from (124), advective heating Q_{adv} from (115), and Φ from (207), we obtain the equation of the heat balance valid in the whole disk, including boundary layer

$$Q_+ = Q_- + Q_{adv} + \frac{1}{4\pi r} \frac{d\Phi}{dr}, \quad (219)$$

which may be written as

$$\dot{M} T \frac{dS}{dr} = \frac{d\Phi}{dr} + \dot{M}(j - j_{in}) \frac{d\Omega}{dr} + \frac{2aT^4 c}{3\kappa \rho h} 4\pi r. \quad (220)$$

The thickness of the disk h is everywhere determined by vertical equilibrium equation (70). Popham and Narayan (1995) used a bit more complicated equations of a heat transfer. Instead of Q_- and Φ from above they considered expressions following from simplified solution of the radiative transfer equation permitting to distinguish between absorption and scattering opacities, similar to the description in Section 1.6, which is valid also in the optically thin case. The equation of state $P = P_g + P_r$ takes into account deviations of the radiation pressure P_r from the equilibrium value, similar to (108).

The boundary conditions used by Popham and Narayan (1995) required angular velocity to be equal to the stellar one Ω_* at the inner boundary at stellar radius r_* , and to the keplerian angular velocity at the outer boundary, specified at $R_{out} = 100R_*$. The boundary conditions for the vertical heat flux had been equivalent to the Q_- energy losses from (124). The radial heat flux from the star $\Phi_* > 0$ was specified on its surface, what is equivalent to the situation described by (210).

Calculations have been performed for cataclismic binaries where a disk accretion goes onto a white dwarf star. Other similar calculations (Popham et al., 1996; Collins et al., 1998) considered white dwarfs or pre-main-sequence stars. Boundary layers in the accretion disks around a neutron star had not been considered in explicit calculations, and had been treated either analytically, or by MAE method (Regev, 1983). Calculations of Popham and Narayan (1995) revealed the existence of a dynamical boundary layer, where there is a rapid drop of the angular velocity and of a velocity of the radial motion, inside the thermal boundary layer. There is a strong radial acceleration of matter when the flow approaches the dynamical boundary layer, and the density is rapidly increasing inside this layer. The heat flux from the boundary layer is propagating radially into the accretion disk and is radiated vertically on the scale of the order of the disk thickness.

Time-dependent calculations for accretion disks with boundary layers around pre-main-sequence stars had been performed in 1-D approximation by Godon

(1996a,b), using nonflux thermal boundary condition $dT/dr = 0$ at $r = r_*$, what is corresponding to $\Phi_* = 0$ in (210). The results of 1-D calculations are qualitatively in accordance with the stationary model of Popham and Narayan (1995). The thermal boundary condition used above does not take into account a possible important heat flux from or inside the star. It seems more consistent to use the thermal boundary condition in the following simplified form

$$\frac{dT_*}{dt} = -\frac{\Phi_*}{C_*}, \quad (221)$$

where C_* is the corresponding heat capacity of a star, and Φ_* is a heat flux on the star boundary from (207), which may be positive or negative, depending on the temperature T_* . In the case of a neutron star or a white dwarf the heat capacity C_* may be estimated from the existing models of their structure, and the heat capacity of the isothermal star could be considered as a rough approximation.

Time-dependent 2-D model had been calculated by Kley (1991). These calculations show oscillations in time of luminosity which amplitude depends on the choice of input parameters. These oscillations could be connected with instabilities, but numerical effects are also cannot be excluded.

3.1.6 Models of accretion disk with a boundary layer constructed by MAE method

Matched asymptotic expansion (MAE) method was used for description of boundary layers in hydrodynamics (Prandtl, 1905), and was first applied for accretion disks by Regev (1983). The structure of the accretion disk and boundary layer with a polytropic equation of state is solved analytically by MAE method (Bisnovatyi-Kogan, 1994), and is described in Section 3.1. Account of thermal processes with the equation of state $P(\rho, T)$ makes the problem more complicated, and analytic solution was not obtained. The equilibrium equations describing the outer solution for the disk may be taken from the standard model without advection with $\Omega = \Omega_K$, valid until the inner boundary of the outer solution at $r = r_*$. Contrary to the standard model, where the integration constant j_{in} was taken as $j_{\text{in}} = \xi \Omega_{K*} r_*^2$ with $\xi = 1$, in the outer MAE solution for the disk the constant ξ is slightly less than unity, and should be found from matching of the inner and outer solutions, like in the polytropic case (see Section 3.1.2).

The thermal equations in the disk may be taken in the form (220), where advective term may be neglected, and (207). The term with Φ in this equation should take into account the heat flux coming from the boundary layer into the accretion disk, which is given by the boundary value $\Phi(r_*) = \Phi_{bl}$. The constant Φ_{bl} should be found from the matching to the inner solution. The second boundary condition for solving two differential equations (220), (207) determines approach of the solution at large r to the standard one with a very

small $\Phi(r)$. It is possible to write the thermal balance equation in the disk in a more simple way. It is evident from the physical model, and also is confirmed by calculations of Popham and Narayan (1995), that the heat flux from the boundary layer Φ_{bl} coming into the disk is radiated from the disk on the scale of the order of the disk thickness h_* near the boundary layer. Instead of solving the differential equation, we may model the radiation flux from the boundary layer by an additional heating term, which is distributed over the distance h_* from the inner boundary by the following profiling

$$\frac{d\Phi}{dr} \approx \frac{\Phi_{bl}}{h_*} \exp\left(-\frac{r-r_*}{h_*}\right). \quad (222)$$

Integration of (222) over the radius between r_* and ∞ gives the additional energy emitted by the disk due to the heat flux from the boundary layer equal to Φ_{bl} , and this flux is emitted in the region $\delta r \sim h_*$, attaching the boundary layer. In this description there is one additional matching condition defining Φ_{bl} , in comparison with the polytropic case.

To obtain the inner MAE solution we should solve the equilibrium equations (171) and (172) together with the equations of the heat production and heat transfer. The constant $\xi_b = 1$ here, like in the polytropic case from the matching condition for $\omega = 1$ at $x = \infty$, equal to the inner keplerian value of the outer solution. Matching the densities of the inner and outer solutions determines the integration constant ξ of the outer solution. Application of MAE to the solution of the boundary layer with thermal processes meets with a definite problem. Using (209) in (207), we write the equation of a heat transfer in the boundary layer in a form

$$\Phi = -4\pi r h \frac{4acT^3}{3\kappa\rho} \frac{dT}{dr} = \frac{GM\dot{M}}{2r_*} [(1-\omega_A)^2 - (1-\omega)^2]. \quad (223)$$

It follows from (223) that the heat flux in the boundary layer consists of the constant value Φ_0 in the first term to the left, and variable part $\sim (1-\omega)^2$. Existence of the constant flux leads to non-physical behaviour of the temperature at large x in MAE method, leading to unrestricted fall of the temperature. Therefore, in the papers of Regev (1983), Regev and Bertout (1995) the solution was obtained at $\Phi_0 = 0$, what determines that all heat produced in the boundary layer heats the star and does not go into the accretion disk, what is opposite to the condition used by Popham and Narayan (1995). As was mentioned above, the maximum of temperature may correspond to the intermediate level in the boundary layer, and heat flux from it may heat simultaneously the star and the boundary layer. In the direct calculations it corresponds to changing of boundary condition, but was not realized. In MAE method solution cannot be obtained directly at non-zero Φ_0 . Additional modification of MAE method are needed for its account.

Note, that large deviations of the ξ value from unity, $\xi=0.61$, obtained by Regev (1983) for $\omega_* = 0.3$, could indicate the step into the region, where the asymptotic expansion begins to be violated. When the stellar angular velocity approaches a critical value, the boundary layer becomes thick (see (191) and the MAE method fails.

3.2 Accretion Disks Around Rapidly Rotating Stars

Investigations of low-mass-X-ray binaries (LMXB) containing a neutron star have lead to the conclusion that the accreting object can rotate rapidly with a surface angular velocity close to Keplerian value. The question of accretion onto a rapidly rotating star also arises in cataclysmic variables, in which the primary is a white dwarf. When the stellar angular velocity reaches its critical value the maximum of the angular velocity and the boundary layer disappear, and a regime of accretion is changing. Disk accretion into a rapidly rotating star, with the Keplerian angular velocity at the equator, had been investigated by Popham and Narayan (1991), Paczynski (1991), Colpi et al. (1991). Self-consistent regime was found by Bisnovatyi-Kogan (1993a), in which star remains to rotate rapidly during the accretion process.

3.2.1 Self-consistent model

When a star reaches the critical rotation rate for which the the surface angular velocity becomes Keplerian, the flux of angular momentum into the star leads to differential rotation inside the star. It is clear that disk properties far away from the star do not change when the star reaches the critical rotation rate, so that the disk remains Keplerian. The properties of the intermediate zone between the star and the disk are determined by the stellar rotational velocity law, but we do not need to know exactly the properties of this transition zone in order to build a self-consistent model. We only have to know that during accretion onto a rapidly rotating star, the transition layer is smooth, all values are monotonous and there is no enhanced heat production in this layer, in contrast to the case of boundary layers between the accretion disk and a slowly rotating star.

The evolution of the star under mass accretion may be characterized by the variations of two values: the mass M and the total angular momentum J and by one function, $j(r)$, determining the angular momentum distribution within the star; $j(r)$ is determined by the viscosity law inside the star. For a given mass flux \dot{M} , determined by conditions far away from the star, the star gradually increase its mass and angular momentum. When the stellar rotation rate is much smaller than the Keplerian limit the specific angular momentum of matter accreting onto the star is approximately equal to $\dot{M}v_{Ke}R_{se}$, ($v_K = (GM/r^3)^{1/2}$ is the Keplerian velocity, R_{se} - the stellar equatorial radius, index "e" refers to values at the stellar equator). When the stellar rotational velocity at the surface is smaller than the Keplerian value, the angular velocity of the disk has

a maximum near R_{se} ; at this point, the viscous flux is zero and the momentum flux is determined only by the convective term $\dot{M}j_e$, $j = v_\phi r$. The maximum of the rotational velocity disappears, when the star rotation is close to the critical velocity and the (negative) viscous momentum flux becomes important.

The demand of self-consistency during accretion onto a rapidly rotating star may be formulated as the condition that **the star absorb the accreted matter with a specific angular momentum such that the star remains in the state of critical rotation**. Depending on the viscosity law, a critically rotating star may have different distributions $j(r)$ and in general, the structure of the star gradually changes with time. If viscosity inside the star is high, the star rotates almost rigidly; this case has been considered in the above mentioned papers. If the star-disc system can be described by a polytropic equation of state, there is a self-similar solution for such a system which does not depend on mass.

3.2.2 Self-similar solution for a polytropic star-disc system in the case of a rigidly rotating star

The equations describing the structure of a rotating star with a polytropic equation of state (41) the equilibrium equations in spherical coordinates are (Chandrasekhar 1989)

$$\frac{1}{\rho} \frac{\partial P}{\partial r} + \frac{\partial \Phi}{\partial r} - \Omega^2 r (1 - \mu^2) = 0 \quad (224)$$

$$\frac{1}{\rho} \frac{\partial P}{\partial \mu} + \frac{\partial \Phi}{\partial \mu} + \Omega^2 r^2 \mu = 0 \quad (225)$$

and the equation for the gravitational potential Φ is

$$\frac{1}{r^2} \frac{\partial}{\partial r} \left(r^2 \frac{\partial \Phi}{\partial r} \right) + \frac{1}{r^2} \frac{\partial}{\partial \mu} \left((1 - \mu^2) \frac{\partial \Phi}{\partial \mu} \right) = 4\pi G \rho \quad (226)$$

Here $\mu = \cos \theta$ and Ω is the angular velocity of the stellar matter. In general Ω is not constant throughout the star, and for a polytropic star in equilibrium depends only on the cylindrical radius $r \sin \theta$. Excluding Φ from Eqs.(2)-(4), we get

$$\begin{aligned} \frac{1}{r^2} \frac{\partial}{\partial r} \left(\frac{r^2}{\rho} \frac{\partial P}{\partial r} \right) + \frac{1}{r^2} \frac{\partial}{\partial \mu} \left(\frac{1 - \mu^2}{\rho} \frac{\partial P}{\partial \mu} \right) + \\ 4\pi G \rho - \frac{1}{x} \frac{d}{dx} (x^2 \Omega^2) = 0 \end{aligned} \quad (227)$$

where $x = r \sin \theta = r \sqrt{1 - \mu^2}$, $\Omega = \Omega(x)$. Introduce the nondimensional polytropic variables

$$\xi = r/r_*, \quad \Theta^n = \rho/\rho_c, \quad \omega = \Omega/\Omega_*, \quad (228)$$

where ρ_c is the central density of the star and r_* and Ω_* are given by

$$r_* = \left(\frac{(n+1)K\rho_c^{\frac{1}{n}-1}}{4\pi G} \right)^{1/2}, \quad \Omega_* = \sqrt{2\pi G\rho_c} \quad (229)$$

In the nondimensional variables (6)-(7) Eq.(5) for $\Omega = \text{const.}$ can be written in the form

$$\frac{1}{\xi^2} \frac{\partial}{\partial \xi} \left(\xi^2 \frac{\partial \Theta}{\partial \xi} \right) + \frac{1}{\xi^2} \frac{\partial}{\partial \mu} \left((1-\mu^2) \frac{\partial \Theta}{\partial \mu} \right) + \Theta^n - \omega^2 = 0 \quad (230)$$

The solution of Eq.(8) is uniquely determined by the boundary conditions

$$\begin{aligned} \Theta = 1, \quad \frac{\partial \Theta}{\partial \xi} = 0 \quad \text{at} \quad \xi = 0, \\ \sqrt{1-\mu^2} \frac{\partial \Theta}{\partial \mu} = 0 \quad \text{at} \quad \mu = 0, \quad \mu = \pm 1, \end{aligned} \quad (231)$$

and by the value of ω ; one also requires that the solution must satisfy the original equilibrium Eqs.(2),(3). The latter condition results from the fact that Eqs.(2) and (3) were differentiated in order to obtain (8), so that a solutions of (8) need not satisfy (2),(3). It is in fact necessary to find a gravitational potential Φ from (4) which, when written in nondimensional form $\phi = \Phi/4\pi G\rho_c r_*^2$ satisfies the scaling conditions of the self-similar solution. For compressible matter with $n > 0$ a solution exists only if $\omega < \omega_c$; for $\omega = \omega_c$ the centrifugal force on the equatorial boundary of the star exactly balances gravity (see the proof in Bisnovaty-Kogan & Blinnikov 1981). Numerical calculations have been done, which gave the structure of rotating polytropic stars for different ω up to the critical value ω_c (James 1964; Blinnikov 1975; Ipser & Monagan 1981; see also Tassoul 1978).

For a given n the structure of a critically rotating star does not depend on its mass. By definition, the mass M and the total angular momentum J are given by

$$M = 2\pi\rho_c r_*^3 \int_{-1}^1 d\mu \int_0^{\xi_{\text{out}}(\mu)} \Theta^n(\xi, \mu) \xi^2 d\xi, \quad (232)$$

$$J = 2\pi\rho_c r_*^5 \omega \sqrt{2\pi G\rho_c} \int_{-1}^1 (1-\mu^2) d\mu \int_0^{\xi_{\text{out}}(\mu)} \Theta^n(\xi, \mu) \xi^4 d\xi. \quad (233)$$

Introducing nondimensional values of the mass \mathcal{M}_n and of the total angular momentum \mathcal{J}_n , defined as

$$\mathcal{M}_n = \frac{1}{2} \int_{-1}^1 d\mu \int_0^{\xi_{\text{out}}(\mu)} \Theta^n(\xi, \mu) \xi^2 d\xi, \quad (234)$$

$$\mathcal{J}_n = \frac{\omega}{2} \int_{-1}^1 (1 - \mu^2) d\mu \int_0^{\xi_{\text{out}}(\mu)} \Theta^n(\xi, \mu) \xi^4 d\xi \quad (235)$$

M and J may be written as

$$M = 4\pi\rho_c r_*^3 \mathcal{M}_n, \quad (236)$$

$$J = 4\pi\rho_c r_*^5 \sqrt{2\pi G \rho_c} \mathcal{J}_n. \quad (237)$$

The average specific angular momentum of the star j_s and the derivative along the critical states $j_a = (dJ/dM)_c$ are written, using (7),(14), as

$$j_s = J/M = r_*^2 \sqrt{2\pi G \rho_c} \mathcal{J}_n / \mathcal{M}_n \quad j_a = \frac{5-2n}{3-n} j_s. \quad (238)$$

Using (14) one may write ρ_c and r_* , which appear in (7), as a function of M

$$\rho_c = \left(\frac{4\pi G}{(n+1)K} \right)^{\frac{3n}{3-n}} \left(\frac{M}{4\pi \mathcal{M}_n} \right)^{\frac{2n}{3-n}}, \quad r_* = \left(\frac{4\pi G}{(n+1)K} \right)^{\frac{n}{n-3}} \left(\frac{M}{4\pi \mathcal{M}_n} \right)^{\frac{1-n}{3-n}}. \quad (239)$$

The specific angular momentum of matter j_e at the stellar equator r_e may be written as

$$j_e = \Omega r_e^2 = r_*^2 \sqrt{2\pi G \rho_c} \xi_e^2 \omega, \quad \xi_e = r_e / r_* = \xi_{\text{out}}(\pi/2). \quad (240)$$

From a comparison of (16) and (18), it follows that the ratio

$$\frac{j_a}{j_e} = \frac{5-2n}{3-n} \frac{j_s}{j_e} = \frac{5-2n}{3-n} \frac{\mathcal{J}_n}{\mathcal{M}_n \xi_e^2 \omega} \quad (241)$$

does not depend on the stellar mass M , and is a function of n and ω only. The nondimensional values of the angular velocity ω_c , the equatorial radius $\xi_{\text{out}}(\theta = \pi/2) = \xi_e$, the mass \mathcal{M}_n , the momentum of inertia around the rotational axis $\mathcal{I}_n = \mathcal{J}_n / \omega_c$, the average specific angular momentum of the star ζ_s , the nondimensional derivative ζ_a

$$\zeta_s = j_s / (r_*^2 \sqrt{2\pi G \rho_c}) = \mathcal{J}_n / \mathcal{M}_n, \quad \zeta_a = \frac{5-2n}{3-n} \zeta_s, \quad (242)$$

and the angular momentum of matter on the stellar equator

$$\zeta_e = j_e / (r_*^2 \sqrt{2\pi G \rho_c}) = \xi_e^2 \omega_c \quad (243)$$

for several polytropic indices n in the state of critical rotation are given in table 1, which is based on calculations of James(1964), Blinnikov(1975) and Ipser and Managan(1981). The ratio of the equatorial and polar radii ξ_e / ξ_p and the nondimensional parameters for nonrotating polytropes (outer radius ξ_{0n} , mass \mathcal{M}_{0n} and momentum of inertia around the symmetry axis \mathcal{I}_{0n} , Chandrasekhar

Table 1: Parameters of non-rotating and critically rotating polytropic stars

n	ξ_{n0}	\mathcal{M}_{n0}	\mathcal{I}_{n0}	ω_c	ξ_e	$\frac{\xi_e}{\xi_p}$	\mathcal{M}_n	\mathcal{I}_n	ζ_s	$\frac{\zeta_a}{\zeta_e} = \beta$
0.5	2.7528	3.7871		0.389 (0.367)		2.51				
0.6				0.362 (0.354)		2.29				
0.808				0.326	4.7652	1.917	5.0248	24.43	1.585	0.3304
1.0	π	π	8.104	0.289	4.8265	1.792	4.289	18.73	1.262	0.2805
1.5	3.65375	2.71406	7.413	0.209	5.36	1.626	3.2138	12.18	0.792	0.176
2.0	4.35287	2.41105	7.074	0.147	6.307	1.555	2.6518	9.62	0.533	0.0894
2.5	5.35528	2.18720	7.013	0.09965	7.7623	1.522	2.30563	8.49	0.367	0.0
3.0	6.89685	2.01824	7.234	0.0639	10.123	1.535	2.0743	8.125	0.250	$-\infty$

1957; James 1964; Blinnikov 1975) are also given.

In nondimensional variables it is obvious that the derivative ζ_a of the angular momentum of the star along the sequence of critically rotating states is always smaller than the equatorial value ζ_e ; ζ_e is equal to the Keplerian value of a critically rotating non-spherical star. The viscous flux of specific angular momentum in the accretion disk around a critically rotating star j_v is therefore negative; near the surface of the star j_v is equal to

$$j_v = j_a - j_e \quad (244)$$

as one requires that the total angular momentum flux into the star is equal to $\dot{M}j_a$ for self-consistency. In the self-consistent model of accretion disk around the rapidly rotating polytropic star the value of the constant ξ in the formulae of the Section 1.4 should be taken equal to ζ_a from the Table 1.

3.2.3 General (nonpolytropic) case of disc accretion into a rapidly rotating star

In realistic cases, thermal processes are very important in the disc, polytropic approximation is not good, and equations of the thermal balance from Section 1.5 should be taken into account. Transition to the rapidly rotating star is accompanied by a substantial change of the integration constant in (71), (ref1.11), what leads to important observational consequences.

The total luminosity of the accretion disc is equal to

$$L = \int_{r_i}^{\infty} 4\pi F r dr = \left(\frac{3}{2} - \beta\right) \dot{M} \frac{GM}{r_i}. \quad (245)$$

When $\beta = 1$ the star accretes matter with Keplerian angular momentum, and only half of the gravitational energy of the accreted matter is radiated from the disc, according to the virial theorem. The fate of the remaining half is different. In the case of a black hole, it is absorbed, increasing the mass and angular

momentum of the black hole without any significant radiation; however matter falling from the last stable orbit to the horizon still emits radiation (Bisnovaty-Kogan & Ruzmaikin 1974).

In the case of accretion onto a (slowly rotating) neutron star there are several possibilities. If the radius of the neutron star r_s is smaller than $3r_g$, then $r_i = 3r_g$; the disk luminosity is the same as in the case of a black hole, and the remaining gravitational energy, including the part gained during free fall onto the neutron star surface, is emitted close to the neutron star surface. If $r_s > 3r_g$, then $r_i = r_s$, the disc luminosity is $GM\dot{M}/2r_s$ and an equal amount of energy is emitted in the boundary layer near the stellar surface, where the accreting matter converts its kinetic energy into heat.

The situation changes gradually while the central object absorbs angular momentum. The black hole moves from Schwarzschild to extreme Kerr solution; the radius of the last stable orbit decreases from $3r_g$ to r_g , and the radius of the horizon changes from r_g to $r_g/2$. The efficiency of the disc energy emission increases from 5.7% to 42% (Novikov & Thorne 1973). The changes go in an opposite direction when a neutron star accelerates its rotation. Let us consider only the case $r_s > 3r_g$. The luminosity of the disc decreases because the stellar radius increases. The fraction of energy emitted by the neutron star also decreases. It changes from $GM\dot{M}/2r_s$ in the case of a nonrotating star to the difference between rotational energy of matter in the disc and at the stellar surface.

A rapid change in the efficiency of energy release and disc luminosity happens when the star rotation reaches its maximum value. The energy emitted near the stellar surface tends towards zero, but the luminosity of the disc suffers a drastic change. The star does not absorb any longer all of the angular momentum coming from the disc, but absorbs only the fraction required to maintain the star in a critically rotating state. The specific angular momentum of matter accreted by the star is equal to $(dJ/dM)_c$ and the remaining part is carried away in the disc by viscous stresses (see sec.2). Viscosity carries not only angular momentum, but also energy, so that the energy production and luminosity of the disk rapidly increase, from the value corresponding to $\beta = 1$ to the value corresponding to $\beta = j_a/j_e$ according to (245); for polytropic stars the values of β are given in the last column of table 1. This implies a rapid increase of the total luminosity by a factor $2 \div 3$, depending on the stellar structure. This rapid increase is easy to understand if one remembers that when a star accelerates its rotation, part of the gravitational energy is converted into rotational energy without heat production. When a star reaches the limiting rotation, the growth rate of its rotational energy strongly diminishes and a correspondingly larger fraction of gravitational energy is transformed into heat. The minimum of luminosity of an accreting neutron star is reached when the stellar angular velocity is slightly below the critical value. A rapid increase in luminosity must be accompanied by a corresponding hardening of the emitted spectrum because the energy release is increased, raising the effective temperature in the inner part

of the disc. Such events may be expected in objects like LMXB or cataclysmic variables. The young T Tauri stars are born rapidly rotating, so their value of β is small from the beginning and close to that of a polytrope $n = 1.5$ with $\beta = 0.176$ given by Table 1. Note, that whereas the standart solution of accretion disk (Shakura, 1972; Shakura and Sunyaev, 1973; Novikov and Thorne, 1973) is not valid in regions close to the inner edge in the case of a black hole (see Paczyński & Bisnovaty-Kogan 1981), the self-consistent solution for accretion onto a rapidly rotating star, may be used down to the very stellar radius, which is the inner edge of the disc.

4 Accretion flows in presence of magnetic fields

4.1 Magnetic Field Amplification in Quasi-Spherical Accretion

Matter flowing into a black hole from a companion star or from the interstellar medium is very likely to be magnetized. Due to the more rapid increase of a magnetic energy in comparison with any other kind of energy, the dynamical and any other role of the magnetic field is becoming more and more important when matter flows inside. Schwartzman (1971) was the first to emphasize the importance of the magnetic field for an energy release during accretion into a black hole. He showed that due to more rapid growth of magnetic energy its density E_M approaches a density of a kinetic energy E_k , and proposed a hypothesis of *equipartition* $E_M \approx E_k$, supported by continuous annihilation of the magnetic field, for the smaller radiuses of the flow where the main energy production happens. This hypothesis is usually accepted in the modern picture of accretion (see e.g Narayan and Yu, 1994). Schwartzman (1971) considered an averaged quasistationary picture with local equipartition, another variant of magnetic accretion, where equipartition and magnetic field annihilation is accompanied by formation of shock waves was considered by Bisnovaty-Kogan and Sunyaev (1972), see also Chang and Ostriker (1985). More accurate account of the heating of matter by magnetic field annihilation was done by Bisnovaty-Kogan and Ruzmaikin (1974), where exact nonstationary solution for a field amplification in the radial accretion flow was also obtained.

Consider the general problem of the field amplification in the accretion flow where gas has an angular momentum and field annihilation is approximated by a finite “turbulent” conductivity. This approach should reproduce a smooth averaged flow, considered by Schwartzman. In the known stationary velocity field $\mathbf{v}(r, \theta)$ the magnetic field \mathbf{B} is described by Maxwell equations in the MHD approximation (without the displacement current), with a finite conductivity

$$\nabla \times \mathbf{B} = \frac{4\pi}{c} \mathbf{j}, \quad \nabla \times \mathbf{E} = -\frac{1}{c} \frac{\partial \mathbf{B}}{\partial t}, \quad \nabla \cdot \mathbf{B} = 0,$$

$$\mathbf{j} = \sigma \left(\mathbf{E} + \frac{1}{c} \mathbf{v} \times \mathbf{B} \right), \quad (246)$$

where σ is the plasma conductivity, \mathbf{j} is the electrical current density, and \mathbf{E} is the electrical field strength. Consider an axisymmetrical picture in a spherical coordinate system r, θ, ϕ where all ϕ derivative are zero, but all vectors $\mathbf{v}, \mathbf{B}, \mathbf{E}, \mathbf{j}$ may have nonzero all three components. The equation containing only magnetic field, following from (246)

$$\frac{\partial \mathbf{B}}{\partial t} = \nabla \times [\mathbf{v} \times \mathbf{B}] + \frac{c^2}{4\pi\sigma} \nabla^2 \mathbf{B}. \quad (247)$$

These equations are completed by the condition of zero divergence of the magnetic field, which for the choosen case has a view

$$\frac{1}{r^2} \frac{\partial}{\partial r} (r^2 B_r) + \frac{1}{r \sin \theta} \frac{\partial}{\partial \theta} (\sin \theta B_\theta) = 0. \quad (248)$$

4.1.1 Time-dependent amplification of a Magnetic field in Spherical Accretion

For a spherical accretion with $\mathbf{v} = (v_r, 0, 0)$ the equation (247) reduces to

$$\frac{\partial B_r}{\partial t} = \frac{1}{r \sin \theta} \frac{\partial}{\partial \theta} (\sin \theta v_r B_\theta) + \frac{c^2}{4\pi\sigma} \quad (249)$$

$$\times \left[\frac{1}{r^2} \frac{\partial}{\partial r} \left(r^2 \frac{\partial B_r}{\partial r} \right) + \frac{1}{r^2 \sin \theta} \frac{\partial}{\partial \theta} \left(\sin \theta \frac{\partial B_r}{\partial \theta} \right) - \frac{2B_r}{r^2} - \frac{2}{r^2 \sin \theta} \frac{\partial}{\partial \theta} (\sin \theta B_\theta) \right],$$

$$\frac{\partial B_\theta}{\partial t} = -\frac{1}{r} \frac{\partial}{\partial r} (r v_r B_\theta) \quad (250)$$

$$+ \frac{c^2}{4\pi\sigma} \left[\frac{1}{r^2} \frac{\partial}{\partial r} \left(r^2 \frac{\partial B_\theta}{\partial r} \right) + \frac{1}{r^2 \sin \theta} \frac{\partial}{\partial \theta} \left(\sin \theta \frac{\partial B_\theta}{\partial \theta} \right) - \frac{B_\theta}{r^2 \sin^2 \theta} + \frac{2}{r^2} \frac{\partial B_r}{\partial \theta} \right],$$

$$\frac{\partial B_\phi}{\partial t} = -\frac{1}{r} \frac{\partial}{\partial r} (r v_r B_\phi) \quad (251)$$

$$+ \frac{c^2}{4\pi\sigma} \left[\frac{1}{r^2} \frac{\partial}{\partial r} \left(r^2 \frac{\partial B_\phi}{\partial r} \right) + \frac{1}{r^2 \sin \theta} \frac{\partial}{\partial \theta} \left(\sin \theta \frac{\partial B_\phi}{\partial \theta} \right) - \frac{B_\phi}{r^2 \sin^2 \theta} \right].$$

For initial nonstationary stage of the field amplification, when field dissipation is negligible, analytical solution may be obtained (Bisnovatyi-Kogan & Ruzmaikin, 1974). From (249) with account of (248), and from (250),(251) we get

$$\frac{d(r^2 B_r)}{dt} = 0, \quad \frac{d(r v_r B_\theta)}{dt} = 0, \quad \frac{d(r v_r B_\phi)}{dt} = 0, \quad (252)$$

where the full Lagrangian derivative is determined as

$$\frac{d}{dt} = \frac{\partial}{\partial t} + v_r \frac{\partial}{\partial r}. \quad (253)$$

A solution of (252)- (253) is determined by 4 first integrals of the characteristic equations

$$C_1 = t - \int \frac{dr}{v_r}, \quad C_2 = r^2 B_r, \quad C_3 = r v_r B_\theta, \quad C_4 = r v_r B_\phi. \quad (254)$$

For a free fall case with $v_r = -\sqrt{\frac{2GM}{r}}$ we get

$$C_1 = t + \frac{2}{3} \frac{r^{3/2}}{\sqrt{2GM}}. \quad (255)$$

The initial condition problem at $t = 0$ is solved separately for poloidal and toroidal fields. For initially uniform field $B_{r0} = B_0 \cos \theta$, $B_{\theta0} = -B_0 \sin \theta$ we obtain the integrals

$$C_1 = \frac{2}{3} \frac{r^{3/2}}{\sqrt{2GM}}, \quad C_2 = r^2 B_0 \cos \theta, \quad C_3 = \sqrt{2GM} r B_0 \sin \theta. \quad (256)$$

The relation between the integrals found at initial moment after excluding $r(C_1)$ is valid at any time, so finally we get from (254) the solution (Bisnovatyi-Kogan, Ruzmaikin, 1974)

$$B_r = \frac{B_0 \cos \theta}{r^2} \left(r^{3/2} + \frac{3}{2} t \sqrt{2GM} \right)^{4/3}, \quad (257)$$

$$B_\theta = -\frac{B_0 \sin \theta}{\sqrt{r}} \left(r^{3/2} + \frac{3}{2} t \sqrt{2GM} \right)^{1/3}.$$

The radial component of the field is growing most rapidly. It is $\sim r^{-2}$ for sufficiently large times, $\sim t^{4/3}$ at given sufficiently small radius, and is growing with time everywhere.

For initially dipole magnetic field $B_{r0} = \frac{B_0 \cos \theta}{r^3}$, $B_{\theta0} = -\frac{B_0 \sin \theta}{2r^3}$ we obtain the following solution

$$B_r = \frac{B_0 \cos \theta}{r^2} \left(r^{3/2} + \frac{3}{2} t \sqrt{2GM} \right)^{-2/3}, \quad (258)$$

$$B_\theta = -\frac{B_0 \sin \theta}{2\sqrt{r}} \left(r^{3/2} + \frac{3}{2} t \sqrt{2GM} \right)^{-5/3}.$$

Here the magnetic field is decreasing everywhere with time, tending to zero. That describes a pressing of a dipole magnetic field to a stellar surface. The

azimuthal stellar magnetic field if confined inside the star. When outer layers of the star are compressing with a free-fall speed, then for initial field distribution $B_{\phi 0} = B_0 r^n f(\theta)$ the change of magnetic field with time is described by a relation

$$B_\phi = -\frac{B_0 f(\theta)}{\sqrt{r}} \left(r^{3/2} + \frac{3}{2} t \sqrt{2GM} \right)^{1/3+n}. \quad (259)$$

4.1.2 Amplification of magnetic Field in Rotating Accretion Flows

In a quasi-spherical accretion flow of a perfectly conducting plasma, $d(\mathbf{B} \cdot d\mathbf{S})/dt = 0$, where $d\mathbf{S}$ is a surface area element and d/dt is the derivative following the flow ($\mathbf{v} = v_r \hat{\mathbf{r}} + v_\phi \hat{\boldsymbol{\phi}}$, in spherical coordinates). With $d\mathbf{S} = r^2 d\Omega \hat{\mathbf{r}}$, $v_r \approx v_r(|\mathbf{r}|)$, and $d\Omega$ a fixed solid angle increment, one finds that $B_r \propto 1/r^2$ independent of the toroidal velocity v_ϕ . Writing $B_r = B_0 (r_{out}/r)^2$, the radius at which $\rho v_K^2/2 = B_r^2/(8\pi)$ is

$$r_{equi} = \left(\frac{g B_0^2 r_0^4}{\sqrt{GM\dot{M}}} \right)^{2/3}, \quad (260)$$

where $v_K \equiv (GM/r)^{1/2}$ and the accretion speed is assumed $v_r = -g v_K$, with $g = \text{const} \leq 1$. For example, for a black hole mass $M = 10^6 M_\odot$, $\dot{M} = 0.1 M_\odot/\text{yr}$, $B_0 = 10^{-5} \text{G}$, $r_0 = 1 \text{pc}$, and $g = 0.1$, we find $r_{equi} \approx 6 \times 10^{14} \text{cm}$, which is much larger than the Schwarzschild radius, $r_S \approx 3 \times 10^{11} \text{cm}$. Thus the magnetic field resulting from flux-freezing is dynamically important in quasi-spherical accretion flows (Shwartzman 1971), and this is independent of dynamo processes or MHD instabilities. Further accretion for $r < r_{equi}$ is possible *only* if magnetic flux is destroyed by reconnection and the magnetic energy is dissipated. Figure 7 shows a sketch of the *instantaneous* poloidal magnetic field configuration.

For example, for a flow with time-averaged velocity $\mathbf{v} = v_r \hat{\mathbf{r}} + v_\phi \hat{\boldsymbol{\phi}}$, an approximate solution for the *time-averaged* magnetic field for infinite conductivity can readily be obtained in the vicinity of the equatorial plane. In this region it is reasonable to assume $\mathbf{B} = B_r \hat{\mathbf{r}} + B_\phi \hat{\boldsymbol{\phi}}$; that is, B_θ is neglected. Thus

$$\nabla \cdot \mathbf{B} = 0 = \frac{1}{r^2} \frac{\partial}{\partial r} (r^2 B_r) + \frac{1}{r \sin \theta} \frac{\partial}{\partial \phi} (B_\phi).$$

Near the equatorial plane, $\sin \theta \approx 1$. This equation is then satisfied by taking

$$B_r = \frac{\text{const}}{r^2} \exp \left(i \int^r dr k_r + im\phi \right), \quad (261)$$

$$B_\phi = f(r) \exp \left(i \int^r dr k_r + im\phi \right), \quad (262)$$

with the actual fields given by the real parts and with

$$\mathbf{k} \cdot \mathbf{B} = k_r B_r + k_\phi B_\phi = 0 , \quad (263)$$

where $\mathbf{k} \equiv \hat{\mathbf{r}}k_r + \hat{\boldsymbol{\phi}} k_\phi$, $k_\phi \equiv m/r$ is the azimuthal wavenumber, and $m = \pm 1, \pm 2$, etc. The stationary magnetic field satisfies $\nabla \times (\mathbf{v} \times \mathbf{B}) = 0$, and this requires

$$\mathbf{v} \times \mathbf{B} = \hat{\boldsymbol{\theta}}(v_\phi B_r - v_r B_\phi) = 0 , \quad \text{or} \quad B_\phi = (v_\phi/v_r)B_r .$$

That is, $\mathbf{v} \propto \mathbf{B}$ and $\mathbf{k} \cdot \mathbf{v} = 0$. Owing to equation (3),

$$k_r = -(v_\phi/v_r)k_\phi . \quad (264)$$

In ADAF accretion models, $v_\phi/v_r = \text{const}$, so that $k_r \propto 1/r$. Thus, $|B_r| = |v_r/v_\phi||B_\phi| \propto 1/r^2$, and $f(r) \propto 1/r^2$.

The nature of the field is most easily obtained from the flux function rA_θ (with \mathbf{A} the vector potential), where

$$B_r = -\frac{1}{r^2} \frac{\partial(rA_\theta)}{\partial\phi} , \quad B_\phi = \frac{1}{r} \frac{\partial(rA_\theta)}{\partial r} ,$$

for $\sin\theta \approx 1$. Note that $(\mathbf{B} \cdot \nabla)(rA_\theta) = 0$. Thus the frozen-in field is described by

$$rA_\theta = \text{const} \exp\left(im \left[\left| \frac{v_\phi}{v_r} \right| \ln r + \phi \right] \right) , \quad (265)$$

where it is assumed that $v_\phi > 0$, $v_r < 0$, and $v_\phi/v_r = \text{const}$. The fact that $|rA_\theta| = \text{const}$ corresponds to the conservation of the ingoing or outgoing flux in a given tube. A given field line satisfies

$$r = \text{const} \exp\left(-\phi \left| \frac{v_r}{v_\phi} \right| \right) . \quad (266)$$

Figure 2 shows the nature of the equatorial field for $m = 2$.

Consider now the problem of magnetic field amplification in an accretion flow which is *not* infinitely conducting. The flow is described by the magneto-hydrodynamics (MHD) equations,

$$\begin{aligned} \rho \frac{d\mathbf{v}}{dt} &= -\nabla p + \rho \mathbf{g} + \frac{1}{c} \mathbf{J} \times \mathbf{B} + \eta \nabla^2 \mathbf{v} , \\ \nabla \times \mathbf{B} &= \frac{4\pi}{c} \mathbf{J} , \quad \nabla \times \mathbf{E} = -\frac{1}{c} \frac{\partial \mathbf{B}}{\partial t} , \\ \mathbf{J} &= \sigma (\mathbf{E} + \mathbf{v} \times \mathbf{B}/c) , \end{aligned} \quad (267)$$

where \mathbf{v} is the flow velocity, \mathbf{B} the magnetic field, p the plasma pressure, σ the plasma conductivity, η the dynamic viscosity (with $\nu = \eta/\rho$ the kinematic

viscosity), \mathbf{J} the current density, and \mathbf{E} the electric field. These equations can be combined to give the induction equation,

$$\begin{aligned} \frac{\partial \mathbf{B}}{\partial t} &= \nabla \times (\mathbf{v} \times \mathbf{B}) - \nabla \times (\eta_m \nabla \times \mathbf{B}) , \\ &\approx \nabla \times (\mathbf{v} \times \mathbf{B}) + \eta_m \nabla^2 \mathbf{B} , \end{aligned} \quad (268)$$

where $\eta_m \equiv c^2/(4\pi\sigma)$ is the magnetic diffusivity, and the approximation involves neglecting $\nabla\eta_m$.

In equations (267) and (268) both the viscosity ν and the magnetic diffusivity η_m have the same units and both are assumed to be due to turbulence in the accretion flow. Thus, it is reasonable to express both transport coefficients using the ‘‘alpha’’ prescription of Shakura (1972) and Shakura and Sunyaev (1973),

$$\nu = \alpha c_s \ell_t , \quad \eta_m = \alpha_m c_s \ell_t , \quad (269)$$

where ℓ_t is the outer scale of the turbulence, and $c_s = \sqrt{p/\rho}$ is the isothermal sound speed. Bisnovatyi-Kogan and Ruzmaikin (1976) introduced α_m and proposed that $\alpha_m \sim \alpha$. Note that α and α_m characterize a turbulent MHD flow in which there is a Kolmogorov cascade of energy from large scales (ℓ_t) to much smaller scales where the actual (microscopic) dissipation of energy occurs.

We obtain stationary \mathbf{B} field solutions for accretion flows with time-averaged flow $\mathbf{v} = \hat{\mathbf{r}}v_r + \hat{\phi}v_\phi$ and with finite diffusivity η_m in the form of equations (261) and (262), but with k_r complex, $k_r = k_r^R + ik_r^I$. Equation (262) still applies, but (264) does not. In its place we have from equation (268),

$$0 \approx i\mathbf{k} \times (\mathbf{v} \times \mathbf{B}) - \eta_m \mathbf{k}^2 \mathbf{B} , \quad (270)$$

where the approximation involves neglect of terms of order $1/(|\mathbf{k}|r) \ll 1$ or smaller. Solution of (270) gives

$$k_r^R v_r + k_\phi v_\phi \approx 0 , \quad \text{and} \quad k_r^I \approx -\frac{\eta_m \mathbf{k}^2}{|v_r|} , \quad (271)$$

where in this equation $\mathbf{k}^2 = (k_r^R)^2 + k_\phi^2$. Consistent with the first part of (12), we take $k_r^R = n_r/r$, where $n_r = \text{const}$. For the ADAF flows, we write the second part of (269) as $\eta_m = \alpha_m c_s r$. The second part of (271) then gives

$$k_r^I = -\left(\frac{\alpha_m c_s}{|v_r|}\right) \frac{n_r^2 + m^2}{r} , \quad (272)$$

where the quantity $\alpha_m c_s / |v_r| = \text{const}$.

The imaginary part of k_r gives an additional radial dependence of B_r and B_ϕ (and rA_θ), multiplying the earlier expressions (261), (262), and (265) by a factor r^δ , where $\delta = (\alpha_m c_s / |v_r|)(n_r^2 + m^2)$. For radial distances $r < r_{\text{equi}}$, we have

equipartition with magnetic energy density $E_m \propto r^{-5/2}$ so that $|\mathbf{B}_p| \propto r^{-5/4}$. This requires $\delta = 3/4$ so that $|rA_\theta| \propto r^{3/4}$, which corresponds to the flux within a given tube decreasing as r decreases. The accretion speed is

$$|v_r| = \frac{4}{3}(n_r^2 + m^2)\alpha_m c_s . \quad (273)$$

Note that for the present solution the accretion depends on the magnetic diffusivity η_m but not the viscosity ν ; more general solutions have v_r dependent on both viscosity and diffusivity. Validity of this solution requires $|k_r^I|/|\mathbf{k}| = (3/4)/\sqrt{n_r^2 + m^2} \ll 1$. The field line pattern is similar to that in Figure 2, but the number of field lines in a tube $\propto r^{3/4}$.

The magnitude of the magnetic field follows from the requirement that the inflow of angular momentum carried by the matter, $\dot{L}_{mech} = 4\pi r^3 < \sin\theta > \rho v_r v_\phi \approx 4\pi r^3 \rho v_r v_\phi < 0$, equal the outflow carried by the field, $\dot{L}_{mag} = -r^3 B_r B_\phi > 0$, which gives $\rho v_r^2 \approx B_r^2/4\pi$. More generally, turbulent viscosity carries away part of the angular momentum in which case the magnetic field strength is reduced. For $r \leq r_{equi}$, we have $B_r = B_0(r_{equi}/r)^{5/4}$, and zero angular momentum flux gives

$$B_0 = \left(\frac{4(n_r^2 + m^2)\alpha_m(c_s/v_\phi)\sqrt{GM\dot{M}}}{3r_{equi}^{5/2}} \right)^{1/2} . \quad (274)$$

This gives $B_0 \approx 55$ G for $r_{equi} = 10^{15}$ cm, $M = 10^6 M_\odot$, $\dot{M} = 0.1 M_\odot/\text{yr}$, $\alpha_m = 0.1$, $c_s/v_\phi = 0.1$, and $n_r^2 + m^2 = 10^2$.

4.2 Stationary picture of the magnetic field distribution in quasi-spherical accretion: turbulence, equipartition and field annihilation; two-temperature advective discs

In the optically thin accretion discs at low mass fluxes the density of the matter is low and energy exchange between electrons and ions due to binary collisions is slow. In this situation, due to different mechanisms of heating and cooling for electrons and ions, they may have different temperatures. First it was realized by Shapiro, Lightman, Eardley (1976) where advection was not included. It was noticed by Narayan and Yu (1995) (see also Ichimaru, 1977), that advection in this case is becoming extremely important. It may carry the main energy flux into a black hole, leaving rather low efficiency of the accretion up to $10^{-3} - 10^{-4}$ (advective dominated accretion flows - ADAF). This conclusion is valid only when the effects, connected with magnetic field annihilation and heating of matter due to it are neglected.

In the ADAF solution the ion temperature is about a virial one $kT_i \sim GMm_i/r$, what means that even at high initial angular momentum the disk

becomes very thick, forming practically a quasi-spherical accretion flow. It is connected also with an “alpha” prescription of viscosity. At high ion temperatures, connected with a strong viscous heating, the ionic pressure becomes high, making the viscosity very effective. So, due to suggestion of “alpha” viscosity in the situation, when energy losses by ions are very low, a kind of a “thermo-viscous” instability is developed, because heating increases a viscosity, and viscosity increases a heating. Development of this instability leads to formation of ADAF.

A full account of the processes, connected with a presence of magnetic field in the flow, is changing considerably the picture of ADAF. It was shown by Schwarzman (1971), that radial component of the magnetic field increses so rapidly in the spherical flow, that equipartition between magnetic and kinetic energy is reached in the flow far from the black hole horizon. In the region where the main enegry prodiction takes place, the condition of equipartition takes place. In presence of a high magnetic field the effiiciency of a radiation during accretion of an interstellar matter into a black hole increase enormously from $\sim 10^{-8}$ up to ~ 0.1 (Schwarzman, 1971), due to efficiency of a magneto-bremstrahlung radiation. So possibility of ADAF regime for a spherical accretion was noticed long time ago. To support the condition of equipartition a continuous magnetic field reconnection is necessary, leading to annihilation of the magnetic flux and heating of matter due to Ohmic heating. It was obtained by Bisnovatyi-Kogan and Ruzmaikin (1974), that due to Ohmic heating the efficiency of a radial accretion into a black hole may become as high as $\sim 30\%$. The rate of the Ohmic heating in the condition of equipartition was obtained in the form

$$T \frac{dS}{dr} = -\frac{3}{2} \frac{B^2}{8\pi\rho r}. \quad (275)$$

In the supersonic flow of the radial accretion equipartition between magnetic and kinetic energy was suggested by Schwarzman (1971):

$$\frac{B^2}{8\pi} \approx \frac{\rho v_r^2}{2} = \frac{\rho GM}{r}. \quad (276)$$

For the disk accretion, where there is more time for a field dissipation, almost equipartition was suggested (Shakura, 1972) between magnetic and turbulent energy, what reduces with account of ”alpha” prescription of viscosity to a relation

$$\frac{B^2}{8\pi} \sim \frac{\rho v_t^2}{2} \approx \alpha_m^2 P, \quad (277)$$

where α_m characterises a magnetic viscosity in a way similar to the turbulent α viscosity. It was suggested by Bisnovatyi-Kogan and Ruzmaikin (1976) the similarity between viscous and magnetic Reynolds numbers, or between turbulent and magnetic viscosity coefficients

$$Re = \frac{\rho v l}{\eta}, \quad Re_m = \frac{\rho v l}{\eta_m}, \quad (278)$$

where the turbulent magnetic viscosity η_m is connected with a turbulent conductivity σ

$$\sigma = \frac{\rho c^2}{4\pi\eta_m}. \quad (279)$$

Taking $\eta_m = \frac{\alpha_m}{\alpha}\eta$, we get a turbulent conductivity

$$\sigma = \frac{c^2}{4\pi\alpha_m h v_s}, \quad v_s^2 = \frac{P_g}{\rho} \quad (280)$$

in the optically thin discs. For the radial accretion the turbulent conductivity may contain mean free path of a turbulent element l_t , and turbulent viscosity v_t in (280) instead of h and v_s . In ADAF solutions, where the ion temperature is of the order of the virial one the two suggestions (276) and (277) almost coincide at $\alpha_m \sim 1$.

The heating of the matter due to an Ohmic dissipation may be obtained from the Ohm's law for a radial accretion in the form

$$T \frac{dS}{dr} = -\frac{\sigma \mathcal{E}^2}{\rho v_r} \approx -\sigma \frac{v_E^2 B^2}{\rho v_r c^2} = -\frac{B^2 v_E^2}{4\pi \rho \alpha_m v_r v_s l_t}, \quad (281)$$

what coincides with (275) when $\alpha_m = \frac{4rv_E}{3v_r l_t}$, or $l_t = \frac{4rv_E^2}{3v_r v_s \alpha_m}$. Here a local electrical field strength in a highly conducting plasma is of the order of $\mathcal{E} \sim \frac{v_E B}{c}$, $v_E \sim v_t \sim \alpha v_s$ for the radial accretion.

Equations for a radial temperature dependence in the accretion disk, separate for the ions and electrons are written as

$$\frac{dE_i}{dt} - \frac{P_i}{\rho^2} \frac{d\rho}{dt} = \mathcal{H}_{\eta i} + \mathcal{H}_{Bi} - Q_{ie}, \quad (282)$$

$$\frac{dE_e}{dt} - \frac{P_e}{\rho^2} \frac{d\rho}{dt} = \mathcal{H}_{\eta e} + \mathcal{H}_{Be} + Q_{ie} - \mathcal{C}_{brem} - \mathcal{C}_{cyc}, \quad (283)$$

Here $\frac{d}{dt} = \frac{\partial}{\partial t} + v_r \frac{\partial}{\partial r}$. A rate of a viscous heating of ions $\mathcal{H}_{\eta i}$ is obtained from (88) as

$$\mathcal{H}_{\eta i} = \frac{2\pi r}{M} Q_+ = \frac{3}{2} \alpha \frac{v_K v_s^2}{r}, \quad \mathcal{H}_{\eta e} \leq \sqrt{\frac{m_e}{m_i}} \mathcal{H}_{\eta i}. \quad (284)$$

The equality in the last equation is related to binary collisions. Combining (70), (92), (86), (90), we get i

$$v_r = \alpha \frac{v_s^2}{v_K \mathcal{J}}, \quad h = \sqrt{2} \frac{v_s}{v_K} r, \quad \rho = \frac{\dot{M}}{4\pi\alpha\sqrt{2}} \frac{v_K^2 \mathcal{J}}{r^2 v_s^3}, \quad (285)$$

where $v_K = r\Omega_K$, $\mathcal{J} = 1 - \frac{jin}{j}$. The rate of the energy exchange between ions and electrons due to the binary collisions was obtained by Landau (1937), Spitzer (1940) as

$$Q_{ie} \approx \frac{4(2\pi)^{\frac{1}{2}} n e^4}{m_i m_e} \left(\frac{T_e}{m_e} + \frac{T_i}{m_i} \right)^{-\frac{3}{2}} \ell n \Lambda (T_i - T_e), \quad (286)$$

with $\ell n \Lambda = \mathcal{O}(20)$ the Coulomb logarithm. Thermodynamic functions must take into account a possible relativistic effects for electrons, which energy may exceed $m_e c^2$. Neglecting pair formation for an low density accretion disk, we may write an exact expression for a pressure

$$P_g = P_i + P_e = n_i k T_e + n_e k T_p = n_e k (T_e + T_i), \quad (287)$$

and an approximate expression for an energy, containing a smooth interpolation between nonrelativistic and relativistic electrons

$$E_g = E_e + E_i \approx \frac{\frac{3}{2} m_e c^2 + 3 k T_e}{m_e c^2 + k T_e} \frac{k T_e}{m_p} + \frac{3 k T_i}{2 m_p}. \quad (288)$$

The electron bremsstrahlung \mathcal{C}_{brem} and magneto-bremsstrahlung \mathcal{C}_{cyc} cooling of maxwellian semi-relativistic electrons, with account of free-bound radiation in nonrelativistic limit, may be written as by inrerpolation of limiting cases (Bisnovaty-Kogan and Ruzmaikin, 1976)

$$\mathcal{C}_{brem} \approx \frac{2 \times 10^{30} m_e c^2 + 3 \times 10^{32} (k T_e)^{3/2}}{m_e c^2 + k T_e} (k T_e)^{1/2}, \quad (289)$$

$$\mathcal{C}_{cyc} \approx \frac{1.7 \times 10^{16} m_e c^2 + 1.7 \times 10^{22} (k T_e)^2}{m_e c^2 + k T_e} k T_e B^2. \quad (290)$$

Effects of the cyclotron self-absorption may be important for nonrelativistic electrons, where radiation itself is low. With increasing of the electron temperature self-absorption effects decrease, because the black-body emission increase with a temperature ($\sim T^4$) more rapidly then magneto-bremsstrahlung volume losses. Account of self-absorption was investigated by Trubnikov (1973).

In the case of a disk accretion there are several characteristic velocities, v_K , v_r , v_s , and $v_t = \alpha v_s$, all of which may be used for determining "equipartition" magnetic energy, and one characteristic length h . Consider three possible choices with $v_B^2 = v_K^2$, v_r^2 , and v_t^2 for scaling $B^2 = 4\pi\rho v_B^2$, note that choice of cross products of different velocities and of v_s , is also possible. We get the following expressions for magnetic field strengths in different cases, with account of (285)

$$\mathbf{a.} \quad v_B = v_K, \quad \frac{B^2}{8\pi} = \frac{\rho v_K^2}{2}, \quad B = \left(\frac{\dot{M}}{\alpha\sqrt{2}} \frac{v_K^4 \mathcal{J}}{r^2 v_s^3} \right)^{1/2},$$

$$\begin{aligned}
\text{b. } \quad v_B = v_r, \quad \frac{B^2}{8\pi} = \frac{\rho v_r^2}{2}, \quad B = \left(\frac{\dot{M} \alpha v_s}{\sqrt{2} \mathcal{J} r^2} \right)^{1/2}, \quad (291) \\
\text{c. } \quad v_B \sim v_t, \quad \frac{B^2}{8\pi} = \frac{\alpha_m^2 \rho v_t^2}{\alpha^2 2}, \quad B = \alpha_m \left(\frac{\dot{M} v_K^2 \mathcal{J}}{\alpha \sqrt{2} r^2 v_s} \right)^{1/2}.
\end{aligned}$$

The expression for an Ohmic heating in the turbulent accretion disk also may be written in different ways, using different velocities v_E in the expression for an effective electrical field

$$\mathcal{E} = \frac{v_E B}{c}. \quad (292)$$

A self-consistency of the model requires, that expressions for a magnetic heating of the matter \mathcal{H}_B , obtained from the condition of stationarity of the flow (275), and from the Ohm's law (281), should be identical. That gives some restrictions for the choice of a characteristic velocity in (292). Comparison between (275) and (281) with account of (280),(285) shows the identity of these two expressions at

$$\frac{\alpha}{\mathcal{J} \alpha_m} \frac{v_E^2}{v_r^2} = \frac{3\sqrt{2}}{4}. \quad (293)$$

That implies $v_E \sim v_r \sim \frac{\alpha v_s^2}{v_K \sqrt{\mathcal{J}}} \simeq \frac{v_t v_s}{v_K \sqrt{\mathcal{J}}} < v_t$ So, the model is becoming self-consistent at the reasonable choice of the parameters. Note, that in the advective models \mathcal{J} is substituted by another function which is not zero at the inner edge of the disk. The heating due to magnetic field reconnection \mathcal{H}_B in the equations (282), (283), obtained from (275) and (291), may be written with account of (284) as

$$\mathcal{H}_B = \frac{3}{16\pi} \frac{B^2}{r\rho} v_r = \frac{1}{2\mathcal{J}} \mathcal{H}_{\eta i} \left(\frac{v_B}{v_K} \right)^2. \quad (294)$$

So, at $v_B = v_K$ the expressions for viscous and magnetic heating are almost identical. The distribution of the magnetic heating between electrons and ions has a critical influence on the model, if we neglect the influence of a plasma turbulence on the energy relaxation, and take into account only the energy exchange by binary collisions from (286). Observations of the magnetic field reconnection in the solar flares show (Tsuneta, 1996), that electronic heating prevails.

It follows from the physical picture of the field reconnection, that transformation of the magnetic energy into a heat is connected with the change of the magnetic flux, generation of the vortex electrical field, accelerating the particles. This vortex field has a scale of the turbulent element and suffers rapid and chaotic changes. The accelerating forces on electrons and protons in this fields are identical, but accelerations themselves differ ~ 2000 times, so during

a sufficiently short time of the turbulent pulsation the electron may gain much larger energy, then the protons. Additional particle acceleration and heating happens on the shock fronts, appearing around turbulent cells, where reconnection happens. In this process acceleration of the electrons is also more effective than of the protons. In the paper of Bisnovatyi-Kogan and Lovelace (1997) the equations (282), (283) have been solved in the approximation of nonrelativistic electrons, $v_B=v_K$, what permitted to unite a viscous and magnetic heating into a unique formula. The combined heating of the electrons and ions were taken as

$$\mathcal{H}_e = (2 - g)\mathcal{H}_{\eta i}, \quad \mathcal{H}_e = g\mathcal{H}_{\eta i}. \quad (295)$$

In the expression for a cyclotron emission self-absorption was taken into account according to Trubnikov (1973). The results of calculations for $g = 0.5 \div 1$ show that almost all energy of the electrons is radiated, so the relative efficiency of the two-temperature, optically thin disk accretion cannot become lower then 0.25. Note again that accurate account of a plasma turbulence for a thermal relaxation and corresponding increase of the term Q_{ie} may restore the relative efficiency to its unity value, corresponding to the optically thick discs.

Studies of the solar corona have led to the general conclusion that the energy build up in the chaotic coronal magnetic field by slow photospheric driving is released by magnetic reconnection events or flares on a wide range of scales and energies (Benz 1997). The observations support the idea of “fast reconnection,” not limited to a rate proportional to an inverse power of the magnetic Reynolds number (Parker 1979, 1990). The data clearly show the rapid acceleration of electrons (e.g., hard X-ray flares, Tsuneta 1996) and ions (e.g., gamma ray line events and energetic ions, Reames *et al.* 1997), but the detailed mechanisms of particle acceleration are not established.

An essential aspect of the coronal heating is the continual input of energy to the chaotic coronal magnetic field due to motion of the photospheric plasma. As emphasized here, there is also a continual input of energy to the chaotic magnetic in a quasi-spherical accretion flow due to compression of the flow. The fact that the ratio of the plasma to magnetic pressures is small in the corona but of order unity in the accretion flow may of course affect the details of the plasma processes.

In magnetic field reconnection plasma flows into the neutral layer from above and below with a speed of the order of the turbulent velocity v_t . Magnetic flux is destroyed in this layer as required for the reasons discussed earlier. Consequently, there is an electric field in the z -direction $\mathcal{E}_z = -(1/c)\partial A_z/\partial t = \mathcal{O}(v_t B_0/c)$, where B_0 is the field well outside of the neutral layer. This is the same as the estimate of the electric field given by Bisnovatyi-Kogan and Lovelace (1997). In the vicinity of the neutral layer ($|y| \ll \ell_t$) this electric field is typically much larger than the Dreicer electric field for electron runaway $E_D = 4\pi e^3(n_e/kT_e) \ln \Lambda$ (Parail & Pogutse 1965), and this leads to streaming motion of electrons in the z -direction. Note that it is much more difficult to

have ion runaway because of the large gyro radii of ions (Bisnovatyi-Kogan and Lovelace, 1997; Lesch, 1991). Of course, in the almost uniform magnetic field assumed by Quataert (1998) there is no runaway of particles.

The streaming of the electrons can give rise to a number of different plasma instabilities the growth of which gives an anomalous resistivity. Galeev and Sagdeev (1983) (see also Li *et al.* 1999) discuss the quasi-linear theory for such conditions and derive expressions for the rate of heating of electrons,

$$\frac{dT_e}{dt} = \frac{1}{n} \int \frac{d^3k}{(2\pi)^3} \gamma_{\mathbf{k}} W_{\mathbf{k}} \frac{\mathbf{k} \cdot \mathbf{u}_e}{\omega_{\mathbf{k}}}, \quad (296)$$

and ions,

$$\frac{dT_i}{dt} = \frac{1}{n} \int \frac{d^3k}{(2\pi)^3} \gamma_{\mathbf{k}} W_{\mathbf{k}}, \quad (297)$$

where $W_{\mathbf{k}}$ is the wavenumber energy spectrum of the turbulence, $\gamma_{\mathbf{k}}$ is the linear growth rate of the mode with real frequency $\omega_{\mathbf{k}}$, n is the number density, and \mathbf{u}_e is the electron drift velocity. If the quantity $\mathbf{k} \cdot \mathbf{u}_e / \omega_{\mathbf{k}}$ is assumed constant and taken out of the integral sign in (19), then the ratio of heating of electrons to that of ions is

$$\frac{dT_e}{dT_i} = \frac{u_e}{(\omega/k)}. \quad (298)$$

This result is independent of the instability type. Galeev and Sagdeev (1983) point out that for most instabilities, relation (21) predicts faster heating of electrons than ions. Earlier, Lesch (1991) and Di Matteo (1998) emphasized the role of reconnection in accelerating electrons to relativistic energies in accretion flows of AGNs.

5 Accretion on to Magnetized Stars

5.1 Disk Accretion on to a Rotating Star with an Aligned Dipole B-Field

5.1.1 Introduction

The problem of matter accretion on to magnetized stars has been of continued interest since the discovery of X-ray pulsars in binary systems (Giacconi *et al.* 1971; Schreier *et al.* 1972; Tananbaum *et al.* 1972). The X-ray pulsars were interpreted as magnetized neutron stars, accreting matter from a companion star (Pringle and Rees 1972; Davidson and Ostriker 1973; Lamb, Pethick, and Pines 1973; Rappaport and Joss 1977). Of the more than 40 of known X-ray pulsars, most are in high-mass ($M_{tot} > 15$) binary systems, while only few are in low-mass ($M_{tot} < 3$) binary systems (see, for example, review by Nagase 1989).

From the early observations, many X-ray pulsars were found to show secular decreases of pulse period (spin-up of the neutron star rotation) with relatively

large rates of change of $-\dot{P}/P = 10^{-2} - 10^{-6} \text{ yr}^{-1}$ (Gursky and Schreier 1975; Schreier and Fabbiano 1976; Rappaport and Joss 1983). The long-term monitoring of X-ray pulsars during the last two decades have shown a wide variety of pulse-period evolution on different time-scales. Some X-ray pulsars show a steady spin-up evolution during many years which rapidly changes to a steady spin-down evolution (e.g., GX 1+4, SMC X-1, 4U 1626-67). Others show the wavy variations of P on time-scales of a few years on a background of systematic spin-up or spin-down (e.g., Cen X-3, Her X-1, Vela X-1) (Nagase 1989; Sheffer *et al.* 1992; Bildsten *et al.*, 1997).

Short-term fluctuations of pulse-period on time-scales of days to months, including clear evidence of spin-down episodes, were found for a number of sources, for example, Her X-1 (Giacconi 1974), Cen X-3 (Fabbiano and Schreier 1977), Vela X-1 (Nagase *et al.* 1984). Detailed observations of Vela X-1 with Hakucho and Tenma satellites, and with HEAO-1 have revealed fluctuations of large amplitude with time-scales about 3-10 days, which were estimated to be random in both amplitude and sign (Nagase 1981). BATSE observations have shown that in some cases (Cen X-3, Her X-1) the timescale of fluctuations is less than one day with the change of sign from spin-up to spin-down and vice-versa (Bildsten *et al.* 1997). Note that some X-ray pulsars (usually the long-period ones) show no evidence of regular spin-up or spin-down (for example, 4U 0115+63, GX 301-2).

In some cases, like Her X-1, the existence of an accretion disk is indicated from various observations in the X-ray and optical bands (for example, Middleditch and Nelson 1976; Bisnovatyi-Kogan *et al.* 1977; Middleditch, Puetter, and Pennypacker 1985). In several other cases, such as Cen X-3, SMC X-1, GX 1+4 (Chakrabarty *et al.* 1997; Cui 1997), and 4U 1626-67, there are also different kinds of evidence, that matter from companion star forms a disk (for example, Tjemkes *et al.* 1986; Nagase 1989). Most of these are short-period pulsars with period about several seconds or less (excluding GX 1+4 with period 122 s.). However, most of long-period pulsars, are supposed to be powered by the capture of stellar wind from companion. However if the companion is the star of Be type with slow rate of outflow, then it is probable that once again the disk first forms, opposite to the case when the companion star is of O-B kind with high speed of matter outflow (see review of Nagase 1989).

Some aspects of matter accretion by magnetized neutron stars were considered for the first time by Bisnovatyi-Kogan and Friedman (1969), and by Shvartsman (1971). Ideas on the spinning-up of pulsars by accretion were first proposed in the case of disk-fed pulsars by Pringle and Rees (1972), Lamb, Pethick and Pines (1973), and Lynden-Bell and Pringle (1974), and for wind-fed pulsars by Davidson and Ostriker (1973), and Illarionov and Sunyaev (1975) (see also Lipunov 1993). The spin-down of a rapidly rotating magnetized star due to “propellar” action of the magnetosphere was suggested by Shvartsman (1971) and Illarionov and Sunyaev (1975), but a detailed model has not been worked out. Pringle and Rees (1972) considered matter accretion from a vis-

cous disk to a magnetized rotating neutron star. Their theory considered the idealized case of an aligned rotator where the magnetic moment of pulsar is aligned parallel or anti-parallel with the pulsar’s spin-axis and the normal to the plane of the accretion disk. They supposed that accreting matter stops at the point where the magnetic pressure of the magnetosphere becomes equal to pressure of matter. At this distance, matter transfers its angular momentum to the star through a thin boundary layer. Another idea regarding the width of the transition zone between the unperturbed accretion disk and magnetosphere, was considered in series of papers by Ghosh and Lamb (1978, 1979a,b). They assumed that magnetic field of the neutron star threads the accretion disk at different radii in a broad “transition” zone, in spite of predominance of the disk stress compared with magnetic stress in this region. Their work is based on the idea of anomalous resistivity connected with the supposed fast reconnection of toroidal component of the magnetic field lines across the disk.

Lovelace, Romanova, and Bisnovaty-Kogan (1995, hereafter LRBK95; Li and Wickramasinghe 1997) proposed an essentially different picture for disk accretion onto a star with an aligned dipole magnetic field. The idea is based on the fact that when there is a large difference between the angular velocity of the star and that of the disk, the magnetic field lines threading the star and the disk undergo a rapid inflation so that the field becomes open with separate regions of field lines extending outward from both the star and the disk. As a result, the magnetosphere consists of an open field line region far from the star and a closed region approximately corotating close to the star. This is shown schematically in Figure 9. The LRBK95 model does not assume an anomalous resistivity, but rather a turbulent magnetic diffusivity proposed by Bisnovaty-Kogan and Ruzmaikin (1976), analogous to the turbulent α viscosity of Shakura (1972) and Shakura and Sunyaev (1973). This corresponds to a resistivity about 10^4 times smaller than that assumed by Ghosh and Lamb (1978,1979a,b). Campbell (1992) has earlier discussed closed field line models of disk accretion onto an aligned dipole star assuming a magnetic diffusivity comparable to the turbulent α viscosity.

The existence of an open magnetic field region of the disk leads to the possibility of magnetically driven outflows. LRBK95 developed a model for magnetohydrodynamic (MHD) outflows and their back influence on the disk using the work on MHD outflows and magnetized disks by Blandford and Payne (1982), Lovelace, Berk, and Contopoulos (1991), Lovelace, Romanova, and Contopoulos (1993), and Lovelace, Romanova, and Newman (1994). In §5.1.1 -5.1.8 we review the arguments of LRBK95. In §5.2 we discuss the magnetic propeller regime of accretion first considered by Illarionov and Sunyaev (1975) and more recently by Lovelace, Romanova and Bisnovaty-Kogan (1999; hereafter LRBK99).

5.1.2 Theory

The basic equations for an assumed stationary plasma configuration are

$$\nabla \cdot (\rho \mathbf{v}) = 0, \quad \nabla \times \mathbf{B} = \frac{4\pi}{c} \mathbf{J}, \quad \nabla \cdot \mathbf{B} = 0, \quad \nabla \times \mathbf{E} = 0,$$

$$\mathbf{J} = \sigma_e (\mathbf{E} + \mathbf{v} \times \mathbf{B}/c), \quad \rho (\mathbf{v} \cdot \nabla) \mathbf{v} = -\nabla p + \rho \mathbf{g} + \frac{1}{c} \mathbf{J} \times \mathbf{B} + \mathbf{F}^{\text{vis}}. \quad (299)$$

Here, \mathbf{v} is the flow velocity, ρ is the density, σ_e is the effective electrical conductivity, \mathbf{F}^{vis} is the viscous force density, $p = \rho k_B T/m$ is the gas pressure (with k_B the Boltzmann constant, m the mean particle mass, and with the radiation pressure assumed negligible), and \mathbf{g} is the gravitational acceleration. Outside of the disk, dissipative effects are considered to be negligible ($\sigma_e \rightarrow \infty$, $\mathbf{F}^{\text{vis}} = 0$, etc.). We neglect the self-gravity of the disk and relativistic effects so that $\mathbf{g} = -\nabla \Phi_g$ with $\Phi_g = -GM/(r^2 + z^2)^{1/2}$, where M is the mass of the central star. Equations (299) are supplemented later by an equation for the conservation of energy in the disk.

A general axisymmetric \mathbf{B} -field can be written as $\mathbf{B} = \mathbf{B}_p + \hat{\phi} B_\phi$, where $\mathbf{B}_p = \nabla \times (\hat{\phi} \Psi/r)$ is the poloidal field, B_ϕ is the toroidal field, and Ψ is the flux function (see, for example, Mestel 1968, or Lovelace *et al.* 1986). We use a non-rotating cylindrical coordinate system so that $\mathbf{B}_p = (B_r, 0, B_z)$. Notice that $\Psi(r, z) = \text{const}$ labels a poloidal field line, $(\mathbf{B}_p \cdot \nabla) \Psi = 0$, or a flux-surface if the poloidal field line is rotated about the z -axis. For the present problem, the \mathbf{B}_p field can be represented as $\Psi = \Psi_* + \Psi'$, with Ψ_* the star's field-assumed to be a dipole $\Psi_* = \mu r^2 (r^2 + z^2)^{-3/2}$ and with Ψ' due to the non-stellar toroidal currents.

5.1.3 Inflation and Opening of Coronal B-Field

Figure 10 shows the poloidal projections of two nearby field lines connecting the star and the disk. Because $\partial/\partial t = 0$, the \mathbf{E} field is electrostatic and the poloidal plane line integral of \mathbf{E} around the loop, $1 \rightarrow 2 \rightarrow 3 \rightarrow 4 \rightarrow 1$, is zero. Because of axisymmetry and the fact that $\mathbf{E} + \mathbf{v} \times \mathbf{B}/c = 0$ outside of the disk, the line integrals of \mathbf{E} along the two curved segments in Figure 10 vanish separately. That is, the electrostatic potential is a constant on any given flux surface (see, for example, Lovelace *et al.* 1986). The potential difference between the points (1,2) on the star's surface is $-\delta \mathbf{r}_{12} \cdot \mathbf{E}_* = \omega_* \delta \Psi/c$, with $\delta \Psi \equiv \Psi_1 - \Psi_2$, where we have assumed that the star is perfectly conducting [$\mathbf{E}_* = -(\mathbf{v} \times \mathbf{B})_*/c$], and where ω_* is the angular rotation rate of the star. Thus, we have $\delta r_{34} (E_r)_d = -\omega_* \delta \Psi/c = -\omega_* r B_z(r, 0) \delta r_{34}/c$, where the path element δr_{34} is in the mid plane of the disk, and the “ d ” subscript indicates that the quantity is evaluated in the disk. In turn, we have $E_r|_d = (J_r/\sigma_e - v_\phi B_z/c)_d$. From Ampère's law, $J_r = -(c/4\pi)(\partial B_\phi/\partial z)$, the fact that B_ϕ is necessarily an odd function of z , and the approximation $\partial B_\phi/\partial z = (B_\phi)_h/h$, we have

$J_r \alpha \approx -(c/4\pi)(B_\phi)_h/h$, where h is the half-thickness of the disk, and the notation $(\dots)_h$ indicates that the quantity is evaluated at $z = h$. Combining these results gives for stationary conditions

$$(B_\phi)_h(r) = -\frac{hr}{\eta_t}[\omega_d(r) - \omega_*]B_z(r), \quad (300)$$

where $\eta_t = c^2/(4\pi\sigma_e)$ is the magnetic diffusivity of the disk, and ω_d is the angular rotation rate of the disk. The fractional variation in B_z between the midplane and surface of the disk is negligible [$O(h/r)$] if the disk is thin in the sense that $h/r \ll 1$. For the conditions of interest here, it follows from (70) that $h/r \leq c_s/v_K$, where $c_s \equiv (k_B T/m)^{1/2}$ the Newtonian sound speed based on the mid-plane temperature of the disk, and $v_K = (GM/r)^{1/2}$ is the Keplerian velocity at r . Campbell (1992) has independently derived equation (300) but does not place any limit on the ratio $|B_\phi/B_z|$.

In contrast with the work of Ghosh and Lamb (1978, 1979a,b), we assume that the magnetic diffusivity of the disk η_t is of the order of magnitude of the disk's effective viscosity (see Bisnovatyi-Kogan and Ruzmaikin 1976; Parker 1979; Campbell 1992). Additionally, we assume that the disk viscosity is the turbulent viscosity as formulated by Shakura (1972) and Shakura and Sunyaev (1973), $\nu_t = (2/3)\alpha c_s h$, where α is a dimensionless quantity less than unity. In this work, we assume that α is in the range 10^{-1} to 10^{-2} . The possible contribution to the turbulent momentum flux due to small-scale magnetic field fluctuations is assumed included in α (Eardley and Lightman 1975; Coroniti 1981; Balbus and Hawley 1992; Kaisig, Tajima, and Lovelace 1992; Rastätter, L. & Schindler, K. 1999). We write $\eta_t = D\nu_t$ where D is dimensionless and of order unity.

With η_t the turbulent diffusivity, equation (300) gives $|(B_\phi)_h/B_z| = (3/2)r|\omega_d(r) - \omega_*|/(\alpha D c_s)$. This ratio is a measure of the twist of the \mathbf{B} field between the star and the disk. For the outer part of the disk $\omega_d(r)$ is expected to be close to the Keplerian value $\omega_K = (GM/r^3)^{1/2}$. Thus, it would appear that the twist $|(B_\phi)_h/B_z|$ can be very much larger than unity, say, > 10 . We argue here that such large values of the twist do not occur.

For a discussion of the limitation on the twist $|(B_\phi)_h/B_z|$ we consider that the plasma outside of the disk is force-free, $\mathbf{J} \times \mathbf{B} = 0$, which is the coronal plasma limit of Gold and Hoyle (1960). This limit is valid under conditions where the kinetic energy density of the plasma is much less than $\mathbf{B}^2/8\pi$. The general response of force-free coronal magnetic field loops to stress (differential twisting) applied to the loop foot points (in the solar photosphere) has been studied intensely by Aly (1984, 1991), Sturrock (1991), and Porter, Klimchuk, and Sturrock (1992). The conclusion of these studies is that a closed field loop with a small twist evolves into an open field-line configuration as the twist is increased. The related problem of the twisting of a force free magnetic field configuration with foot points at different radii in a Keplerian disk has been

studied by Newman, Newman and Lovelace (1992), and Lynden-Bell and Boily (1994). The twisting due to the differential rotation of the disk acts to increase the total magnetic energy of the coronal field and this in turn acts to “inflate” the field.

An alternative measure of the field twist between the star and the disk is simply the difference in the azimuthal location, $\Delta\phi$, of the stellar and disk foot points of a given flux tube. We have $r d\phi/dl_p = B_\phi(r, z)/|\mathbf{B}_p(r, z)|$, where dl_p is the length element along a poloidal field line $\Psi(r, z) = \text{const}$. Because $rB_\phi(r, z)$ depends only on Ψ in a force-free plasma, we have

$$\Delta\phi = [r(B_\phi)_h]_{disk} \int_{star}^{disk} \frac{dl_p}{r|\nabla\Psi|}. \quad (301)$$

For small $\Delta\phi$ (say, < 1), the poloidal field is close to that of a dipole, and the integral gives $\Delta\phi = C_t[(B_\phi)_h/B_z]_d$ with $C_t = 8/15$. For increasing $\Delta\phi$, the value of C_t increases because of the longer path length and the smaller value of $|\nabla\Psi|$. The present situation is analogous to a current-carrying plasma column with a longitudinal B field. For the plasma column there is the well-known Kruskal-Shafranov stability condition (see, for example, Bateman 1980) on the twist $\Delta\phi$ of the field (at the column’s surface) over the length of the column. This condition, $\Delta\phi < 2\pi$, is required for stability against symmetry changing kink perturbations. A related, non-axisymmetric instability may accompany the above mentioned inflation and opening of the star/disk field in response to increasing $\Delta\phi$.

LRBK95 argued that there is a definite upper limit on the twist $\Delta\phi$ of any field lines connecting the star and the disk. This limit implies a corresponding limit on $|(B_\phi)_h/B_z|_d$ in equation (300). If $\Delta\phi$ is larger than this limit, then the field is assumed to be open as indicated in Figure 9.

5.1.4 Equations for Disk

The flow velocity in the disk is $\mathbf{v}(r) = -u(r)\hat{r} + v_\phi(r)\hat{\phi}$, where u is the accretion speed. The surface density of the disk is σ . The main equations are:

1. Mass conservation:

$$\dot{M} = 2\pi r \sigma u, = \text{const}. \quad (302)$$

We assume that the change of \dot{M} with r due to possible MHD outflows is small.

2. Radial force balance:

$$\frac{\sigma v_\phi^2}{r} = \frac{GM\sigma}{r^2} - \frac{(B_r B_z)_h}{2\pi} + \frac{d}{dr} \int_{-h}^h dz p. \quad (303)$$

3. Angular momentum conservation:

$$\frac{d}{dr}(\dot{M}F) = -r^2(B_\phi B_z)_h, \quad F \equiv r^2\omega + \frac{r^2 v_t}{u} \frac{d\omega}{dr}, \quad (304)$$

where $\omega = v_\phi/r$. The term $-r^2(B_\phi B_z)_h$ represents the outflow of angular momentum from the $\pm z$ surfaces of the disk (that is, a torque on the disk). We assume that the angular momentum carried by the matter of the outflow is small compared with that carried by the field. If the B field at r is open as discussed in § 5.1.3, then the angular momentum outflow from the disk is carried to infinity. On the other hand, if the field is closed, then the angular momentum outflow from (or inflow to) the disk is carried by the coronal B field to (or from) the star.

4. Energy conservation:

$$\sigma\nu_t \left(r \frac{d\omega}{dr} \right)^2 + \frac{4\pi}{c^2} \int_{-h}^h dz \eta_t \mathbf{J}^2 = \frac{4acT^4}{3\kappa\sigma} \equiv 2\sigma_B T_{eff}^4. \quad (305)$$

The first term is the viscous dissipation, the second is the Ohmic dissipation, while the third term is the power per unit area carried off by radiation (in the $\pm z$ directions) from the disk which is assumed optically thick. Here, κ is the opacity assumed due to electron scattering, a and $\sigma_B = ac/4$ are the usual radiation constants, T is the midplane temperature of the disk, and T_{eff} is disk's effective surface temperature.

5. Conservation of magnetic flux for a general time-dependent disk:

$$\frac{\partial}{\partial t}(rB_z) = \frac{\partial}{\partial r} \left[rB_z u - \frac{\eta_t r}{h} (B_r)_h \right],$$

where the generally small radial diffusion of the B_z field has been neglected (see LRN). The first term inside the square brackets represents the advection of the field while the second term represents the diffusive drift. In a stationary state,

$$\beta_r(r) \equiv \frac{(B_r)_h}{B_z} = \frac{uh}{\eta_t}. \quad (306)$$

6. Vertical hydrostatic equilibrium: The z -component of the Navier-Stokes equation (299) gives the condition for vertical hydrostatic balance which can be written as

$$\left(\frac{h}{r} \right)^2 + b \left(\frac{h}{r} \right) - \left(\frac{c_s}{v_K} \right)^2 = 0, \quad (307)$$

where c_s is the Newtonian sound speed based on the midplane temperature of the disk, and $b \equiv r \left[(B_r)_h^2 + (B_\phi)_h^2 \right] / (4\pi\sigma v_K^2)$ (Wang, Lovelace, and Sulkanen 1990). Radiation pressure is negligible for the conditions of interest. For $b \ll 2c_s/v_K$, this equation gives the well-known relation $h/r = c_s/v_K$ (Shakura and Sunyaev 1973), while for $b \gg 2c_s/v_K$ it gives $h/r = b^{-1}(c_s/v_K)^2$ which is smaller than c_s/v_K owing to the compressive effect of the magnetic field external to the disk (Wang et al. 1990) It is useful to write $b = \epsilon \beta^2$, where $\epsilon \equiv rB_z^2(r,0)/(2\pi\sigma v_K^2)$ and $\beta^2 \equiv [(B_r)_h^2 + (B_\phi)_h^2]/(2B_z^2)$. In § 5.1.6, we discuss that

$\beta = O(1)$ in order to have outflows from the disk, and $\beta \leq 1$ with no outflows. Thus, the Alfvén speed in the midplane of the disk is $v_A = v_K \epsilon^{\frac{1}{2}} (h/r)^{\frac{1}{2}}$. We may term the magnetic field as weak if $\epsilon < c_s/v_K \approx h/r$. In this limit, $v_A/c_s \approx (\epsilon r/h)^{\frac{1}{2}} \leq 1$, and the magnetic compression of the disk is always small. In the opposite, strong field limit, $\epsilon > c_s/v_K$. If at the same time $\beta = O(1)$, then the disk is magnetically compressed, and for $\epsilon \gg c_s/v_K$, $v_A/c_s = 1/\beta$.

Note that with the magnetic field terms neglected these equations give the Shakura-Sunyaev (1973) solution for region “b”.

5.1.5 Magnetically Driven Outflows

Consider the outer region of the disk where the value of the field twist $\Delta\phi$ given by equation (301) [or $|(B_\phi)_h/B_z|$ of equation (300)] is larger than a critical value. In this region the B field threading the disk is open as discussed in § 5.1.3. The angular momentum flux carried by the disk is $\dot{M}F$. If the angular rotation of the disk is approximately Keplerian, $\omega(r) \approx \omega_K(r)$, then the viscous transport contribution to F is $r^2(\nu/u)(d\omega/dr) \approx -(3/2)r^2\omega[h/(\beta_r r)]$. As discussed in detail below a necessary condition for MHD outflows is that $\beta_r = O(1)$. Consequently, the viscous contribution to F in equation (304) is smaller than the bulk transport term by the small factor $h/r \ll 1$, and $F \approx \omega r^2$.

In equation (304) we therefore have $d(\dot{M}F)/dr \approx \dot{M}\omega_K r/2$. In equation (304) we let $(B_\phi)_h = -\beta_\phi B_z(r, 0)$. Studies of MHD outflows (Blandford and Payne 1982, LBC, LRC) indicate that $\beta_\phi = \text{const} = O(1)$. As a result, equation (304) implies that

$$[B_z(r, 0)]_w = k/r^{5/4}, \text{ with } k = [\dot{M}(GM)^{\frac{1}{2}}/(2\beta_\phi)]^{\frac{1}{2}}, \quad (308)$$

where the w subscript indicates the wind region of the disk. Of course at a sufficiently small radius, denoted r_{wi} , the outflow ceases, and the dependence of $B_z(r, 0)$ reverts to approximately the stellar dipole field, μ/r^3 . As a consistency condition we must have

$$\mathcal{E} = (k/r_{wi}^{5/4})/(\mu/r_{wi}^3) = \left[\frac{\dot{M}(GM)^{1/2} r_{wi}^{7/2}}{\mu^2 (2\beta_\phi)} \right]^{\frac{1}{2}} < 1. \quad (309)$$

The transition between the dipole and outflow field dependences is handled by letting $B_z(r, 0) = (\mu/r^3)g(r) + (k/r^{5/4})[1 - g(r)]$, where, for example, $g(r) = \{1 + \exp[(r - r_{wi})/\Delta r]\}^{-1}$ and $\Delta r/r_{wi} \ll 1$.

Equations (302) – (307) can be used to obtain the disk parameters in the region of outflow. As shown below the viscous dissipation is much larger than the Ohmic, and then Eq. (305) gives $T = [81\dot{M}^2(GM)^{1/2}\kappa/(128\pi^2\alpha D\beta_r^2 ac)]^{1/4} r^{-7/8}$. For illustrative values, $M = 1M_\odot$, $\dot{M} = 10^{17}\text{g/s} \approx 1.6 \times 10^{-9}M_\odot/\text{yr}$, $\alpha = 0.1$, $\beta_r = 0.58$, and $D = 1$, we find at the representative distance $r = 10^8\text{cm}$ that $T \approx 0.44 \times 10^6\text{K}$, $v_K = 1.15 \times 10^9\text{cm/s}$, $c_s = 7.6 \times 10^6\text{cm/s}$, $u = 0.88 \times 10^6\text{cm/s}$, $\sigma = 180\text{g/cm}^2$, and $h/r = 6.6 \times 10^{-3}$. The ratio of the ohmic dissipation to

that due to viscosity is: $(4/27)\alpha D\beta_r^3 \ll 1$. The ratio of the viscous dissipation to the power output of the outflows (the $\pm z$ Poynting fluxes) (per unit area of the disk) is: $(9/2)(h/r)(\beta_r D)^{-1} \ll 1$. Thus, most of the accretion power for $r > r_{wi}$ goes into the outflows. However, the fraction of the total accretion power in outflows is small if $r_{wi} \gg r_*$, where r_* is the star's radius ($\sim 10^6$ cm for a neutron star). Note that $\dot{M} = 10^{17}$ g/s and $M = 1M_\odot$ correspond to a total accretion power or luminosity $L_0 = GM\dot{M}/r_* \approx 1.33 \times 10^{37}$ (erg/s) (10^6 cm/ r_*).

Conservation of the poloidal flux threading the disk implies that there is an outer radius, denoted r_{wo} , of the outflow from the disk. That is, we have $\int_{r_{wi}}^{r_{wo}} r dr (k/r^{5/4}) = \int_{r_{wi}}^{r_{wo}} r dr (\mu/r^3)$. So, the outer radius is $r_{wo} \approx r_{wi} (f\mathcal{E})^{-4/3}$, where $f \approx 1$ for $1 - \mathcal{E} \ll 1$ and $f = 3/4$ for $\mathcal{E} \ll 1$. For $r > r_{wo}$, $B_z(r, 0)$ rapidly approaches zero.

Equation (307) gives the disk thickness. From equation (308), we have $\epsilon = rB_z^2/(2\pi\sigma v_K^2) = (u/c_s)(c_s/v_K)/(2\beta_\phi)$. The magnetic compression of the disk is small if $\epsilon < c_s/v_K$ or equivalently if $u/c_s < 1$. Our numerical solutions have $u/c_s < 1$ in the region of outflow.

5.1.6 Necessary Condition for MHD Outflows

A necessary condition on β_r for MHD outflows from the disk can be obtained by considering the net force \mathcal{F}_p on a fluid particle in the direction of its poloidal motion above the disk. Notice that for stationary flows, the poloidal flow velocity \mathbf{v}_p is parallel to \mathbf{B}_p owing to the assumed axisymmetry and perfect conductivity. However, in general $\mathbf{v} \times \mathbf{B} \neq 0$ so that the fluid particles do not move like "beads on a wire". Above, but close to the disk ($h \leq z \ll r$), we assume that the poloidal field lines are approximately straight. Thus, the poloidal position of a fluid particle above the disk is $\mathbf{r} = (r_o + S \sin(\theta))\hat{\mathbf{r}} + S \cos(\theta)\hat{\mathbf{z}}$, where S is the distance along the path from the starting value $S_o = h/\cos(\theta)$ at a radius r_o , $\tan(\theta) = (B_r)_h/B_z = \beta_r$, and $z = S \cos(\theta)$. The effective potential is $U(S) = -(1/2)\omega_o^2(r_o + S \sin(\theta))^2 - GM/|\mathbf{r}|$ (LRN), and the force in the direction of the particle's poloidal motion is $\mathcal{F}_p = -\partial U/\partial S$. For distances z much less than the distance to the Alfvén point, $\omega_o \approx \omega_K(r_o)$. In this way we find

$$\mathcal{F}_p = -(\omega_K^2 - \omega^2)r \left(\frac{B_r}{|\mathbf{B}_p|} \right) + \omega_K^2 z (3\beta_r^2 - 1) \left(\frac{B_z}{|\mathbf{B}_p|} \right), \quad (310)$$

for $h \leq z \ll r$, where we assume $B_z > 0$.

The slow magnetosonic point of the outflow occurs where $\mathcal{F}_p = 0$ (LRC) at the distance

$$z_s = r \left(1 - \frac{\omega^2}{\omega_K^2} \right) \frac{\beta_r}{3\beta_r^2 - 1}. \quad (311)$$

The factor $1 - (\omega/\omega_K)^2$ can be obtained from the radial force balance equation (303). The radial pressure force is small compared with the magnetic force for

the conditions we consider, $\alpha\beta_r^2/(3\beta_\phi) > h/r \ll 1$. Thus,

$$\frac{z_s}{h} = \left(\frac{2\alpha DB_z^2 r}{3M\omega_K} \right) \frac{\beta_r^3}{3\beta_r^2 - 1}. \quad (312)$$

For $r_{wi} < r < r_{wo}$, the quantity in brackets is simply $\alpha/(3\beta_\phi)$ owing to equation (308). Note that the minimum of $\beta_r^3/(3\beta_r^2 - 1)$ is $1/2$ at $\beta_r = 1$. If the gas near the surface of the disk ($h \leq z \leq z_s$) is assumed isothermal with temperature $T_1 \ll T$ and sound speed $c_{s1} \equiv (k_B T_1/m)^{1/2}$, then the density at the slow magnetosonic point ρ_s can be obtained using the MHD form of Bernoulli's equation. At the slow magnetosonic point, the poloidal flow speed is $v_p = c_{s1} |\mathbf{B}_p|/|\mathbf{B}| \equiv v_{sm}$, the slow magnetosonic speed, and $\rho_s = \rho_h \exp\{-1/2 - [U(z_s) - U(h)]/c_{s1}^2\}$, where U is now regarded as a function of z . In turn, the mass flux density from the $+z$ surface of the disk is $\rho_s v_{sm} \cos(\theta) = \rho_s c_{s1} B_z/|\mathbf{B}|$.

The consistency of the magnetically driven outflow solutions requires $z_s \geq h$. If this were not the case, the outflows would be matter rather than field dominated near the disk. There are two possible regimes having $z_s \geq h$: one is with $\alpha D/(3\beta_\phi) < 1$ [or $\alpha D/(3\beta_\phi) \ll 1$] and $\beta_r \geq 1/\sqrt{3}$; another is with $\alpha D/(6\beta_\phi) > 1$ and $\beta_r > 1$. In the present work, we consider the first regime which is consistent in the following respect: The magnetic pinching force on the inner part of the outflow ($r < r_{wo}$) increases as the mass flux in the outflow increases (LBC). In turn, an increase in the pinching force acts to decrease $\beta_r = (B_r)_h/B_z$ thereby increasing z_s/h and decreasing the mass flux in the outflow.

In addition to the condition $z_s \geq h$, the slow magnetosonic point must be at a distance z_s *not* much larger than h , say $2h$, in order for the outflow to have a non-zero mass flux. At the inner radius of the outflow, r_{wi} , the $B_z(r, 0)$ field in the disk is $\mu/(2r_{wi}^3)$ as discussed in § 5.1.5. We then have

$$r_{wi} \geq \left[\frac{\alpha D \mu^2}{24 \dot{M} (GM)^{1/2}} \right]^{2/7} \quad (313)$$

$$\approx 0.75 \times 10^8 \text{cm} \left[\left(\frac{\alpha D}{0.1} \right) \left(\frac{\mu}{10^{30} \text{Gcm}^3} \right)^2 \left(\frac{10^{17} \text{g/s}}{\dot{M}} \right) \left(\frac{M_\odot}{M} \right)^{1/2} \right]^{2/7},$$

from equation (312). Note that from equation (309), we get $\mathcal{E} \geq [\alpha D/(48\beta_\phi)]^{1/2}$ or $\mathcal{E} \geq 0.046$ and $r_{wo} \leq 90r_{wi}$ for $\alpha = 0.1$, $D = 1$ and $\beta_\phi = 1$.

5.1.7 MHD Outflows and Spin-Up ($r_{to} < r_{cr}$)

We have numerically integrated equations (302) – (307) assuming magnetically driven outflows from the disk. We integrate the equations inward starting from a large radial distance $r < r_{wo}$. The inner radius of the region of outflow is determined as discussed above. For $r < r_{wi}$, $dF/dr = 0$, and the solutions in

this range of r all exhibit a “turn-over radius”, r_{to} , where $d\omega/dr = 0$. This “turn over” results from the radially outward magnetic force in equation (303) which becomes stronger as r decreases. In the region close to the turnover, the magnetic compression of the disk becomes strong in that $\epsilon = O(1)$. From a least squares fitting of many integrations, we find

$$r_{to} \approx 0.91 \times 10^8 \text{cm} \left(\frac{\alpha D}{0.1}\right)^{0.3} \left(\frac{\mu}{10^{30} \text{Gcm}^3}\right)^{0.57} \left(\frac{10^{17} \text{g/s}}{\dot{M}}\right)^{0.3} \left(\frac{M_\odot}{M}\right)^{0.15}. \quad (314)$$

The turn-over radius is less than but in all cases close to r_{wi} . Thus, equation (314) is compatible with (313). Our radius r_{to} has a role similar to that of the Alfvén radius r_A of Ghosh and Lamb (1978, 1979a,b). The dependences we find of r_{to} on μ , \dot{M} , and M are close to those of r_A . However, our analysis shows an important dependence on αD which is proportional to the magnetic diffusivity of the disk. Furthermore, our r_{to} is smaller than r_A by a factor of about $(\alpha D/12)^{0.3}$, which is ≈ 0.24 for $\alpha D = 0.1$.

The turn-over radius is important in the respect that the inward angular momentum flux carried by the disk ($\dot{M}F$) is $\dot{M}\omega_{to}r_{to}^2$ because $d\omega/dr = 0$ at $r = r_{to}$. [Note that we do not consider here the possibility of significant poloidal current flow along the open field lines extending from the polar caps of the star ($B_\phi > 0$ for $z > 0$ in figure 9) which would act to remove angular momentum from the star to infinity.] From numerical integrations, we find to a good approximation that $\omega_{to} = (GM/r_{to}^3)^{1/2}$, so that the influx of angular momentum to the star is $\dot{M}F_{to} = \dot{M}(GMr_{to})^{1/2}$. Thus, the rate of increase of the star’s angular momentum J is:

$$\frac{dJ}{dt} = \dot{M}(GMr_{to})^{1/2}. \quad (315)$$

With I the moment of inertia of the star, $J = I\omega_*$, and $dJ/dt = (dI/dM)\dot{M}\omega_* + I(d\omega_*/dt)$. For the situation of interest, the term proportional to dI/dM is negligible because r_{to} is much larger than the star’s radius. Thus, we have “spin-up” of the star,

$$\frac{d\omega_*}{dt} = \frac{\dot{M}(GMr_{to})^{1/2}}{I},$$

or

$$\frac{1}{P} \frac{dP}{dt} \approx -5.8 \times 10^{-5} \frac{1}{\text{yr}} \left(\frac{P}{1\text{s}}\right) \left(\frac{\dot{M}}{10^{17} \text{g/s}}\right) \left(\frac{10^{45} \text{gcm}^2}{I}\right) \left(\frac{M}{M_\odot}\right)^{1/2} \left(\frac{r_{to}}{10^8 \text{cm}}\right)^{1/2}, \quad (316)$$

where $P = 2\pi/\omega_*$ is the pulsar period. Because the total accretion luminosity $L = GM\dot{M}/r_*$ with r_* the star’s radius, $\dot{P} \propto -P^2 L^{0.85} \mu^{0.285}$ for constant αD , r_* , and M .

Our outflow solutions are consistent only in the case where $\omega_{to} = (GM/r_{to}^3)^{1/2} > \omega_*$. In this case, with r decreasing from r_{to} , the rotation rate of the disk $\omega(r)$ decreases and approaches the rotation rate of the magnetosphere ($\approx \omega_*$) from

above where it matches onto the magnetospheric rotation through a radially thin turbulent boundary layer. We find no consistent stationary solutions when $\omega(r)$ decreases below ω_* . The condition $\omega_{to} > \omega_*$ is the same as

$$r_{to} < r_{cr} \equiv \left(\frac{GM}{\omega_*^2} \right)^{\frac{1}{3}} \approx 1.5 \times 10^8 \text{ cm} \left(\frac{M}{M_\odot} \right)^{\frac{1}{3}} \left(\frac{P}{1 \text{ s}} \right)^{\frac{2}{3}}, \quad (317)$$

where r_{cr} is commonly referred to as the ‘‘co-rotation radius’’. Note that r_{cr} decreases during spin-up. Thus, r_{cr} approaches r_{to} if r_{to} does not decrease rapidly.

5.1.8 Magnetic Braking of Star by Disk; Spin-Up or Spin-Down ($r_{to} > r_{cr}$)

For $r_{to} > r_{cr}$, the B field in the outer part of the disk ($r \gg r_{cr}$) is open as discussed above, but there are no consistent stationary MHD outflows, $(B_\phi)_h = 0$, $\beta_r = hu/\eta_t \ll 1$, and the Ohmic dissipation is small compared with that due to viscosity. Thus, the outer part of the disk obeys essentially the equations of Shakura and Sunyaev (1973) for a Keplerian disk with $F = \text{const.} \equiv F_\infty$ in equation (304) undetermined. We show below that F_∞ can be determined self-consistently by considering the region near r_{cr} where the Keplerian accretion flow is brought into co-rotation with the star. Because there are no outflows, the angular momentum influx to the star is $\dot{M}F_\infty$ which is equal to dJ_*/dt .

In the region of the disk where $\omega(r)$ is close to ω_* , that is, where $r \sim r_{cr}$, $|(B_\phi)_h/B_z|$ given by equation (300) is *not* much larger than unity. In this region, closed but twisted field lines link the star and the disk. The twist of the field acts to remove (or add) angular momentum from (to) the disk if $B_\phi B_z > 0$ (or < 0). The angular momentum removed from the disk is deposited on the star via the B field. In this region of the disk the key equations are (300) and (304) which we rewrite as

$$\frac{d\omega}{dr} = \frac{u}{r^2\nu_t}(F - \omega r^2), \quad \frac{dF}{dr} = \frac{hr}{D\nu_t}(\omega - \omega_*) \left(\frac{r^2 B_z^2}{M} \right) H\left(\frac{\tau}{\tau_{max}} \right). \quad (318)$$

Here, $H(x)$ is a Heaviside function such that $H(x) = 1$ for $|x| < 1$ and $H(x) = 0$ for $|x| > 1$;

$$\tau(r) \equiv \frac{(B_\phi)_h(r)}{B_z(r, 0)} = -\frac{hr}{D\nu_t}(\omega - \omega_*)$$

is a measure of the field twist; $\tau_{max} = \text{const}$ is the maximum value of the twist; and

$$F(r) \equiv r^2\omega + \frac{r^2\nu_t}{u} \frac{d\omega}{dr}.$$

We consider τ_{max} to be a universal constant. For $|\tau| > \tau_{max}$ the field configuration becomes open. In equations (316), B_z is assumed to be the star’s dipole field. The other equations of §4.1.4 are still needed. Note that both the viscous

and Ohmic heating must be retained in the energy equation (305). The viscous dissipation is dominant for $r > r_{cr}$, while the Ohmic dissipation dominates for $r < r_{cr}$. Equations (303) and (306) can be combined to give u as a function of r, T , and ω . In turn, this expression for u can be combined with the energy conservation equation (305) to give both u and T as functions of r, ω , and $\partial\omega/\partial r$ if viscous heating dominates, or as functions of r and ω if Ohmic heating dominates. Furthermore, $\nu_t = (2/3)\alpha c_s h$ in equation (318) can be derived from T and h/r from equation (307) using β_r from equation (306), $\beta_\phi = -\tau$, and ϵ from B_z and u .

We have solved the equations (303, 305-307, & 318) by numerical integration starting from the outside, at a distance where $\tau > \tau_{max}$ and $F = \text{const} = F_\infty$, and integrating inward through r_{cr} . The fact that the value of F_∞ is not known a priori points to the use of a ‘‘shooting method’’ for its determination. Using this approach, we find that there is in general a unique value of F_∞ , denoted F_∞^0 , such that the solution for $\omega(r)$ smoothly approaches ω_* for r decreasing below r_{cr} . If F_∞ is smaller than F_∞^0 , then $\omega(r)$ follows the Keplerian law as r decreases below r_{cr} . On the other hand, if F_∞ is larger than F_∞^0 , then $\omega(r)$ goes through a maximum and decreases rapidly to values much less than ω_* . The only physical solution is that with $F_\infty = F_\infty^0$. Hereafter, the zero superscript on F_∞ is implicit.

The behavior of equations (318) can be understood qualitatively by noting that if $\omega(r)$ were to decrease linearly through r_{cr} , then the radial width of the region of braking, $dF/dr < 0$ where $\omega < \omega_*$, would equal that the width of the region of acceleration, $dF/dr > 0$ where $\omega > \omega_*$. Consequently, F would change by only a small fractional amount. However, if within the braking region $F(r)$ attains a value equal to ωr^2 , then $d\omega/dr = 0$ at this point and $d\omega/dr$ remains small and $\omega \approx \omega_*$ for smaller r . A rough estimation gives the radial width of the braking region as $\Delta r \sim \tau_{max} D c_s / \omega_K$, where c_s is based on the temperature just outside of this region, and the jump in F as $\Delta F \sim \tau_{max} \Delta r (r^2 B_z^2 / \dot{M})$.

Figure 11 shows the dependence of F_∞ on μ and on \dot{M} for sequences of cases where r_{cr} is assumed comparable to r_{to} . This is clearly not a necessary choice; that is, r_{to} could differ significantly from r_{cr} . However, with $r_{cr} = r_{to}$, Figure 11 allows a direct comparison of the angular momentum influx to the star ($\dot{M} F_K$) for the case of outflows ($r_{to} \leq r_{cr}$) with the influx ($\dot{M} F_\infty$) in the case of no outflows and magnetic braking ($r_{to} > r_{cr}$). Figure 11 suggests that a bimodal behavior can occur where the star switches between spin-up and spin-down, owing to some extraneous perturbation.

5.2 Magnetic Propeller Regime

5.2.1 Introduction

Observations of some X-ray pulsars show remarkable ‘jumps’ between states where the pulsar is spin-ning-down to one where it is spinning-up. Examples include the objects Cen X-3 (Bildsten *et al.* 1997) and GX 1+4 (Chakrabarty

et al. 1997; Cui 1997). The theoretical problem of disk accretion on to a rotating magnetized star has been discussed in many works over a long period (Pringle & Rees 1972; Lynden-Bell & Pringle 1974; Ghosh & Lamb 1979a,b; Wang 1979; Lipunov 1993; Lovelace, Romanova, & Bisnovaty-Kogan 1995 (referred to as LRBK95); Li & Wickramasinghe 1997). However, except for the work by Li & Wickramasinghe (1997), the studies do not specifically address the “propeller” regime (Illarionov & Sunyaev 1975) where the rapid rotation of the star’s magnetosphere acts to expell most of the accreting matter and where the star spins-down. Recent computer simulation studies of disk accretion on to a rotating star with an aligned dipole magnetic field (Hayashi, Shibata, & Matsumoto 1996; Goodson, Winglee, & Böhm 1997; Miller & Stone 1997) provide evidence of time-dependent outflows but do not give definite evidence for a “propeller” regime with spin-down of the star. Recent computer simulation studies of disk accretion on to a rotating star with an aligned dipole magnetic field (Hayashi, Shibata, & Matsumoto 1996; Goodson, Winglee, & Böhm 1997; Miller & Stone 1997) provide evidence of time-dependent outflows but do not give definite evidence for a “propeller” regime with spin-down of the star.

Lovelace, Romanova, and Bisnovaty-Kogan (1999, hereafter LRBK99) developed a model for magnetic “propeller”-driven outflows which were first considered by Illarionov and Sunyaev (1975). Such outflows can cause a rapidly rotating magnetized star accreting from a disk to spin-down. Energy and angular momentum lost by the star goes into expelling most of the accreting disk matter. The envisioned geometry is shown in Figure 9. The theory gives an expression for the effective Alfvén radius R_A (where the inflowing matter is effectively stopped) which depends on the mass accretion rate, the star’s mass and magnetic moment, *and* the star’s rotation rate. The model points to a mechanism for ‘jumps’ between spin-down and spin-up evolution and for the reverse transition, which are changes between two possible equilibrium configurations of the system. In for example the transition from spin-down to spin-up states the Alfvén radius R_A decreases from a value larger than the corotation radius to one which is smaller. In this transition the “propeller” goes from being “on” to being “off.” The ratio of the spin-down to spin-up torque (or the ratio for the reverse change) in a jump is shown to be of order unity.

5.2.2 Theory

Consider disk accretion on to a rapidly rotating star so that the disk-star configuration is as sketched in Figure 12. Consider the flow of mass, angular momentum, and energy into and out of the annular region indicated by the box $A'ACC'$ in this figure, where $A'A$ is at radius r_1 and CC' is at r_2 . Notice that at this point the values of r_1 and r_2 are *unknown*. They are determined by the physical considerations discussed here.

Consider first the outer surface CC' through the disk. The influx of mass

into the considered region is

$$\dot{M}_{accr} = 2\pi r_2 \int_{-h}^h dz [\rho (-v_r)]_2 > 0 , \quad (319)$$

where h is the half-thickness of the disk, and the 2 subscript indicates evaluation at $r = r_2$. We assume that mass accretion rate for $r \geq r_2$ is approximately constant equal to \dot{M}_{accr} . That is, we consider that outflow from the disk is negligible for $r \geq r_2$. The influx of angular momentum into the considered region is

$$\dot{L}_{accr} = \dot{M}_{accr}(rv_\phi)_2 - T_2 , \quad T_2 = 2\pi r_2^2 \int_{-h}^h dz (T_{r\phi}^{vis})_2 , \quad (320)$$

where $T_{r\phi}^{vis}$ is the viscous contribution to the stress tensor which includes *both* the turbulent hydrodynamic and turbulent magnetic stresses. The influx of energy into the considered region is

$$\dot{E}_{accr} = \dot{M}_{accr} \left(-\frac{GM}{2r_2} + w_2 \right) - \omega_2 T_2 , \quad (321)$$

where $\omega \equiv v_\phi/r \approx v_K/r$ with $v_K \equiv \sqrt{GM/r}$ the Keplerian speed and M the mass of the star, and where w_2 is the enthalpy. For conditions of interest here the disk at r_2 is geometrically thin so that $w \sim c_s^2 \ll v_K^2$, where c_s is the sound speed.

Consider next the fluxes of mass, angular momentum, and energy across the surface AA' in Figure 12. For the physical regime considered, where $v_K(r_1)/r_1 \ll \omega_*$ (ω_* = the angular rotation rate of the star), the mass accretion across the AA' surface is assumed to be small compared with \dot{M}_{accr} . The reason for this is that any plasma which crosses the AA' surface will be ‘spun-up’ to an angular velocity ω_* (by the magnetic force) which is substantially larger than the Keplerian value, and thus it will be thrown outwards. Thus the efflux of angular momentum across this surface from the considered region is $\dot{L}_1 = -T_1$. The efflux of energy across this surface is $\dot{E}_1 = -\omega_* T_1$, where ω_* is the angular rotation rate of the star and the inner magnetosphere as shown in Figure 12. For the conditions considered, the star slows down and loses rotational energy so that $T_1 > 0$.

We have $\dot{E}_1/\dot{L}_1 = \omega_*$. Because the interaction of the star with the accretion flow is by assumption entirely across the surface AA' , this is consistent with the spin-down of a star with constant moment of inertia I ; that is, $\Delta E_*/\Delta L_* = I_* \omega_* \Delta \omega_*/(I_* \Delta \omega_*) = \omega_*$.

Next we consider the mass, angular momentum, and energy fluxes across the surfaces $A'C'$ and AC in Figure 12. As mentioned, accretion on to the star is small for $r_{cr} \ll r_1$ where r_{cr} is the corotation radius as indicated in Figure 12. Thus, the mass accretion goes mainly into outflows, $\dot{M}_{out} \approx \dot{M}_{accr}$, where “out”

stands for outflows. The angular momentum outflow across the surfaces $A'C'$ and AC , \dot{L}_{out} , must be the difference between the angular momentum lost by the star and the incoming angular momentum of the accretion flow. The angular momentum carried by radiation from the disk is negligible because $(v_K/c)^2 \ll 1$, where c is the speed of light. That is, $\dot{L}_{out} = \dot{L}_{accr} - \dot{L}_1$. The energy outflow across the $A'C'$ and AC surfaces is $\dot{E}_{out} + \dot{E}_{rad} = \dot{E}_{accr} - \dot{E}_1$, where \dot{E}_{rad} is the radiation energy loss rate from the disk surfaces between $r = r_1$ and r_2 , and \dot{E}_{out} is the rate of energy loss carried by the outflows.

Angular momentum conservation gives

$$\dot{L}_{out} = \dot{M}_{accr}(rv_\phi)_2 - T_2 + T_1 . \quad (322)$$

We have

$$\dot{E}_{out} + \dot{E}_{rad} = -\frac{GM\dot{M}_{accr}}{2r_2} - \omega_2 T_2 + \omega_* T_1 . \quad (323)$$

We can solve equation (322) for T_2 and thereby eliminate this quantity from the energy equation (323). This gives

$$\dot{E}_{out} + \dot{E}_{rad} = -\frac{3GM\dot{M}_{accr}}{2r_2} + \omega_2 \dot{L}_{out} + (\omega_* - \omega_2) T_1 . \quad (324)$$

The preceding equations are independent of the nature of the outflows from the disk. At this point we consider the case of magnetically driven outflows as treated by Lovelace, Berk, and Contopoulos (1991, hereafter LBC). In the LBC model the outflows come predominantly from an annular inner region of the disk of radius $\sim R_A$ where the disk rotation rate is $\omega_0 = \sqrt{GM/R_A^3}$. Thus we assume that the outflows come from a region of the disk which is approximately in Keplerian rotation. For the present situation, shown in Figure 1, it is clear that we must have $r_1 < R_A < r_2$. Further, we will assume R_A is close in value to r_1 with $(R_A - r_1)/R_A \lesssim 1$. For conditions where the outflow from the disk is relatively low temperature (sound speed much less than Keplerian speed), equations (16) and (18) of LBC imply the general relation $\dot{E}_{out} = \omega_0 \dot{L}_{out} - 3GM\dot{M}_{out}/(2R_A)$. This equation can be used to eliminate \dot{L}_{out} in favor of \dot{E}_{out} in equation (324). Recalling that $\dot{M}_{out} = \dot{M}_{accr}$ we have

$$(1 - \delta^{\frac{3}{2}})\dot{E}_{out} + \dot{E}_{rad} = (\omega_* - \omega_2) T_1 - \frac{3GM\dot{M}_{accr}}{2r_2} (1 - \delta^{\frac{1}{2}}) , \quad (325)$$

where $\delta \equiv R_A/r_2 < 1$.

The energy dissipation in the region of the disk $r = r_1$ to r_2 heats the disk and this heat energy is transformed into outgoing radiation \dot{E}_{rad} . Thus we have

$$\dot{E}_{rad} = \frac{3}{2} \int_{r_1}^{r_2} dr \frac{GM\dot{M}_{disk}(r)}{r^2} , \quad (326)$$

(Shakura 1973; Shakura & Sunyaev 1973), where $\dot{M}_{disk}(r_2) = \dot{M}_{accr}$ and $\dot{M}_{disk}(r_1) \approx 0$. The essential change in $\dot{M}_{disk}(r)$ occurs in the vicinity of R_A so that $\dot{E}_{rad} \approx (3GM\dot{M}_{accr}/2)(R_A^{-1} - r_2^{-1})$. Thus equation (325) becomes

$$(1 - \delta^{\frac{3}{2}})\dot{E}_{out} = (\omega_* - \omega_2)T_1 - \frac{3GM\dot{M}_{accr}}{2R_A}(1 - \delta^{\frac{3}{2}}). \quad (327)$$

Thus the power from the spin-down of the star ω_*T_1 must be larger than a certain value in order to drive the outflow.

For magnetically driven outflows, the value of \dot{E}_{out} can be written as

$$\dot{E}_{out} = \frac{3}{2} \mathcal{F}_0^{\frac{2}{3}} \omega_0^{\frac{4}{3}} R_A^{\frac{8}{3}} B_0^{\frac{4}{3}} \dot{M}_{accr}^{\frac{1}{3}}, \quad (328)$$

(equation 34 of LBC), where \mathcal{F}_0 is a dimensionless numerical constant $\gtrsim 0.234$, and B_0 is the poloidal magnetic field at the base of the outflow at $r = R_A$. We take the simple estimate $B_0 = \mu/R_A^3$, which omits corrections for example for compression of the star's field by the inflowing plasma.

Next we consider the torque on the star T_1 . Because most of the matter inflowing in the accretion disk at $r = r_2$ is driven off in outflows at distances $r > r_1$, the stress is necessarily due to the magnetic field. The magnetic field in the vicinity of r_1 has an essential time-dependence owing to the continual processes of stellar flux leaking outward into the disk, the resulting field loops being inflated by the differential rotation (LRBK95), and the reconnection between the open disk field and the closed stellar field loops. The time scale of these processes is $t_1 \lesssim 2\pi r_1/v_K(r_1)$. We make the estimate of the torque $T_1 = -2\pi r_1^2(2\Delta z)\langle B_r B_\phi \rangle_1/(4\pi)$, where Δz is the vertical half-thickness of the region where the magnetic stress is significant, and where the angular brackets denote a time average of the field quantities at $r \sim r_1$. The magnetic field components, B_r, B_ϕ , with $B_\phi \propto -B_r$ necessarily, must be of magnitude less than or of the order of the dipole field $B_1 = \mu/r_1^3$ at $r = r_1$. The fact that B_ϕ has the opposite sign to that of B_r is due to the fact that the B_ϕ field arises differential rotation between the region $r < r_1$, which rotates at rate ω_* , and the region $r > r_1$, which rotates at rate $\omega_K(r_1) < \omega_*$. Also, it is reasonable to assume $\Delta z \lesssim r_1$. Therefore,

$$T_1 \approx \bar{\alpha}_1 r_1^3 B_1^2 \equiv \bar{\alpha} \frac{\mu^2}{R_A^3}, \quad (329)$$

where $\bar{\alpha} \leq 1$ (the time average of $\alpha(t)$) is a dimensionless constant analogous to the α -parameter of Shakura (1973) and Shakura & Sunyaev (1973). (Note that because $r_1 \lesssim R_A$, $\bar{\alpha}$ and $\bar{\alpha}_1 = (r_1/R_A)^3 \bar{\alpha}$ are of the same order of magnitude.)

Substituting equations (328) and (329) into equation (327) gives

$$\frac{3}{2} (1 - \delta^{\frac{3}{2}}) \mathcal{F}_0^{\frac{2}{3}} \left(\frac{r_A}{R_A} \right)^{\frac{7}{3}} = \frac{\bar{\alpha} r_A^{\frac{7}{2}}}{R_A^2 r_{cr}^{\frac{3}{2}}} \left[1 - \left(\frac{r_{cr}}{R_A} \right)^{\frac{3}{2}} \delta^{\frac{3}{2}} \right] - \frac{3}{2} (1 - \delta^{\frac{3}{2}}). \quad (330)$$

Here, we have introduced two characteristic radii – the corotation radius,

$$r_{cr} \equiv \left(\frac{GM}{\omega_*^2} \right)^{1/3} \approx 1.5 \times 10^8 \text{cm} M_1^{1/3} P_1^{2/3},$$

with $P_1 \equiv (2\pi/\omega_*)/1\text{s}$ the pulsar period and $M_1 \equiv M/M_\odot$. [For a young stellar object, $r_{cr} \approx 1.36 \times 10^{12} M_1^{1/3} P_{10d}^{2/3}$, where P_{10d} is the period in units of 10 days.] The second is the *nominal* Alfvén radius

$$R_A \equiv \left[\frac{\mu^2}{\dot{M}_{accr} \sqrt{GM}} \right]^{2/7} \approx 3.6 \times 10^8 \text{cm} \frac{\mu_{30}^{4/7}}{\dot{M}_{17}^{2/7} M_1^{1/7}}, \quad (330a)$$

where $\dot{M}_{17} \equiv \dot{M}_{accr}/(10^{17} \text{g/s})$ is the accretion rate with $10^{17} \text{g/s} \approx 1.6 \times 10^{-9} M_\odot/\text{yr}$ and $\mu_{30} \equiv \mu/(10^{30} \text{Gcm}^2)$ with the magnetic field at the star's equatorial surface $\mu/r^3 = 10^{12} \text{G}(10^6 \text{cm}/r)^3$. [For a young stellar object $r_A \approx 1.81 \times 10^{12} \text{cm} \mu_{36.5}^{4/7} / (\dot{M}^{2/7} M_1^{1/7})$, where the normalization corresponds to a stellar radius of 10^{11}cm , a surface magnetic field of $3 \times 10^3 \text{G}$, and an accretion rate of $1.6 \times 10^{-8} M_\odot/\text{yr}$.] The corotation radius is the distance from the star where the centrifugal force on a particle corotating with the star ($\omega_*^2 r$) balances the gravitational attraction (GM/r^2). The Alfvén radius r_A is the distance from a *non-rotating* star where the free-fall of a quasi-spherical accretion flow is stopped, which occurs (approximately) where the kinetic energy-density of the flow equals the energy-density of the star's dipole field. Note that the assumptions leading to equation (330a) require $R_A > r_{cr}$.

Notice that R_A (or $r_1 \sim R_A$) is the *effective* Alfvén radius for a *rotating* star. It depends on *both* r_A and r_{cr} in contrast with the common notion that the Alfvén radius is given by r_A even for a rotating star. From equation (329), the *spin-down* rate of the star is $I(d\omega_*/dt) = -\bar{\alpha} \mu^2/R_A^3$, where I is the moment of inertia of the star (assumed constant). Thus the spin-down rate depends on both r_A and r_{cr} .

Figure 13 shows the dependence of R_A on r_A and r_{cr} for a sample case. For conditions of a newly formed disk around a young pulsar, the initial system point would be on the upper left-hand part of the curve. Due to the pulsar slowing down (assuming μ and \dot{M} constant), the system point would move downward and to the right as indicated by the arrow. In this region of the diagram, $R_A \approx \sqrt{\bar{\alpha}} r_A^{7/4}/r_{cr}^{3/4} \propto \sqrt{\omega}$ (for $\delta \ll 1$), so that the torque on the star is $T_1 \approx (GM\dot{M})^{3/2}/(\mu\sqrt{\bar{\alpha}}\omega^{3/2})$. Thus the braking index is $n = -3/2$, where n is defined by the relation $\dot{\omega}_* = -\text{const} \omega_*^n$. Numerically,

$$\frac{1}{P} \frac{dP}{dt} = \frac{1.55 \times 10^{-5}}{\text{yr}} \frac{P_1^{5/2} (M_1 \dot{M}_{17})^{3/2}}{\sqrt{\bar{\alpha}} \mu_{30} I_{45}}, \quad (331)$$

where $I_{45} \equiv I/(10^{45} \text{g cm}^2)$. For $R_A \gg r_{cr}$, the mass accretion rate to the star is small compared with \dot{M}_{accr} , but some accretion may occur due to ‘leakage’

of relatively low angular momentum plasma across field lines near r_1 (Arons & Lea 1976).

As R_A decreases, the spin-down torque on the star increases. Over a long interval, R_A will decrease to a value larger than r_{cr} but not much larger. In this limit, mass accretion on to the star \dot{M}_1 may become significant. Our treatment can be extended to this limit by noting that $\dot{M}_1 = \dot{M}_2 - \dot{M}_{out}$, $\dot{L}_1 = \dot{M}_1 \omega_1 r_1^2 - T_1$, and $\dot{E}_1 = \dot{M}_1 (-GM/2r_1) - \omega_* T_1$, where T_1 is given by equation (329). In this limit the accretion luminosity is $GM\dot{M}_1/r_*$, where r_* is the star's radius. Figure 13 is not changed appreciably for $\dot{M}_1 < \dot{M}_{accr}$.

Further spin-down of the star will cause the system point in Figure 13 to approach the right-most part of the curve. Further spin-down of the star is impossible. At this point of the evolution, the only possibility is a transition to the spin-up regime. In this regime the effective Alfvén radius is the ‘turnover radius’ r_{to} of the disk rotation curve calculated by LRBK99, the star spins-up at the rate $Id\omega_*/dt = \dot{M}_{accr}(GMr_{to})^{1/2}$, and most of the disk accretion \dot{M}_{accr} falls onto the star. The dashed horizontal line in Figure 13 indicates r_{to} which is necessarily less than r_{cr} .

The location of the turnover line r_{to} in Figure 13 suggests the possible evolution shown by the sequence of points $a \rightarrow b \rightarrow c \rightarrow d \rightarrow a$. The system can jump down from point a where the star spins-down to point b where it spins-up. The spin-down torque at a is $-\bar{\alpha}\mu^2/R_{Aa}^3$ (where R_{Aa} is the effective Alfvén radius at point a), whereas the spin-up torque at b is $\dot{M}_{accr}(GMr_{to})^{1/2}$. The magnitude of the ratio of these torques is

$$\frac{\text{spin-down}}{\text{spin-up}} = \bar{\alpha} \left(\frac{r_A}{R_{Aa}} \right)^{7/2} \left(\frac{R_{Aa}}{r_{to}} \right)^{1/2}. \quad (332)$$

With the system on the r_{to} line, it evolves to the left. Because $r_{to} \leq r_{cr}$, there must be an upward jump from point c to point d . For this case the torque ratio is given by equation (332) with $R_{Aa} \rightarrow R_{Ad}$. From point d the system evolves to the right. For the example shown in Figure 2, the torque ratio is ≈ 3.45 for $a \rightarrow b$ whereas it is ≈ 0.87 for $c \rightarrow d$. The vertical line $c \rightarrow d$ is at the left-most position allowed for the considered conditions, but this transistion could also occur if the line is shift to the right. The line $a \rightarrow b$ can be displaced slightly to the right or it can be displaced to the left to be coincident with the $c \rightarrow d$ line. In the latter case the torque ratio for the spin-down to spin-up jump is approximately equal to the torque ratio for the spin-up to spin-down jump and is ≈ 0.87 . The smaller the horizontal separation of the $a \rightarrow b$ and the $c \rightarrow d$ lines, the shorter is the time interval between jumps.

Summarizing, we can say that the horizontal locations of the transistions, $a \rightarrow b$, and $c \rightarrow d$, are indeterminate within a definite range. The locations of the jumps in the (R_A, r_{cr}) plane may in fact be a stochastic or chaotic in nature and give rise to chaotic hysteresis in the of the spin-down/spin-up behavior of the pulsar. The jumps could be triggered by small variations in the accretion

flow (\dot{M} for example) and magnetic field configuration (the time-dependence of α in the torque T_1). Analysis of the accreting neutron star system Her X-1 (Voges, Atmanspacher, & Scheingraber 1987; Morfill *et al.* 1989) suggests that the intensity variations are described by a low dimensional deterministic chaotic model. The transitions between spin-down and spin-up and the reverse transitions may be described by an analogous model.

The allowed values in Figure 13 have $r_{cr}/r_A \leq \text{const} \equiv k$, where $k \approx \bar{\alpha}^{2/3}$. This corresponds to pulsar periods

$$P \leq 5.2\text{s} \left(\frac{\bar{\alpha}}{M_1^{5/7}} \right) \left(\frac{\mu_{30}^2}{\dot{M}_{17}} \right)^{3/7}. \quad (333)$$

For some long period pulsars such as GX 1+4 this inequality points to magnetic moment values μ_{30} appreciably larger than unity. Periods much longer than allowed by (333) can result for pulsars which accrete from a stellar wind (Bisnovaty-Kogan 1991). [For a young stellar object, equation (333) gives $P \leq 8d(\bar{\alpha}/M_1^{5/7})(\mu_{36.5}^2/\dot{M}_{18})^{3/7}$.]

5.3 Cyclotron emission from magnetic poles in X-ray pulsars

Accretion flow into a strongly magnetized neutron star is analyzed by the magnetic field and is falling into magnetic poles. Observational spectra of X-ray pulsars are formed by combination of black body and comptonization in the hot coronal layer. In presence of a strong magnetic fields $\sim 10^{10} - 10^{13}$ Gs the cyclotron or synchrotron emission of electrons also falls into an X-ray band. There are a lot of observations of the spectral feature, interpreted as a cyclotron line in the X-ray spectrum of the pulsar Her X-1 (Trümper *et al.*, 1978; Tueller *et al.*, 1984; Ubertini *et al.*, 1980; Voges *et al.*, 1982; Gruber *et al.*, 1980; McCray *et al.*, 1982; Mihara *et al.*, 1990; Sheepmaker *et al.* 1981) at 39-58 KeV (see Table 2). Magnetic field intensity was usually calculated from the non-relativistic formula

$$H = \frac{mc\omega}{e}, \quad (334)$$

where ω is the cyclic frequency of the photons, m is the mass of the electron. From observations of the line frequency in the Table the magnetic field strengths are of the order of $(3 - 5) \cdot 10^{12}$ Gs. But as large as this value comes into conflict with some theoretical reasonings like interpretation of the observations of pulsar spin acceleration (Bisnovaty-Kogan and Komberg, 1973), condition for the transparency for the outgoing of the directed radiation (Bisnovaty-Kogan, 1973, 1974), consideration of the interrelation between radio and X-ray pulsars (Bisnovaty-Kogan and Komberg, 1974), interpretation of beam variability during the 35-day cycle (Sheffer *et al.*, 1992; Deeter *et al.*, 1998; Scott *et al.*,

2000), see also Lipunov (1987). It seems likely that the reason of this conflict is an unsuitability of the non-relativistic formula in this case. According to Bisnovaty-Kogan and Fridman (1969), the temperature of the electrons emitting a cyclotron line could be $\sim 10^{11} K$, and therefore they are ultrarelativistic. By this means the mean energy of the cyclotron line is broadened and shifted relativistically by a factor of $\gamma \simeq \frac{kT}{mc^2}$. In the paper of Baushev and Bisnovaty-Kogan (1999) the spectral profile of the cyclotron line had been calculated for various electron distributions. Furthermore, the model of the hot spot on the pulsar magnetic pole was considered and it was shown that the overall observed X-ray spectrum (from 0.2 to 120 KeV) could arise in presence of the surface magnetic field ($\sim 5 \cdot 10^{10}$ Gs) which is well below then those, obtained from (334).

5.3.1 The spectrum of the cyclotron radiation of the anisotropic relativistic electrons

According to Bisnovaty-Kogan (1973), Gnedin and Sunyaev (1973), in the magnetic field near the pulsar the component of a momentum perpendicular to the magnetic field emits rapidly, while the parallel component of a velocity remains constant. Hence the momentum distribution of the electrons is anisotropic

$$p_{\perp}^2 \ll p_{\parallel}^2, \quad (335)$$

where $p_{\perp} \ll mc$, $p_{\parallel} \gg mc$. Assume for simplicity that the transverse electron distribution is two-dimensional Maxwellian

$$dn = \frac{N}{T_1} \exp\left(-\frac{mu^2}{2T_1}\right) d\frac{mu^2}{2}, \quad (336)$$

where $T_1 \ll mc^2$. Let us calculate the cyclotron emission of N such particles that move at a rate V along the magnetic field.

For a single particle, having the transverse velocity u , we find (Ginzburg, 1975):

$$j(\theta) = \frac{e^4 H^2 u^2 (1 - \frac{V^2}{c^2})^2 [(1 + \cos \theta)(1 + \frac{V^2}{c^2}) - 4\frac{V}{c} \cos \theta]}{8\pi c^5 m^2 (1 - \frac{V}{c} \cos \theta)^5}, \quad (337)$$

where θ is an observational angle in a laboratory frame of reference. Integrating over the distribution (336), we obtain for N particles:

$$J(\theta) = \int j(\theta) dn = N \frac{e^4 H^2 T_1 (1 - \frac{V^2}{c^2})^2 [(1 + \cos \theta)(1 + \frac{V^2}{c^2}) - 4\frac{V}{c} \cos \theta]}{4\pi c^5 m^3 (1 - \frac{V}{c} \cos \theta)^5}. \quad (338)$$

For the spectrum we find:

$$\omega(\theta) = \omega_H \frac{\sqrt{1 - \frac{V^2}{c^2}}}{1 - \frac{V}{c} \cos \theta}, \quad \omega_H = \frac{eH}{mc}. \quad (339)$$

When $V \simeq c$ the cyclotron radiation is highly directed and diagram has a pencil beam along V ($\theta \simeq 0$). Under these conditions ($\theta = 0$, $V \simeq c$) we obtain from (338),(339):

$$J(0) = \frac{2Ne^4 H^2 T_1}{\pi c^5 m^3 (1 - \frac{V}{c})}, \quad (340)$$

$$\omega(0) = \omega_H \sqrt{\frac{1 + \frac{V}{c}}{1 - \frac{V}{c}}} \approx 2\omega_H \frac{E_{\parallel}}{m_e c^2}, \quad (341)$$

what gives

$$1 - \frac{V}{c} = \frac{2\omega_H^2}{\omega^2}. \quad (342)$$

Let us consider the parallel momentum distribution of the electrons as:

$$dn = f(p_{\parallel}) dp_{\parallel}. \quad (343)$$

Substituting of dn for N and using

$$p_{\parallel} = \frac{mc}{2} \frac{\omega}{\omega_H}; \quad 1 - \frac{V}{c} = \frac{2\omega_H^2}{\omega^2}, \quad (344)$$

we obtain for the spectral density:

$$J_{\omega} = \frac{e^2 T}{2\pi c^2 \omega_H} \omega^2 f\left(-\frac{mc}{2} \frac{\omega}{\omega_H}\right) d\omega. \quad (345)$$

Let us consider two important cases. When f is a relativistic Maxwell:

$$f = \frac{n_0 c}{T_2} \exp\left(-\frac{p_{\parallel} c}{T_2}\right), \quad T_2 \gg mc^2 \gg T_1, \quad (346)$$

where n_0 is a number of emitting electrons. Then the spectrum is:

$$J_{\omega} = \frac{n_0 e^2}{2\pi c \omega_H} \frac{T}{T_2} \omega^2 \exp\left(-\frac{mc^2 \omega}{2\omega_H T_2}\right) d\omega. \quad (347)$$

This spectrum has a single maximum at

$$\frac{\omega}{\omega_H} = \frac{4T_2}{mc^2}. \quad (348)$$

In the second case consider the function f as

$$f = \frac{n_0}{\sqrt{\pi}\sigma} \exp\left(-\frac{(p_{\parallel} - a)^2}{\sigma^2}\right). \quad (349)$$

The spectrum of radiation is

$$J_{\omega} = \frac{n_0 e^2}{2\pi c^2 \omega_H} \omega^2 \exp\left(-\frac{(\frac{mc}{2} \frac{\omega}{\omega_H} - a)^2}{\sigma^2}\right) d\omega. \quad (350)$$

When $\sigma \ll a$ this spectrum has a single maximum at

$$\omega \simeq \frac{2a}{mc} \omega_H. \quad (351)$$

Notice that in all cases the maximum is shifted to

$$\frac{\omega}{\omega_H} \sim \frac{\bar{E}_e}{mc^2}. \quad (352)$$

It is a common property of relativistic cyclotron line, that is independent of the particular form of f . We had approximated experimental spectrum taken from Mihara et al. (1990) (solid line) by (347),(350), representing the second variant with better coincidence by the dot line in Figure 14. The spectrum from McCray et al. (1982) was approximated by (350) only (see Figure 15).

Setting in accordance with Bisnovatyi-Kogan and Fridman (1969) the longitude electron temperature as $\sim 2 \cdot 10^{11}$ K, that is $T_2 = 2 \cdot 10^{11}$ K and $a = 7 \cdot 10^{-4} \frac{\text{eV}\cdot\text{s}}{\text{cm}}$, we obtain for the magnetic field strength $B = 4 \cdot 10^{10}$ Gs, $8 \cdot 10^{10}$ Gs, and $4 \cdot 10^{10}$ Gs respectively. Here we estimate the spectral form of the cyclotron line averaged over the pulsar period, supposing a uniform distribution of $f(p_{\parallel})$ over the polar cap. In this model the beam of the cyclotron feature is determined by the number distribution of the emitting relativistic electrons, moving predominantly along the magnetic field, over the polar cap.

5.3.2 Model of the X-ray spectrum of Her X-1.

In order to obtain the whole experimental spectrum of the Her X-1 the following model of the hot spot is considered (see Figure 16). A collisionless shock wave is generated in the accretion flow near the surface on the magnetic pole of a neutron star. In it's front the ultrarelativistic electrons are generated having small pitch-angle values, so the condition (335) is fulfilled automatically. Behind the shock there is a hot turbulent zone with a temperature T_e , and optical depth τ_e , and under this zone a heated spot on the surface of the neutron star with a smaller temperature is situated.

The whole X-ray spectrum of pulsar Her X-1 taken from McCray et al. (1982) is represented in Figure 15 by the solid line, and in Figure 16 together with the schematic picture of the emission region of Her X-1.

Table 2: Observations of the cyclotron line in Her X-1

Date	References	ω_{\max} (KeV)	Line width (KeV)
May 1978	Trümper et al. (1978)	58	11^{+26}_{-11}
September 1977	Voges et al. (1982)	51	21^{+9}_{-7}
February 1978	Gruber et al. (1980)	48	28 ± 7
April 1980	Gruber et al. (1980)	54	11^{+14}_{-11}
May 1980	Ubertini et al. (1980)	49.5	18^{+6}_{-3}
September 1980	Tuller et al. (1984)	39	27^{+21}_{-20}

There are three main regions in the spectrum: a quasi-Plankian spectrum between 0,3 and 0,6 KeV, that is generated near the magnetosphere of the X-ray pulsar; power-law spectrum (0.6 ÷ 20) KeV with a rapid decrease at 20 KeV, and the cyclotron feature.

The power-law spectrum area appears as follows. A surface emits the black-body spectrum with a temperature T_s . Travelling through the turbulent zone this radiation is comptonized. This comptonized spectrum has been calculated according to Sunyaev and Titarchuk (1980). Setting the neutron star radius equal to 10 km, distance from the X-ray pulsar 6 Kps, hot spot area $S = 2 \cdot 10^{12}$ cm², we have found the best approximation conditions at $T_s = 1$ KeV, $T_e = 8$ KeV, $\tau_e = 14$. The best approximation of the X-ray spectrum of the pulsar Her X-1 is represented in Figure 15 by the dashed line. It agrees nicely with the experimental curve.

Observation of the variability of the cyclotron line is reported in Mihara et al. (1997). Ginga detected the changes of the cyclotron energies from 4 pulsars. The change is as much as 40 % in the case of 4U 0115+63. Larger luminosity of the source corresponds to smaller average energy of the cyclotron feature. These changes might be easily explained in our model. The velocity of the accretion flow decreases with increasing of the pulsar's luminosity because locally the luminosity is close to the Eddington limit. As a result the shock wave intensity drops as well as the energy of the ultrarelativistic electrons in it's front. The cyclotron energy decreases in accordance with (352).

Observations on Beppo-Sax and RXTE satellites (Santangelo et al., 1999; Heindl et al., 1999) revealed 4 cyclotron-like spectral features (harmonics) in the spectrum of the X-ray pulsar 4U 0115+63. Interpretation of these features is still not completed.

6 Magnetohydrodynamic Origin of Jets from Accretion Disks

6.1 Introduction

Powerful, highly-collimated, oppositely directed jets are observed in active galaxies and quasars (see for example Bridle & Eilek 1984), and in the “micro-quasars” – old compact stars in binaries (Mirabel & Rodriguez 1994; Eikenberry *et al.* 1998). Further, highly collimated emission line jets are seen in young stellar objects (Mundt 1985; Bührke, Mundt, & Ray 1988). Different ideas and models have been put forward to explain astrophysical jets (see reviews by Begelman, Blandford, & Rees 1984; Bisnovatyi-Kogan 1993b; Lovelace *et al.* 1999b). Recent observational and theoretical work favors models where twisting of an ordered magnetic field threading an accretion disk acts to magnetically accelerate the jets as first proposed by Lovelace (1976) and Blandford (1976). The nature of the ordered magnetic field threading an accretion disk envisioned by Bisnovatyi-Kogan and Ruzmaikin (1976) is shown in Figure 17. Figure 18 shows the outflows from a disk with such an ordered field from Lovelace (1976). Two main regimes have been considered in theoretical models, the *hydromagnetic regime* where the energy and angular momentum is carried by both the electromagnetic field and the kinetic flux of matter, and the *Poynting flux regime* where the energy and angular momentum outflow from the disk is carried predominantly by the electromagnetic field.

The theory of the origin of hydromagnetic outflows has been developed by many authors (Blandford & Payne 1982; Pudritz & Norman 1986; Sakurai 1987; Koupelis & Van Horn 1989; Lovelace, Berk & Contopoulos 1991; Pelletier & Pudritz 1992; Königl & Ruden 1993; Lovelace, Romanova, & Contopoulos 1993; Cao & Spruit 1994; Contopoulos & Lovelace 1994; Contopoulos 1995; Ostriker 1997). Physical understanding of the hydromagnetic outflows from disks has developed from MHD simulations (Uchida & Shibata 1985; Shibata & Uchida 1986; Bell 1994; Ustyugova *et al.* 1995, 1999; Koldoba *et al.* 1995; Romanova *et al.* 1997, 1998; Meier *et al.* 1997; Ouyed & Pudritz 1997; Krasnopolsky, Li, & Blandford 1999; Koide *et al.* 2000).

Recent work on hydromagnetic outflows assumes the geometry sketched in Figure 19. A strong case for hydromagnetic jets as an explanation of jets in protostellar systems emerges because the temperature of the inner regions of these systems is insufficient to permit driving by thermal or radiation pressure (Königl & Ruden 1993). Part of the investigations have been analytical or semi-analytical and outgrowths of the self-similar solution of Blandford & Payne (1982) (Pudritz & Norman 1986; Königl 1989; Pelletier & Pudritz 1992; Contopoulos & Lovelace 1994). The outflows in this model are often referred to as “centrifugally driven” owing to the driving force close to the disk: Close to the disk, MHD fluid particles move along the magnetic field lines (sometimes described as “beads on a wire”). If the poloidal magnetic field lines threading the disk diverge away from the z -axis as shown in Figure 17 (making an angle with the z -axis of more than 30°), then the sum of the gravitational and centrifugal forces is outward, away from the disk. The self-similar models are

unsatisfactory in the respect that they must be cutoff at small cylindrical radii, $r \leq r_{min}$. This is the most important region of the jet flow. Observations of optical stellar jets (Mundt 1985) reveal jet velocities $\sim 200 - 400$ km/s, which are comparable to the Keplerian disk velocity close to the star's surface. This suggests that the jets originate from the inner region of the disk close to the star (Shu et al. 1988; Pringle 1989).

The limitations of analytical models has motivated efforts to study jet formation using MHD simulations. Simulation studies of hydromagnetic jet formation have addressed two main regions: The jet formation region where the matter enters with sub slow-magnetosonic speed and exits with super fast-magnetosonic speed. The second region includes the disk and the problem of the Velikhov (1959) - Chandrasekhar (1981) instability (Balbus-Hawley 1998) and the resulting 3D MHD turbulence. A number of studies have addressed the coupled problem of the disk and near jet regions (Uchida & Shibata 1985; Shibata & Uchida 1986; Stone & Norman 1994; Bell and Lucek 1995;). MHD simulations of the near jet region have been carried out by several groups (Bell 1994; Ustyugova et al. 1995, 1999; Koldoba et al. 1995; Romanova et al. 1997, 1998; Meier et al. 1997; Ouyed & Pudritz 1997).

The powerful jets observed from active galaxies and quasars are probably *not* hydromagnetic outflows but rather Poynting flux dominated jets. The motion of these jets measured by very long baseline interferometry correspond to bulk Lorentz factors of $\Gamma = \mathcal{O}(10)$ which is much larger than the Keplerian disk velocity predicted for hydromagnetic outflows. Furthermore, the low Faraday rotation measures observed for these jets at distances $< \text{kpc}$ from the central object implies a very low plasma densities. Similar arguments indicate that the jets of microquasars are *not* hydromagnetic outflows but rather Poynting jets. Poynting jets have been proposed to be the driving mechanism for gamma ray burst sources (Katz 1997) Theoretical studies have developed models for Poynting jets from accretion disks (Lovelace, Wang, & Sulkanen 1987; Colgate & Li 1998; Lynden-Bell 1996; Romanova & Lovelace 1997; Levinson 1998; Romanova 1999; Lovelace *et al.* 2001; and Li *et al.* 2001). Stationary Poynting flux dominated outflows were found by Romanova *et al.* (1998) and Ustyugova *et al.* (2000) in axisymmetric MHD simulations of the opening of magnetic loops threading a Keplerian disk.

Here, we first review recent results on MHD simulations of hydromagnetic jet formation and later discuss the Poynting flux regime. Section 4.3 discusses general considerations of hydromagnetic outflows. Sections 4.4 discusses MHD simulations which give non-stationary and stationary hydromagnetic outflows. Sections 4.5 describes the Poynting flux regime which remains to be fully explored by simulations. Section 4.6 gives the conclusions.

6.2 Basics of MHD Outflows from Disks

The main forces which drive a hydromagnetic outflow from a disk threaded by a magnetic field are the centrifugal force and the magnetic pressure gradient force. If disk has a hot corona, the pressure gradient may also be important. We neglect the radiative force but in this regard see Phinney (1987). Accreting matter of the disk carries magnetic field inward thus generating a B_r component of the magnetic field as sketched in Figure 19. On the other hand, rotation of the disk acts to generate a toroidal component of the field B_ϕ (< 0 if $B_z > 0$).

For a sufficiently inclined magnetic field (θ in Figure 19 sufficiently large), outflows can result from the centrifugal force (Blandford & Payne 1982) and/or the magnetic pressure gradient force ($-\nabla_z B_\phi^2/(8\pi)$) (Lovelace et al. 1989, 1991; Koupelis & Van Horn 1989). This depends on the ratio of energy densities at the base of the outflow at the inner radius of the disk denoted r_i . Thus, the main parameters are $\varepsilon_{th} = (c_s/v_K)_i^2$ and $\varepsilon_B = (v_A/v_K)_i^2$, where v_K is Keplerian velocity, c_s the sound speed, v_A the Alfvén speed, and the i subscript indicates evaluation on the surface of the disk at its inner radius, $r = r_i$. For $\varepsilon_B \sim 1$ the outflow is magneto-centrifugally driven, whereas for $\varepsilon_{th} \sim 1$, the flow is thermally driven.

Processes in the disk are of course coupled to the outflows (Lovelace et al. 1994, 1997; Falcke, Malkan, & Biermann 1995). However, it is difficult to simultaneously simulate the disk and the outflow regions because the time scales of the accretion and outflow are in general very different. The radial accretion speed of the disk is typically $|v_r| \ll c_s \ll v_K$, where c_s is the sound speed in the disk, and v_K is the Keplerian velocity. On the other hand the velocity of magnetic outflows from disks is of the order of v_K . Clearly, it is “easier” (less computation time is required) to simulate the outflows.

Furthermore, processes in the disk may involve the small scale MHD instability of Chandrasekhar-Velikhov instability emphasized by Balbus, and Hawley, and therefore require high spatial resolution. Stone & Norman (1994) attempted to simultaneously simulate the internal MHD dynamics of a disk and MHD dynamics of outflows. This proved impractical because essentially all of the spatial resolution was needed for treating the unstable dynamics of the disk. Also, there was the problem that the initial configuration was far from equilibrium. Simulation of the internal MHD disk dynamics has led several groups to the problem of simulating 3D MHD turbulence in a sheared flow of a patch of a disk (for example, Hawley et al. 1995; Brandenburg et al. 1995). This is a much larger project than that of understanding MHD outflows. At the same time it is widely thought, and observations of cataclysmic variables support the view, that the disk turbulence - including MHD turbulence - can be modeled approximately using the Shakura (1973), Shakura & Sunyaev (1973) “alpha” viscosity model (Eardley & Lightman 1975; Coroniti 1981; see also section 1.5). In contrast with the internal disk dynamics, there is theoretical and simulation evidence that the outflows can be treated using axisymmetric (2D) MHD (Blandford &

Payne 1982; Lovelace et al. 1991; Ustyugova et al. 1995). Here, we consider outflows from a disk represented as a boundary condition. This approach has subsequently been adopted by other groups (Meier et al. 1997; Ouyed & Pudritz 1997). This treatment of the disk is justified for outflows from a disk where the accretion speed is small compared with the Keplerian speed (Ustyugova et al. 1995).

6.3 Theory of Stationary MHD Flows

The theory of stationary, axisymmetric, ideal MHD flows was developed by Chandrasekhar (1956), Woltjer (1959), Mestel (1968), Kulikovskiy & Lyubimov (1962), and others. Under these conditions the MHD equations can be reduced to a single equation for the “flux function” $\Psi(r, z)$ in cylindrical (r, ϕ, z) coordinates (Heinemann & Olbert 1978; Lovelace et al. 1986). The flux function Ψ labels flux surfaces so that $\Psi(r, z) = \text{const}$ represents the poloidal projection of a field line. The equation for Ψ is commonly referred to as the Grad-Shafranov equation (Lovelace et al. 1986). The discussion of this section follows that of Ustyugova *et al.* (1999).

6.3.1 Integrals of Motion

For axisymmetric conditions the flow field can be written as $\mathbf{v} = \mathbf{v}_p + v_\phi \mathbf{e}_\phi$ where \mathbf{v}_p is the poloidal (r, z) component, $v_\phi = \omega r > 0$ is the toroidal component, and \mathbf{e}_ϕ is the unit toroidal vector. Similarly, the magnetic field can be written as $\mathbf{B} = \mathbf{B}_p + B_\phi \mathbf{e}_\phi$. The ideal MHD equations then imply that certain quantities are constants on any given flux surface $\Psi(r, z) = \text{const}$ or equivalently they are constants along any given stream line or a given magnetic field line. These integrals are functions of Ψ (see for example Lovelace et al. 1986),

$$\mathbf{v}_p = \frac{K(\Psi)}{4\pi\rho} \mathbf{B}_p \quad (353)$$

$$\omega r^2 - \frac{rB_\phi}{K} = \Lambda(\Psi) \quad (354)$$

$$\omega - \frac{KB_\phi}{4\pi\rho r} = \Omega(\Psi) \quad (355)$$

$$S = S(\Psi) \quad (356)$$

$$w + \Phi - \frac{\Omega^2 r^2}{2} + \frac{\mathbf{v}_p^2}{2} + \frac{1}{2}(\omega - \Omega)^2 r^2 = E(\Psi) \quad (357)$$

Here, S is the entropy, w is the enthalpy, and Φ is the gravitational potential. The quantity K corresponds to the conservation of mass along a streamline, Λ to the conservation of angular momentum, Ω to the conservation of helicity, S to the conservation of entropy, and E (Bernoulli’s constant) to the conservation of energy.

The remaining MHD equation (which cannot be written in the integral form) is the Euler force equation across the poloidal magnetic field line (Bogovalov 1997),

$$(\mathbf{v}_p^2 - v_{Ap}^2) \frac{\partial \theta}{\partial s} - \frac{\cos \theta}{r} (v_\phi^2 - v_{A\phi}^2) + \frac{1}{\rho} \frac{\partial}{\partial n} \left(p + \frac{\mathbf{B}^2}{8\pi} \right) + \frac{\partial \Phi}{\partial n} = 0, \quad (358)$$

which is equivalent to the Grad-Shafranov equation. Here, $\partial/\partial n$ is the derivative in the direction perpendicular to magnetic field lines and directed outward from the axis, θ is the angle of inclination of the poloidal magnetic field line away from the z -axis, s is the distance from the disk along a magnetic field line, $v_{Ap} \equiv |\mathbf{B}_p|/\sqrt{4\pi\rho}$ and $v_{A\phi} \equiv |B_\phi|/\sqrt{4\pi\rho}$ are the poloidal and azimuthal Alfvén velocities. The quantity $\partial\theta/\partial s$ is the curvature of magnetic field line. The first two terms in equation (6) are determined by the non-diagonal (tension) part of the stress tensor, $\rho v_i v_k + (p + \mathbf{B}^2/8\pi) \delta_{ik} - B_i B_k/4\pi$. The third term is determined by the total (matter plus magnetic) pressure $p + \mathbf{B}^2/8\pi$ and the gravity force $\partial\Phi/\partial n$.

To clarify the physical sense of the integrals of motion, it is useful to derive the fluxes of mass, angular momentum (about the z -axis), and energy. The corresponding conservation laws for stationary conditions are

$$\nabla \cdot (\rho \mathbf{v}_p) = 0, \quad (359)$$

$$\nabla \cdot \left(r \rho \mathbf{v}_p v_\phi - \frac{\mathbf{B}_p r B_\phi}{4\pi} \right) = 0, \quad (360)$$

$$\nabla \cdot \left[\rho \mathbf{v}_p \left(\frac{\mathbf{v}^2}{2} + \frac{\mathbf{B}^2}{4\pi\rho} + w + \Phi \right) - \frac{\mathbf{B}_p (\mathbf{v} \cdot \mathbf{B})}{4\pi} \right] = 0. \quad (361)$$

Because $\mathbf{v}_p \parallel \mathbf{B}_p$, the vector flux densities are directed along the field lines.

Consider the fluxes through an annular region with surface area element $d\mathbf{S}$. The matter flux through the axisymmetric surface \mathbf{S} extending out from the z -axis is

$$\mathcal{F}_M = \int_{\mathbf{S}} d\mathbf{S} \cdot \rho \mathbf{v}_p = \frac{1}{4\pi} \int_{\mathbf{S}} d\mathbf{S} \cdot \mathbf{B}_p K(\Psi), \quad (362)$$

where we took into account the integral (353). $d\mathbf{S} \cdot \mathbf{B}_p$ is the magnetic flux through the annular region bounded by flux surfaces Ψ and $\Psi + d\Psi$. Thus we can change from space integration to integration over Ψ . Because $B_r = -(1/r)\partial\Psi/\partial z$ and $B_z = (1/r)\partial\Psi/\partial r$, we have

$$\mathcal{F}_M(\Psi) = \frac{1}{2} \int_0^\Psi d\Psi' K(\Psi'), \quad (363)$$

where $\Psi = 0$ corresponds to the z -axis. Similarly,

$$\begin{aligned}\mathcal{F}_L(\Psi) &= \int d\mathbf{S} \cdot \left(r\rho\mathbf{v}_p v_\phi - \frac{\mathbf{B}_p r B_\phi}{4\pi} \right) \\ &= \frac{1}{2} \int_0^\Psi d\Psi' \Lambda(\Psi') K(\Psi') ,\end{aligned}\tag{364}$$

$$\begin{aligned}\mathcal{F}_E(\Psi) &= \int d\mathbf{S} \cdot \rho\mathbf{v}_p \left[\left(\frac{\mathbf{v}^2}{2} + \frac{\mathbf{B}^2}{4\pi\rho} + w + \Phi \right) - \frac{\mathbf{B}_p \mathbf{v} \cdot \mathbf{B}}{4\pi} \right] \\ &= \frac{1}{2} \int_0^\Psi d\Psi' (E + \Lambda\Omega) K .\end{aligned}\tag{365}$$

Thus, $Kd\Psi/2$ is the matter flux between the flux surfaces separated by $d\Psi$, $\Lambda Kd\Psi/2$ is the angular momentum flux, and $(E + \Lambda\Omega)Kd\Psi/2$ is the energy flux. Note that $\Lambda(\Psi)$ is the specific angular momentum carried along the magnetic field line $\Psi = \text{const}$, $E(\Psi) + \Lambda\Omega(\Psi)$ is the specific energy, and $\Omega(\Psi)$ is the angular velocity of the disk at the point where the magnetic field line or flux surface $\Psi = \text{const}$ intersects the disk (for $|\mathbf{v}_p| \rightarrow 0$ at the disk).

6.3.2 Alfvén Surface

Conditions at the Alfvén surface are known to be important for the global properties of MHD flows (Weber & Davis 1967). Equations (2) and (3) constitute a linear system of equations for ω and B_ϕ . The determinant of this system is zero if $K^2 = 4\pi\rho$. Under this condition a solution exists if $\Lambda = r^2\Omega$ (Weber & Davis 1967) which corresponds to $\mathbf{v}_p = \mathbf{B}_p/\sqrt{4\pi\rho} = \mathbf{v}_{Ap}$. This is the condition which defines the Alfvén surface. Figure 20 shows the Alfvén surface for a sample case. The radius at which this field line intersects the disk is $r_d(\Psi)$. The radius at which it crosses the Alfvén surface is $r_A(\Psi)$. The density at this point on the Alfvén surface is $\rho_A(\Psi)$. Thus,

$$\rho_A(\Psi) = K^2(\Psi)/4\pi , \quad r_A^2(\Psi) = \Lambda(\Psi)/\Omega(\Psi) .\tag{366}$$

Equations (354) and (355) give

$$\omega = \Omega \frac{1 - \rho_A r_A^2 / \rho r^2}{1 - \rho_A / \rho} ,\tag{367}$$

$$B_\phi = r\Omega\sqrt{4\pi\rho_A} \frac{1 - r_A^2/r^2}{1 - \rho_A/\rho} .\tag{368}$$

Taking into account equations (366) - (368), one can express the fluxes of mass, angular momentum and energy, using only the values of physical quantities on the Alfvén surface:

$$\mathcal{F}_M(\Psi) = \int_0^\Psi d\Psi' \sqrt{\pi\rho_A} , \quad (369)$$

$$\mathcal{F}_L(\Psi) = \int_0^\Psi d\Psi' \sqrt{\pi\rho_A} \Omega r_A^2 , \quad (370)$$

$$\mathcal{F}_E(\Psi) = \int_0^\Psi d\Psi' \sqrt{\pi\rho_A} (E + \Omega^2 r_A^2) . \quad (371)$$

6.3.3 Forces

For understanding the plasma acceleration, we project the different forces onto the poloidal magnetic field lines. As mentioned, in a stationary state, matter flows along the poloidal magnetic field lines. The acceleration in the poloidal (r, z) plane is

$$(\mathbf{v}_p \cdot \nabla) \mathbf{v}_p + v_\phi (\mathbf{e}_\phi \cdot \nabla) (v_\phi \mathbf{e}_\phi) . \quad (372)$$

The last term represents the centrifugal acceleration $-(v_\phi^2/r)\mathbf{e}_r = -r\omega^2\mathbf{e}_r$. To get the force per unit mass along a magnetic field line, we multiply the Euler equation by a unit vector $\hat{\mathbf{b}}$ parallel to \mathbf{B}_p . This gives

$$f = \omega^2 r \sin \theta - \frac{1}{\rho} \frac{\partial p}{\partial s} - \frac{\partial \Phi}{\partial s} + \frac{1}{4\pi\rho} \hat{\mathbf{b}} \cdot [(\nabla \times \mathbf{B}) \times \mathbf{B}] , \quad (373)$$

where θ is the inclination angle of the field line to the z -axis. The final term of (373) is the projection of the magnetic force in the direction of $\hat{\mathbf{b}}$, which can be transformed to

$$f_M = \frac{1}{4\pi\rho} \hat{\mathbf{b}} \cdot [(\nabla \times \mathbf{B}) \times \mathbf{B}] = -\frac{1}{8\pi\rho r^2} \frac{\partial (rB_\phi)^2}{\partial s} ,$$

which is useful for understanding our results.

When magnetic field lines are inclined outward, away from the symmetry axis, the gravitational force $f_G = \partial\Phi/\partial s$ opposes the outflow of matter from the disk. If the matter is relatively cold then the pressure gradient force $f_P = -(1/\rho)(\partial p/\partial s)$ is unimportant. Then matter is accelerated outward by the centrifugal force $f_C = \omega^2 r \sin \theta$ and/or the magnetic force f_M . This determines the driving mechanisms of the outflow, centrifugal and/or magnetic. The centrifugal force always acts to accelerates matter outward if the distance between magnetic field line and the axis increases. However, under the same condition,

the magnetic force can act to accelerate or decelerate the flow depending on the direction of $-\nabla(rB_\phi)^2$ (see discussion in Ustyugova *et al.* 1999).

Thus, magnetic and centrifugal forces may both accelerate matter, but this depends on the configuration of magnetic field and current-density lines.

6.3.4 Collimation

Consider now the collimation of the flow. From equation (358), taking into account that $\cos\theta = \partial r/\partial n$, we have

$$(\mathbf{v}_p^2 - v_{Ap}^2) \frac{\partial\theta}{\partial s} = -\frac{1}{8\pi\rho r^2} \frac{\partial}{\partial n} (rB_\phi)^2 + \frac{\cos\theta v_\phi^2}{r} - \frac{1}{\rho} \frac{\partial}{\partial n} \left(p + \frac{\mathbf{B}_p^2}{8\pi} \right) - \frac{\partial\Phi}{\partial n}. \quad (374)$$

At large distances from the Alfvén surface $r \gg r_A$, the density $\rho \ll \rho_A$, but values ρr^2 and \mathbf{v}_p^2 remain finite (Heyvaerts and Norman 1989). Then $v_{Ap}^2 = (\rho/\rho_A)^2 \mathbf{v}_p^2 \ll \mathbf{v}_p^2$, so that the second term on the left-hand side of (374) is negligible. On the right-hand side, only the first term is important for $r \gg r_A$. Then, equation (374) simplifies to

$$v_p^2 \frac{\partial\theta}{\partial s} = -\frac{1}{8\pi\rho r^2} \frac{\partial}{\partial n} (rB_\phi)^2. \quad (375)$$

Thus, the curvature of magnetic field lines in the region $r \gg r_A$ is determined by the gradient $(rB_\phi)^2$. This force can act either to “collimate” the flow or “anticollimate” it depending on the orientation of the $rB_\phi(r, z) = \text{const}$ and $\Psi(r, z) = \text{const}$ surfaces (Ustyugova *et al.* 1999). The simulation study of Ustyugova *et al.* (1999) in fact finds only very small collimation of the hydromagnetic outflows over distances of the order of 100 times the inner disk radius. Recent work by Ustyugova *et al.* (2001) extends this conclusion by showing only small collimation out to distances of > 1000 times the inner disk radius. The collimation observed in protostellar jets at small distances, for example, in HH 30 observed with the space telescope, may result from the pressure of the external medium (Lovellace *et al.* 1991).

The conclusion by Heyvaerts and Norman (1989) that the magnetic collimation of MHD jets is a mathematical rather than physical result. The conclusion is based on the premise that the entire half-space above the disk is described by a stationary solution $\Psi(r, z)$ of the Grad-Shafranov equation. In reality, MHD jets result from initial conditions at the disk (as in the simulation studies) which result in the outward propagation of the jet into a highly conducting ionized external (interstellar or intergalactic) medium. At a given time, the region inside the surface $r = \mathcal{R}(z, t)$ is filled by the jet flow and the region outside it is filled by external plasma. The net axial current carried by the jet $2\pi \int_0^{\mathcal{R}} r dr J_z$ (for say $z > 0$) is necessarily zero for any (z, t) . Therefore, the toroidal magnetic field is zero on the surface \mathcal{R} , and there is *no* magnetic confinement of the

flow. Of course, it is possible that a fraction of the flux Ψ is collimated along the z -axis while the remaining flux is “anti-collimated” (that is, pushed away) from the z -axis. Exactly such a case is discussed in §1.5 below for the case of Poynting jets. This case also has the physical condition that the jet carries no net magnetic flux, $2\pi \int_0^{\mathcal{R}} r dr B_z = 0$. As in Landau’s (1946) treatment of the damping of plasma waves, the physically correct treatment of the collimation of MHD jets requires consideration of an initial value problem.

6.4 Numerical Simulations of MHD Outflows

In order to test and more fully understand analytical models of stationary outflows, MHD simulations of flows from a disk treated as a boundary condition have been carried out by a number of groups.

6.4.1 Non-Stationary Outflows

The initial magnetic field configuration was chosen so that the magnetic field was significantly inclined to the disk ($\theta > 30^\circ$) over most of the disk surface (Ustyugova et al. 1995; Koldoba et al. 1995). The simulations involve solving the complete system of ideal non-relativistic MHD equations using a Godunov-type code assuming axisymmetry but taking into account all three components of velocity and magnetic field. Matter of the corona was initially in thermal equilibrium with the gravitating center. At $t = 0$, the disk is set into rotation with Keplerian velocity and at the same time matter is pushed from the disk with a small poloidal velocity equal to a fraction of the slow magnetosonic velocity ($v_p = \alpha v_{sm}$, with $\alpha = 0.1 - 0.9$). A relatively high temperature and small magnetic field was considered. We found that at the maximum of the outflow, matter is accelerated to speeds in excess of the escape speed and in excess of the fast magnetosonic speed within the simulation region ($\sim 100r_i$). The acceleration is due to both thermal and magnetic pressure gradients. The outflow collimates within the simulation region due to strong amplification, ‘wrapping up’ of the toroidal magnetic field and the associated pinching force.

However, the outflows are *not stationary*. The matter flux grows to a peak and then decreases to relatively small values. The strong collimation of the outflow reduces the divergence of the field away from the z -axis ($\theta < 30^\circ$) and this “turns off” the outflow of matter and leads to flow velocities less than the escape speed. Thus, this simulation is an example of a temporary outburst of matter to a jet. Unfortunately, this type of flow has a significant dependence on the initial conditions.

6.4.2 Stationary Outflows

More recently, stationary magnetohydrodynamic outflows from a rotating accretion disk have been obtained by time-dependent axisymmetric simulations by

Romanova et al. (1997) and systematically analyzed by Ustyugova et al. (1999). The initial magnetic field in the latter work was taken to be a split-monopole poloidal field configuration (Sakurai 1987) frozen into the disk. The disk was treated as a perfectly conducting, time-independent density boundary $[\rho(r)]$ in Keplerian rotation which is different from the earlier specification of a small velocity outflow (§4.3.1, Ustyugova et al. 1995). The outflow velocity from the disk is determined self-consistently from the MHD equations. The temperature of the matter outflowing from the disk is small in the region where the magnetic field is inclined away from the symmetry axis ($c_s^2 \ll v_K^2$), but relatively high ($c_s^2 \lesssim v_K^2$) at very small radii in the disk where the magnetic field is not inclined away from the axis. We have found a large class of stationary MHD winds.

Figure 20 shows the nature of the stationary MHD outflows found by Ustyugova *et al.* (1999). The outflows are approximately spherical, with only small collimation within the simulation region. The *collimation distance* over which the flow becomes collimated (with divergence less than, say, 10°) is much larger than the size of our simulation region. Because the flow is super fast-magnetosonic (see below), the flow is not expected to magnetically collimate at larger distances. Notice for example that the solar wind is also super fast-magnetosonic and essentially uncollimated. Collimation may however result from the pressure of external plasma (Lovelace *et al.* 1991).

Figure 21 shows the variation of the flow speed and other characteristic speeds along a sample streamline. The outflow accelerates from thermal velocity ($\sim c_s$) to a much larger asymptotic poloidal flow velocity of the order of one-half $\sqrt{GM/r_i}$ where M is the mass of the central object and r_i is the inner radius of the disk. This asymptotic velocity is much larger than the local escape speed and is larger than fast magnetosonic speed by a factor of ~ 1.75 . The *acceleration distance* for the outflow, over which the flow accelerates from ~ 0 to, say, 90% of the asymptotic speed, occurs at a flow distance of about $80r_i$. Close to the disk the outflow is driven by the centrifugal force while at all larger distances the flow is driven by the magnetic force which is proportional to $-\nabla(rB_\phi)^2$, where B_ϕ is the toroidal field.

The stationary MHD flow solutions allow us (353) to compare the results with MHD theory of stationary flows, (354) to investigate the influence of different outer boundary conditions on the flows, and (355) to investigate the influence of the shape of the simulation region on the flows. The ideal MHD integrals of motion (constants on flux surfaces discussed by Lovelace et al. 1986) were calculated along magnetic field lines and were shown to be constants with accuracy 5 – 15%. Other characteristics of the numerical solutions were compared with the theory, including conditions at the Alfvén surface.

Different outer boundary conditions on the toroidal component of the magnetic field can significantly influence the calculated flows. The commonly used “free” boundary condition on the toroidal field leads to artificial magnetic forces on the outer boundaries, which can give spurious collimation of the flows. New

outer boundary conditions which do not give artificial forces have been proposed and investigated by Ustyugova et al. (1999).

The simulated flows may also depend on the shape of the simulation region. Namely, if the simulation region is elongated in the z -direction, then Mach cones on the outer cylindrical boundaries may be partially directed inside the simulation region. Because of this, the boundary can have an artificial influence on the calculated flow. This effect is reduced if the computational region is approximately square or if it is spherical as in Figure 20. Simulations of MHD outflows with an elongated computational region can lead to *artificial* collimation of the flow.

Recent simulation studies have treated MHD outflows from disks with more general initial \mathbf{B} field configurations, for example, that where the poloidal field has different polarities as a function of radius (Hayashi, Shibata, & Matsumoto 1996; Goodson, Winglee, & Böhm 1997; Romanova et al. 1998). The differential rotation of the foot-points of \mathbf{B} field loops at different radii on the disk surface causes twisting of the coronal magnetic field, an increase in the coronal magnetic energy, and an opening of the loops in the region where the magnetic pressure is larger than the matter pressure ($\beta \lesssim 1$) (Romanova et al. 1998). In the region where $\beta \gtrsim 1$, the loops may be only partially opened. Current layers form in the narrow regions which separate oppositely directed magnetic field. Reconnection occurs in these layers as a result of the small numerical magnetic diffusivity. In contrast with the case of the solar corona, there can be a steady outflow of energy and matter from the disk surface. We find that the power output mainly in the form of a Poynting flux. Opening of magnetic field loops and subsequent closing can give reconnection events which may be responsible for X-ray flares in disks around both stellar mass objects and massive black holes (Hayashi et al. 1996; Goodson, Winglee, & Böhm 1997; Romanova et al. 1998).

6.5 Poynting Jets

In a very different regime from the hydromagnetic flows discussed in §2 - 4, a Poynting outflow or jet transports energy and angular momentum mainly by the electromagnetic fields with only a small contribution due to the matter (Lovelace *et al.* 1987; Colgate & Li 1998; Romanova *et al.* 1998; Ustyugova *et al.* 2000; Li *et al.* 2001; Lovelace *et al.* 2001). A steady Poynting jet can be characterized in the lab frame by its asymptotic (large distance) magnetic field $B_\phi = -B_0[r_o/r_j(z)]$ at the jet's edge, $r = r_j(z)$, where r_o is the jet's radius at $z = 0$ and B_0 is the poloidal field strength at this location. The electric field in the jet is $\mathbf{E} = -\mathbf{v} \times \mathbf{B}/c$ and consequently the energy flux or luminosity of the jet is $L_j = vB_0^2r_o^2/8 \sim 4 \times 10^{45} \text{erg/s} (v/c)(r_o/10^{14} \text{cm})^2 (B_0/10^4 \text{G})^2$. Propagating disturbances in such field dominated jets provide a simple, but self-consistent physical model for the gamma ray flares observed in Blazars (Romanova & Lovelace 1997; Levinson 1998; Romanova 1999). Owing to pair production

close to the black hole, the main constituent of a Poynting flux jet may be electron-positron pairs.

6.5.1 Theory of Poynting Jets

Consider the coronal magnetic field of a differentially rotating Keplerian accretion disk for a given poloidal field threading the disk. That is, the disk is perfectly conducting with a very small accretion speed. Further, consider “coronal or force-free” magnetic fields in the non-relativistic limit. We use cylindrical (r, ϕ, z) coordinates as in §3 and consider axisymmetric field configurations. Thus the magnetic field has the form $\mathbf{B} = \mathbf{B}_p + B_\phi \hat{\phi}$, with $\mathbf{B}_p = B_r \hat{\mathbf{r}} + B_z \hat{\mathbf{z}}$. Because $\nabla \cdot \mathbf{B} = 0$, $\mathbf{B} = \nabla \times \mathbf{A}$ with \mathbf{A} the vector potential. Consequently, $B_r = -(1/r)(\partial\Psi/\partial z)$, $B_z = (1/r)(\partial\Psi/\partial r)$, where $\Psi(r, z) \equiv rA_\phi(r, z)$. The $\Psi(r, z) = \text{const}$ lines label the poloidal field lines; that is, $(\mathbf{B}_p \cdot \nabla)\Psi = 0 = \mathbf{B} \cdot \nabla\Psi = 0$. Note that $2\pi\Psi(r, z)$ is the magnetic flux through a horizontal, coaxial circular disk of radius r .

The magnetic field threading the disk at $z = 0$ is assumed to evolve slowly so that it can be considered approximately time-independent, $\Psi(r, z = 0) = \Psi_0(r)$. However, the magnetic field above the disk will in general be time-dependent, $\Psi = \Psi(r, z, t)$, due to the differential rotation of the disk. Figure 22 shows a possible vacuum poloidal magnetic field threading the disk. This field may be regarded as the “initial” field for the considered case where the space exterior to the disk is filled with a low density plasma.

The non-relativistic equation of plasma motion in the corona of an accretion disk is

$$\rho d\mathbf{v}/dt = -\nabla p + \rho \mathbf{g} + \mathbf{J} \times \mathbf{B}/c, \quad (376)$$

where \mathbf{v} is the flow velocity, p is the pressure, and \mathbf{g} is the gravitational acceleration. The equation for the \mathbf{B} field is $\nabla \times \mathbf{B} = \frac{4\pi}{c}\mathbf{J}$, because the displacement current is negligible in the non-relativistic limit. In the “coronal or force-free plasma limit,” the magnetic energy density $\mathbf{B}^2/(8\pi)$ is much larger than the kinetic or thermal energy densities; that is, sub-Alfvénic flow speeds \mathbf{v} , $\mathbf{v}^2 \ll v_A^2 = \mathbf{B}^2/4\pi\rho$, where v_A is the Alfvén velocity. Equation (376) then simplifies to $0 \approx \mathbf{J} \times \mathbf{B}$; therefore, $\mathbf{J} = \lambda \mathbf{B}$ (Gold & Hoyle 1960). Because $\nabla \cdot \mathbf{J} = 0$, $(\mathbf{B} \cdot \nabla)\lambda = 0$ and consequently $\lambda = \lambda(\Psi)$, as well-known. Thus Ampère’s law becomes $\nabla \times \mathbf{B} = 4\pi\lambda(\Psi)\mathbf{B}/c$.

The r and z components of this equation imply $rB_\phi = H(\Psi)$, and $dH(\Psi)/d\Psi = 4\pi\lambda(\Psi)/c$, where $H(\Psi)$ is another function of Ψ . Thus, $H(\Psi) = \text{const}$ are lines of constant poloidal current density; $\mathbf{J}_p = (c/4\pi)(dH/d\Psi)\mathbf{B}_p$ so that $(\mathbf{J}_p \cdot \nabla)H = 0$. The toroidal component of Ampère’s law gives

$$\Delta^* \Psi = -H(\Psi) \frac{dH(\Psi)}{d\Psi}, \quad (377)$$

which is the Grad-Shafranov equation for Ψ (see for example Batemann 1980; Lovelace *et al.* 1986). Here, $\Delta^* \equiv \partial^2/\partial r^2 - (1/r)(\partial/\partial r) + \partial^2/\partial z^2$ is the adjoint Laplacian operator. Note that $\Delta^*\Psi = r(\nabla^2 - 1/r^2)A_\phi$ and that $H(dH/d\Psi) = 4\pi r J_\phi/c$. From Ampère's law, $\oint d\mathbf{l} \cdot \mathbf{B} = (4\pi/c) \int d\mathbf{S} \cdot \mathbf{J}$, so that $rB_\phi(r, z) = H(\Psi)$ is $(2/c)$ times the current flowing through a circular area of radius r (with normal $\hat{\mathbf{z}}$) labeled by $\Psi(r, z) = \text{const}$. Equivalently, $-H[\Psi(r, 0)]$ is $(2/c) \times$ the current flowing into the area of the disk $\leq r$. For all cases studied here, $-H(\Psi)$ has a maximum so that the total current flowing into the disk for $r \leq r_m$ is $I_{tot} = \frac{2}{c}(-H)_{max}$, where r_m is such that $-H[\Psi(r_m, 0)] = (-H)_{max}$ so that r_m is less than the radius of the O -point, r_0 . The same total current I_{tot} flows out of the region of the disk $r = r_m$ to r_0 .

The function $H(\Psi)$ must be determined before the GS equation can be solved. Lynden-Bell and Boily (1994) determined the form of $H(\Psi)$ by requiring that the solution $\Psi(\mathbf{r})$ be a self-similar function of $|\mathbf{r}|$. Their stationary solution has *no* energy or angular momentum outflow from the disk. However, in general the magnetic field threading a disk will have definite length-scales and the field solution will not be self-similar.

For definiteness we consider the *initial value problem* where the disk at $t = 0$ is threaded by a poloidal field such as shown in Figure 22. Such a field can arise from a disk-dynamo driven by star-disk collisions as discussed by Pariev, Finn, & Colgate (2001). We assume for simplicity that the field threading the disk has the symmetry of a dipole although it is predicted in the reference above that the quadrupole field grows somewhat faster.

The form of $H(\Psi)$ is then determined by the differential rotation of the disk: The azimuthal *twist* of a given field line going from an inner footpoint at r_1 to an outer footpoint at r_2 is fixed by the differential rotation of the disk. The field line slippage speed through the disk due to the disk's finite magnetic diffusivity is estimated to be negligible compared with the Keplerian velocity. For a given field line we have $r d\phi/B_\phi = ds_p/B_p$, where $ds_p \equiv \sqrt{dr^2 + dz^2}$ is the poloidal arc length along the field line, and $B_p \equiv \sqrt{B_r^2 + B_z^2}$. The total twist of a field line loop is

$$\Delta\phi(\Psi) = \int_1^2 ds_p \frac{-B_\phi}{rB_p} = -H(\Psi) \int_1^2 \frac{ds_p}{r^2 B_p}, \quad (378)$$

with the sign included to give $\Delta\phi > 0$. For a Keplerian disk around an object of mass M the angular rotation is $\omega_K = \sqrt{GM/r^3}$ so that the field line twist after a time t is

$$\Delta\phi(\Psi) = \omega_0 t \left[\left(\frac{r_0}{r_1} \right)^{3/2} - \left(\frac{r_0}{r_2} \right)^{3/2} \right] = (\omega_0 t) \mathcal{F}(\Psi/\Psi_0) \quad (379)$$

where r_0 is the radius of the O -point, $\omega_0 \equiv \sqrt{GM/r_0^3}$, and \mathcal{F} is a dimensionless function (the quantity in the square brackets). At sufficiently small r_1 one reaches the inner radius of the disk r_i ($\ll r_0$) where we assume ω_K saturates

at the value $\omega_{Ki} = \sqrt{GM/r_i^3}$. For the dipole-like field of Figure 22, $\mathcal{F} \approx 3^{9/8}(\Psi_0/\Psi)^{3/4}$ for $\Psi/\Psi_0 \ll 1$, while $\mathcal{F} \approx 3.64(1 - \Psi/\Psi_0)^{1/2}$ for $1 - \Psi/\Psi_0 \ll 1$.

The quantity $T \equiv \omega_0 t$ (in radians) we refer to as the ‘‘twist’’ of the disk. For the dashed field lines of Figure 22, T is the twist $\Delta\phi(\Psi_1)$ of the field line with $\Psi_1/\Psi_0 \approx 0.932$ which has footpoints at $r_1 \approx 0.73r_0$ and $r_2 \approx 1.4r_0$. For $\Psi/\Psi_0 = 0.1$, where the footpoints are at $r_1 \approx 0.14r_0$ and $r_2 \approx 7.8r_0$, the field line twist is $\Delta\phi \approx 18.3$ rad. for $T = 1$.

For example, for an accretion disk around a massive $M = M_8 10^8 M_\odot$ black hole in the nucleus of galaxy, the twist is $T = (t/3.17\text{d})(r_0/10^{15}\text{cm})^{3/2}/\sqrt{M_8}$. The inner radius of the disk is $r_i \approx M_8 9 \times 10^{13}$ cm for a Schwarzschild black hole.

The Grad-Shafranov equation (377) is an elliptic equation and can be readily solved by the method of Successive Over-Relaxation (SOR) (see for example, Potter 1973). Figure 23 shows a sample high twist solution exhibiting a Poynting jet (Lovelace *et al.* 2001). These high-twist solutions consist of a region near the axis which is *magnetically collimated* by the toroidal B_ϕ field and a region far from the axis, on the outer radial boundary, which is *anti-collimated* in the sense that it is pushed against the outer boundary. The field lines returning to the disk at $r > r_0$ are anti-collimated by the pressure of the toroidal magnetic field.

Figure 24 shows a three dimensional view of two sample field lines for the same case as Figure 23.

6.5.2 Analytic Model of Poynting Jets

Figure 24 shows that most of the twist $\Delta\phi$ of a field line occurs along the jet from $z = 0$ to Z_{max} . Because $-r^2 d\phi/H(\Psi) = dz/B_z$, we have

$$\frac{\Delta\phi(\Psi)}{-H(\Psi)} = \frac{(\omega_0 t)\mathcal{F}(\Psi/\Psi_0)}{-H(\Psi)} \approx \frac{Z_{max}}{r^2 B_z}, \quad (380)$$

where $r^2 B_z(r, z)$ is evaluated on the straight part of the jet at $r = r(\Psi)$. In the core of the jet $\Psi \ll \Psi_0$, we have $\mathcal{F} \approx 3^{9/8}(\Psi_0/\Psi)^{3/4}$, and in this region we can take

$$\Psi = C\Psi_0 \left(\frac{r}{r_0}\right)^q, \quad \text{and} \quad H = -\mathcal{K} \left(\frac{\Psi_0}{r_0}\right) \left(\frac{\Psi}{\Psi_0}\right)^s, \quad (381)$$

where C , q , \mathcal{K} , and s are dimensionless constants. The GS equation for the straight part of the jet, $\Psi_{rr} - \Psi_r/r = -HH'$ implies $q = 1/(1-s)$ and $C^{2(1-s)} = s(1-s)^2 \mathcal{K}^2/(1-2s)$. In turn, equation (381) implies $s = 1/4$ so that $q = 4/3$, $C = [9/32]^{2/3} \mathcal{K}^{4/3}$, and $\mathcal{K} = 3^{1/8} 4(r_0 \omega_0 t / Z_{max})$.

In order to have a Poynting jet, we must have \mathcal{K} larger than ≈ 0.5 . For the case of uniform expansion of the top boundary, $Z_{max} = V_z t$, this condition is the same as $V_z < 9.2(r_0 \omega_0)$. For the case of Figures 23 and 24, $\mathcal{K} \approx 0.844$.

The field components in the straight part of the jet are

$$B_\phi = -\sqrt{2}B_z = -\sqrt{2} \left(\frac{3}{16}\right)^{1/3} \mathcal{K}^{4/3} \left(\frac{\Psi_0}{r_0^2}\right) \left(\frac{r_0}{r}\right)^{2/3}. \quad (382)$$

These field components of course satisfy the radial force balance equation $d(B_z^2)/dr + (1/r^2)d(r^2B_\phi^2)/dr = 0$ which is equivalent to the GS equation. These dependences agree approximately with those found independently in the numerical simulations of Poynting jets by Ustyugova *et al.* (2000). On the disk, $\Psi \approx 3^{3/2}\Psi_0(r/r_0)^2$ for $r < r_0/3^{3/4}$. Using this and equation (16) for $\Psi(r)$ gives the relation between the radius of a field line in the disk, denoted r_d , and its radius in the jet, $r/r_0 = 2^{5/2}3^{1/8}(r_d/r_0)^{3/2}\mathcal{K}^{-1}$. Thus the power laws apply for $r_1 < r < r_2$, where $r_1 = 3^{1/8}2^{5/2}r_0(r_i/r_0)^{3/2}/\mathcal{K}$ and $r_2 = (2^{5/2}/3)r_0/\mathcal{K}$, with r_i the inner radius of the disk. The outer edge of the Poynting jet has a transition layer where the axial field changes from $B_z(r_2)$ to zero while (minus) the toroidal field increases from $-B_\phi(r_2)$ to $(-H)_{max}/r_2$. Using equations (19), which are only approximate at r_2 , gives $(-H)_{max} \approx (3/2)^{1/2}\mathcal{K}\Psi_0/r_0$. This expression agrees approximately with our numerical results.

6.5.3 MHD Simulations of Poynting Jets

Ustyugova *et al.* (2000) did full, axisymmetric MHD simulations of a Keplerian disk initially threaded by a dipole-like magnetic field as shown in Figure 22. For these simulations the outer boundaries at $r = R_{max}$ and $z = Z_{max}$ were treated as free boundaries following the methods of Ustyugova *et al.* (1999). These simulations established that a quasi-stationary collimated Poynting jet arises from the inner part of the disk while a steady uncollimated hydromagnetic outflow arises in the outer part of the disk. Figure 25 shows the evolution towards a stationary Poynting jet.

Quasi-stationary Poynting jets from the two sides of the disk within r_0 give an energy outflow per unit radius of the disk $d\dot{E}_B/dr = rv_K(-B_\phi B_z)_h$, where the h subscript indicates evaluation at the top surface of the disk. This outflow is $\sim r_0 d\dot{E}_B/dr \sim v_K(r_0)(\Psi_{max}/r_0)^2 \sim 10^{45}(\text{erg/s})r_{015}^{3/2}\sqrt{M_8}[B_z(0)/6\text{kG}]^2$ where r_{015} is in units of 10^{15}cm , and M_8 in units of $10^8 M_\odot$. This formula agrees approximately with the values derived from the simulations. The jets also give an outflow of angular momentum from the disk which causes disk accretion (without viscosity) at the rate $\dot{M}_B(r) \equiv -2\pi\Sigma v_r = -2(r^2/v_K)(B_\phi B_z)_h \sim 2\Psi_{max}^2/[r_0^2 v_K(r_0)]$, where Σ is the disk's surface mass density. (Lovelace *et al.* 1997). The Poynting jet has a net axial momentum flux $\dot{P}_z = (1/4) \int r dr (B_\phi^2 - B_z^2) \sim 0.5(\Psi_{max}/r_0)^2$, which acts to drive the jet outward through an external medium. Further, the Poynting jet generates toroidal magnetic flux at the rate $\dot{\Phi}_t \sim -12[v_K(r_0)/r_0]\Psi_{max}$.

For long time-scales, the Poynting jet is of course time-dependent due to the angular momentum it extracts from the inner disk ($r < r_0$). This loss of

angular momentum leads to a “global magnetic instability” and collapse of the inner disk (Lovelace *et al.* 1997). An approximate model of this collapse can be made if the inner disk mass M_d is concentrated near the O -point radius $r_0(t)$, if the field line slippage through the disk is negligible (Lovelace *et al.* 1997), $\Psi_{max} = \text{const}$, and if $(-rB_\phi)_{max} \sim \Psi_{max}/r_0(t)$ (as found here). Then, $M_d dr_0/dt = -2\Psi_{max}^2(GMr_0)^{-1/2}$. If t_i denotes the time at which $r_0(t_i) = r_i$ (the inner radius of the disk), then $r_0(t) = r_i[1 - (t - t_i)/t_{coll}]^{2/3}$, for $t \leq t_i$, where $t_{coll} = \sqrt{GM} M_d r_i^{3/2} / (3\Psi_{max}^2)$ is the time-scale for the collapse of the inner disk. (Note that the time-scale for r_0 to decrease by a factor of 2 is $\sim t_i(r_0/r_i)^{3/2} \gg t_i$ for $r_0 \gg r_i$.) The power output to the Poynting jets is $\dot{E}(t) = (2/3)(\Delta E_{tot}/t_{coll})[1 - (t - t_i)/t_{coll}]^{-5/3}$, where $\Delta E_{tot} = GMM_d/2r_i$ is the total energy of the outburst. Roughly, $t_{coll} \sim 2\text{day}M_8^2(M_d/M_\odot)(6 \times 10^{32}\text{Gcm}^2/\Psi_{max})^2$ for a Schwarzschild black hole, where validity of the analysis requires $t_{coll} \gg t_i$.

6.6 Summary Regarding Jets from Accretion Disks

MHD simulations carried out by a number of groups over the last several years support the idea that an ordered magnetic field of an accretion disk can give powerful outflows or jets of matter, energy, and angular momentum. Most of the studies have been in the hydromagnetic regime and find asymptotic flow speeds of the order of the maximum Keplerian velocity of the disk, v_{K_i} . These flows are clearly relevant to the jets from protostellar systems which flow speeds of the order of v_{K_i} . In contrast, observed VLBI jets in quasars and active galaxies point to bulk Lorentz factors $\Gamma \sim 10$ - much larger than the disk Lorentz factor. The large Lorentz factors as well as the small Faraday rotation measures point to the fact that these jets are in the Poynting flux regime. These jets may involve energy extraction from a rotating black hole (Blandford and Znajek 1977; Livio *et al.* 1999).

7 Discussion

Observational evidence for massive black holes at the center of our Galaxy and in the nuclei of other galaxies (Cherepashchuk, 1996; Ho, 1998; Haswell, 1999; Richstone *et al.* 1998; Gebhardt *et al.* 2000; Merritt & Ferrarese 2001) make it necessary to revise theoretical models of the disk accretion. A large part of the high energy radiation originates close to the black hole, where the standard accretion disk model is not appropriate. Improvements of the accretion models have been made by taking into account the advective terms and including the important consequences of ordered and disordered magnetic fields. The conclusions obtained from ADAF solutions - for optically thin accretion flows at low mass accretion rates - are open to question because of omission of all magnetic field effects. Heating due to the annihilation of the magnetic field in the accre-

tion flow is predicted to be important. Further, the energy exchange between electrons and ions may be increased substantially by the turbulent electric fields in the plasma. Account of the magnetic field leads to the conclusion that the radiative efficiency of the accretion is *not* smaller than about 0.25 the efficiency for standard disk accretion (Bisnovatyi-Kogan & Lovelace, 1997, 2000) It is expected that more accurate treatment of the relaxation connected with the plasma turbulence will increase the efficiency further, making it close to unity (see also Fabian and Rees, 1995).

Some observational data which were interpreted as an evidence for the existence of the ADAF regime have disappeared after additional accumulation of data. The most interesting example of this sort is connected with the claim of the proof of the existence of event horizon of the black holes due to manifestation of the ADAF regime of accretion (Narayan *et al.*, 1997). Analysis of a more complete set of observational data (Chen *et al.*, 1997) had shown the disappearance of the statistical effect claimed as an evidence for ADAF. This example shows how dangerous is to base a proof of the theoretical model on the preliminary observational data. It is even more dangerous, when the model is physically not fully consistent. Then even a reliable set of the observational data cannot serve as a proof of the model. The classical example from astrophysics of this kind gives the theory of the origin of the elements presented in the famous book of Gamov (1952), where the model of the hot universe was developed. In addition to rich advantages of this model, the author also wanted to explain the origin of heavy elements in the primordial explosion, neglecting the problems connected with an absence of the stable elements with the number of barions equal to 5 and 8. Gamov considered the good coincidence of his calculations, where the mentioned problem was neglected, and the observational curve, as a proof of his theory of the origin of the elements. Further developments have shown that his outstanding theory explains many things, but not the origin of the heavy elements which are produced due to stellar evolution.

It appears difficult explain under-luminous AGNs with ADAF solutions where the radiative efficiency is much smaller than for standard accretion disk models. Possible explanations include the fact that the mass accretion rates to the black holes may have been overestimated. More importantly, other mechanisms of energy loss may be involved in the accretion flows, for example, in the form of accelerated particles, as in the radio-pulsars, where the energy carried by the relativistic wind far exceeds the electromagnetic radiation (e.g., the Crab pulsar). Winds and/or jets are likely to happen in the presence of a large scale magnetic field which can have a key role in their the formation. To extend this, we may suggest that under-luminous AGN loose significant part of their energy to the formation of winds and/or jets. A search for a correlation between the occurrence of outflows or jets and low luminosity could be very informative. [Note that the ADAF model of Blandford and Begelman (1999) takes into account outflows, but it requires the same assumption as earlier ADAF models that there is no magnetic field and no heating of electrons by field annihilation.

As we have argued, these assumptions are implausible.]

The behavior of accretion disks in the presence of ordered and disordered magnetic fields was discussed. The interaction of an accretion disk with a rotating magnetized star was reviewed including the formation of magnetohydrodynamic (MHD) outflows, magnetic braking of the star's rotation, and the propeller effect. The discussed problems of the MHD origin of jets in both in the hydromagnetic and Poynting flux regimes are currently under active study. Both regimes are being studied by different groups using axisymmetric and more recently 3D MHD simulations. Many simulation papers have been published on MHD outflows and jets, but the results often represent the time evolution for only a short interval (typically the period of rotation at the inner edge of the disk). These results are therefore strongly dependent on the initial conditions which are unknown. Furthermore, the boundary conditions used in the simulation codes can give false results, for example, collimation of an MHD flow when there actually is no collimation (see e.g. Ustyugova *et al.*, 1999). The difficulty of obtaining generally valid results from MHD simulations is even more challenging in the case of relativistic MHD (Komissarov, 1999) including the Kerr metric near a rapidly rotating black hole (Koide *et al.* 2000). Energy losses connected with magnetohydrodynamic (MHD) outflows and jets from the accretion disk may be very important and represent an alternative explanation of under-luminous AGN black holes.

References

- [1] Abramowicz M.A., Czerny B., Lasota J.P., Szuszkiewicz E. 1988, ApJ, **332**, 646
- [2] Abramowicz M. A., & Zurek W. H. 1981, ApJ, **246**, 314
- [3] Abramowicz M. A., & Kato S. 1989, ApJ, **336**, 304
- [4] Agol E., Krolik J. 1998, ApJ, **507**, 304
- [5] Agol E., Krolik J., Turner N.J. & Stone J.M. 2000, preprint
- [6] Aly, J.J. 1984, ApJ, **283**, 349.
- [7] Aly, J.J. 1991, ApJ Lett., **375**, L61.
- [8] Artemova I.V., Bisnovatyi-Kogan G.S., Björnsson G., Novikov I.D. 1996, ApJ, **456**, 119
- [9] Artemova I.V., Bisnovatyi-Kogan G.S., Igumenshchev I. Novikov I.D. 2000, astro-ph/0003058; ApJ (2001) **549**, No.2
- [10] Balbus, S.A., & Hawley, J.F. 1992, ApJ, **400**, 610.

- [11] Balbus S.A. & Hawley J.F. 1998, *Rev. Mod. Phys.* **70**, 1
- [12] Bateman, G. 1980, *MHD Instabilities* (Cambridge: MIT Press) Chap. 6.
- [13] Basko M.M., Sunyaev R.A. 1976, *MNRAS*, **175**, 395
- [14] Baushev A.N. and Bisnovatyi-Kogan G.S. 1999, *Astron. Reports*, **43**, 241
- [15] Benz A.O. 1997, in *Solar and Heliospheric Plasma Physics*, G.M. Simnett, C.E. Alissandrakis, & L. Vlahos, eds. (Heidelberg: Springer), 201.
- [16] Begelman M.C., Blandford R.D., & Rees M.J. 1984, *Rev. Mod. Phys.*, **56**, 255.
- [17] Bell A.R. 1994. *Phys. Plasmas*, **1**, 1643.
- [18] Bell A.R., & Lucek S.G. 1995, *Mon. Not. R.A.S.*, **277**, 1327.
- [19] Beloborodov A. M. 1998, *MNRAS*, **297**, 739
- [20] Biermann L., & and Lust R. 1960. "Nonthermal phenomena in stellar atmospheres", in: *Stellar Atmospheres*, Univ. Chicago Press, Chap. 6
- [21] Bildsten L., Chakrabarty D., Chiu J., Finger M. H., Koh D. T., Nelson R. W., Prince T. A., Rubin B. C., Scott D. M., Stollberg M., Vaughan B. A. Wilson C. A., Wilson R. B. 1997, *ApJ Suppl* **113**, 367.
- [22] Bisnovatyi-Kogan G.S. 1973, *AZh*, **50**, 902
- [23] Bisnovatyi-Kogan G.S. 1974, *AZh*, **51**, 443
- [24] Bisnovatyi-Kogan G.S. 1991, *A& A*, **245**, 528
- [25] Bisnovatyi-Kogan G.S. 1993a, *A& A*, **274**, 796
- [26] Bisnovatyi-Kogan G.S. 1989, "Physical Problems of the Theory of Stellar Evolution", Moscow, Nauka (in Russian)
- [27] Bisnovatyi-Kogan, G.S. 1993b, in *Stellar Jets and Bipolar Outflows*, eds. L. Errico & A. A. Vittone (Dordrecht: Kluwer), p. 369.
- [28] Bisnovatyi-Kogan G.S. 1994, *MNRAS* **269**, 557
- [29] Bisnovatyi-Kogan G.S. 1999a, *Proc. Conf. "Observational evidences for the black holes in the Universe"*, Calcutta, 1998. Kluwer, p.1
- [30] Bisnovatyi-Kogan G.S. 1999b, *astro-ph/9911275*
- [31] Bisnovatyi-Kogan G. S. 2001. *Stellar Physics*, Vol.1. Springer. Heidelberg
- [32] Bisnovatyi-Kogan G. S. and Blinnikov S.I. 1976, *Sov. Astron. Lett.*, **2**, 191

- [33] Bisnovatyi-Kogan G. S. and Blinnikov S.I. 1977, A&A, **59**, 111
- [34] Bisnovatyi-Kogan G. S. and Blinnikov S.I. 1978, Sov. Astron. Lett , **4**, 290
- [35] Bisnovatyi-Kogan G. S. and Blinnikov S.I. 1978a, Astrophysics, **14**, 316
- [36] Bisnovatyi-Kogan G. S. and Blinnikov S.I. 1979, Astrophysics, **15**, 99
- [37] Bisnovatyi-Kogan G.S., Blinnikov S.I., 1981, Sov. Astron., **25**, 175
- [38] Bisnovatyi-Kogan G.S. and Fridman A.M. 1969, AZh, **46**, 721
- [39] Bisnovatyi-Kogan, G.S., Goncharskii, A.V., Komberg, B.V., Cherepashchuk, A.M. & Yagola, A.G. 1977, Sov. Astron., **21**, 133.
- [40] Bisnovatyi-Kogan G.S. and Komberg B.V. 1973, Astron. cirk., No. 784, 721
- [41] Bisnovatyi-Kogan G.S. and Komberg B.V. 1974, AZh, **51**, 373
- [42] Bisnovatyi-Kogan G.S. and Lovelace R.V.L. 1997, ApJ Lett, **486**, L43
- [43] Bisnovatyi-Kogan G.S. and Lovelace R.V.L. 2000, ApJ, **529**, 978
- [44] Bisnovatyi-Kogan G.S., & Ruzmaikin A.A., 1974, Astrophys. and Space Sci., **28**, 45
- [45] Bisnovatyi-Kogan G.S., & Ruzmaikin A.A., 1976, Astrophys. and Space Sci., **42**, 401
- [46] Bisnovatyi-Kogan G.S. and Sunyaev R.A. 1972, Soviet Astron., **15**, 697
- [47] Blackman E.G. 1999, MN R.A.S., **302**, 723
- [48] Blandford R.D. 1976, Mon. Not. R.A.S., **176**, 465.
- [49] Blandford R.D. & Begelman M.C. 1999, MNRAS, **303**, L1.
- [50] Blandford, R.D., & Payne, D.G. 1982, MNRAS, **199**, 883.
- [51] Blandford R.D., & Znajek R.L. 1977, Mon. Not. R.A.S., **179**, 433.
- [52] Blinnikov S.I., 1975, Sov. Astron., **19**, 151
- [53] Bogovalov S.B. 1997, A&A, **323**, 634.
- [54] Boldt E. 1977, Ann. New York Acad. Sci. **302**, 329.
- [55] Bondi H. 1952, MN R.A.S., **112**, 195
- [56] Bondi H., Hoyle F. 1944, MN R.A.S., **104**, 273

- [57] Brandenburg A., Nordlund A., Stein R.F., & Torkelson U. 1995, ApJ, **446**, 741.
- [58] Bridle A.H., & Eilek, J.A. (eds) 1984, in *Physics of Energy Transport in Extragalactic Radio Sources*, Greenbank: NRAO.
- [59] Bührke T., Mundt R., & Ray T.P. 1988, A&A, **200** 99.
- [60] Camenzind, M. 1990. Rev. Mod. Astron. (Berlin: Springer) 3, 234.
- [61] Campbell, C.G. 1992, Geophys. Astrophys. Fluid Dynamics, **63**, 179.
- [62] Cannizzo J., Ghosh P. and Wheeler J.C. 1982, ApJ Lett., **260**, L83.
- [63] Cannizzo J.K., Greenhill L.J., Herrnstein J.R., Moran J.M., Mushotsky R.E. 1998, AAS Meeting, **192**, #41.03
- [64] Cao, X. & Spruit, H.C. 1994, A&A, 287, 80.
- [65] Chakrabarti S.K. 1996, ApJ, **464**, 1996
- [66] Chakrabarti S.K., Molteni D. 1993, ApJ, **417**, 671
- [67] Chakrabarty, D. et al. 1997, ApJ, **481**, L101.
- [68] Chandrasekhar, S. 1956, ApJ, **124**, 232.
- [69] Chandrasekhar S., 1957, An Introduction in the Study of Stellar Structure, Dover Pub. INC.
- [70] Chandrasekhar S. 1981, *Hydrodynamic and Hydromagnetic Stability*, (New York: Dover).
- [71] Chandrasekhar S., 1989, Selected papers, vol.1, p.185; Chicago Univ press.
- [72] Chang K.M, Ostriker J.P. 1985, ApJ, **288**, 428
- [73] Chapman S., Cowling T.G., 1939, The mathematical theory of nonuniform gases. Camb. Univ. Press
- [74] Chen W., Cui W., Frank J., King A., Livio M., Zhang S.N. 1998, AIP Conf. Proc. **431**, 347
- [75] Cherepashchuk A.M. 1996, Uspekhi Fiz. Nauk, **166**, 809
- [76] Cherepashchuk A.M. 2000, Space Sci. Rev. **93**, 473
- [77] Colgate S.A. & Li H. 1998, in *Proc. of VII International Conference and Lindau Workshop on Plasma Astrophysics and Space Physics*, Lindau, Germany.

- [78] Collins T.J.B., Helfer H.L., Van Horn H.M. 1998, ApJ, **502**, 730
- [79] Colpi M., Nammorelli M., Calvani M., 1991, Mon.Not.R.A.S., **253**, 55
- [80] Contopoulos J., & Lovelace R.V.E. 1994, ApJ, **429**, 139.
- [81] Contopoulos, J. 1995, ApJ, 450, 616
- [82] Coppi B. & Coppi, P., 2001, Phys. Rev. Lett., **87**, 051101. 2000, MIT (RLE) Report PTP 00/09
- [83] Coroniti, F.V. 1981, ApJ, **244**, 587.
- [84] Cui, W. 1997, ApJ, **482**, L163.
- [85] Davidson, K., & Ostriker, J.P. 1973, ApJ, **179**, 585.
- [86] Deeter, J.E., Scott, D.M., Boynton, P.E., Miyamoto, S., Kitamoto, S., Takahama, S., & Nagase, F. 1998, ApJ, **502**, 802.
- [87] Di Matteo, T., Fabian, A.C., Rees, M.J., Carilli, C.L., & Ivison, R.J., 1999, MNRAS, 305, 492 (astro-ph/9807245).
- [88] Dullemond C. P. & Turolla R. 1998, ApJ, **503**, 361
- [89] Eardley, D. M., & Lightman, A. P. 1975, ApJ, **200**, 187.
- [90] Eikenberry S., Matthews K., Morgan E.H., Remillard R.A., & Nelson R.W. 1998, ApJ Lett., **494**, L61.
- [91] Fabian A.C. and Rees M.J. 1995, Month. Not. R.A.S., **277**, L55
- [92] Fabbiano, G., & Schreier, E.J. 1977, ApJ, **214**, 235.
- [93] Falcke H., Malkan M.A., & Biermann P.L. 1995, A&A, **298**, 375.
- [94] Field, G.B., & Rogers, R.D. 1993, ApJ, **403**, 94.
- [95] Finn, J.M., & Chen, J. 1990, ApJ, **349**, 345.
- [96] Fujita M. & Okuda T. 1998, Publ. Astron. Soc. Jap. **50**, 639.
- [97] Fukue J. 1987, PASJ, **39**, 309
- [98] Galeev, A. A., Rosner, R., & Vaiana, G. S.1979, ApJ, **229**, 318.
- [99] Galeev, A.A., & Sagdeev, R.Z. 1983, Chap. 6, in *Handbook of Plasma Physics*, Vol. 1, eds. Rosenbluth, M.N., & Sagdeev, R.Z. (Amsterdam: North-Holland Pub.), Ch. 6.1.
- [100] Gamow G. 1952, *The Creation of the Universe*, (Viking Press: NY).

- [101] Gebhardt, K., Bender, R., Bower, G., Dressler, A., Faber, S. M., Filippenko, A. V., Green, R., Grillmair, C., Ho, L. C.; Kormendy, J. Lauer, T. R., Magorrian, J. Pinkney, J. Richstone, D., & Tremaine, S. 2000, ApJ, **439**, L13.
- [102] Ghosh, P., & Lamb, F.K. 1978, ApJ, **223**, L83.
- [103] Ghosh, P., & Lamb, F.K. 1979a, ApJ, **232**, 259.
- [104] Ghosh, P., & Lamb, F.K. 1979b, ApJ, **234**, 296.
- [105] Giacconi R., Gursky H, Paolini F.R., and Rossi B.B. 1962, Phys. Rev. Lett. **9**, 439
- [106] Giacconi, R., Gursky, H., Kellogg, E., Schreier, E., & Tananbaum, U. 1971, ApJ, **167**, L67.
- [107] Giacconi, R., 1974, in *Astrophysics and Gravitation* (Bruxelles: l'Universite de Bruxelles) p. 27.
- [108] Ginzburg V.L. 1975, Theoretical physics and astrophysics, "Nauka", Moscow
- [109] Glatzel W. 1989, J. Fluid. Mech., **202**, 515
- [110] Glatzel W., 1992, Mon.Not.R.A.S., **257**, 572
- [111] Gnedin Yu.N., Sunyaev R.A. 1973, Astron.Ap., **25**, 233
- [112] Godon P. 1996, MNRAS, **279**, 1071
- [113] Godon P. 1996, ApJ, **463**, 674
- [114] Gold, T. & Hoyle, F. 1960, MNRAS, **120**, 7.
- [115] Goldreich P. & Julian W.H. 1969, ApJ, **157**, 869.
- [116] Goodson, A.P., Winglee, R.M., & Böhm, K.H. 1997, ApJ, **489**, 390.
- [117] Gruber D.E., et al. 1980, ApJ Lett., **240**, L27
- [118] Gursky, H. & Schreier, E. 1975, in *Neutron Stars, Black Holes and Binary X-Ray Sources*, ed. H. Gursky and R. Ruffini (D. Reidel Publishing Company, Dordrecht), p. 175.
- [119] Hartmann, L., Hewett, R., & Calvet, N. 1994, ApJ, **426**, 669.
- [120] Haswell, C. 1999, in *Observational Evidence for Black Holes in the Universe*, ed. S. Chakrabarty (Dordrecht: Kluwer).
- [121] Hawley J.F., Gammie C.F., & Balbus S.A. 1995, ApJ, **440**, 742.

- [122] Hayashi, M.R., Shibata, K., & Matsumoto, R. 1996, ApJ, **468**, L37.
- [123] Heindl W.A. et al. 1999, ApJ Lett., **521**, L49
- [124] Heinemann M., & Olbert S. 1978, J. Geophys. Res., **83**, 2457.
- [125] Heyvaerts J., & Norman C.A. 1989, ApJ, **347**, 1055.
- [126] Herrnstein J.R., Greenhill L.J., Moran J.M., Diamond P.J., Inoue M., Nakai N., Miyoshi M., 1998, ApJ Lett., **497**, L69
- [127] Ho L. 1999, Proc. Conf. "Observational evidences for the black holes in the Universe", Calcutta, 1998. Kluwer, p.157
- [128] Hōshi R., 1977, Prog. Theor. Phys., **58**, 1191
- [129] Hōshi R., Shibazaki N. 1977, Prog. Theor. Phys., **58**, 1759
- [130] Ichimaru S. 1977, ApJ, **214**, 830
- [131] Igumenshchev I.V. 2000, MNRAS, **314**, 54.
- [132] Igumenshchev I.V. & Abramowicz M.A. 1999, MNRAS, **303**, 309.
- [133] Igumenshchev I.V. & Abramowicz M.A. 2000, ApJ Suppl., **130**, 463.
- [134] Igumenshchev I.V., Abramowicz M.A. & Narayan R. 2000, ApJ Lett., **537**, L27.
- [135] Illarionov, A.F., & Sunyaev, R.A. 1975, Astron. & Astrophys., **39**, 185.
- [136] Ipser J.R., Managan R.A., 1981, ApJ **250**, 362
- [137] James R.A., 1964, ApJ, **140**, 552
- [138] Kadomtsev, B.B. 1963, *Reviews of Plasma Physics*, 2, 188.
- [139] Kaisig, M., Tajima, T., & Lovelace, R.V.E. 1992, ApJ, **386**, 83.
- [140] Kato S., Fukue J. & Mineshige S. 1998, Black-Hole Accretion Disks (Kyoto: Kyoto Univ. Press)
- [141] Katz J.I. 1997, ApJ, **490**, 633.
- [142] Klieber R., Glatzel W. 1999, Month. Not. R.A.S., **303**, 107
- [143] Kley W. 1991, A&A, **247**, 95
- [144] Koide S., Meier D.L., Shibata K., & Kudo T. 2000, ApJ, **536**, 668.
- [145] Koldoba A.V., Ustyugova G.V., Romanova M.M., Chechetkin V.M., & Lovelace R.V.E. 1995, Astrophys. Sp. Sci, **232**, 241.

- [146] Komissarov, S.S. 1999, MNRAS, **303**, 343.
- [147] Königl A. 1989, ApJ, **342**, 208.
- [148] Königl A., & Ruden S.P. 1993, *Protostars and Planets III*, E.H. Levy and J. Lunine, Tucson: Univ. of Arizona Press, 641.
- [149] Koupelis T., & Van Horn H.M. 1989, ApJ, **342**, 146.
- [150] Krasnopolsky, R., Li, Z.-Y., & Blandford, R.D. 1999, ApJ, **526**, 631.
- [151] Kulikovskiy, A.G., & Lyubimov, G.A. 1962, *Magnetic Hydrodynamics*, (Moscow: PhysMatGiz) (in Russian).
- [152] Lamb, F.K., Pethick, C.J., & Pines, D. 1973, ApJ, **184**, 271.
- [153] Landau L.D. 1937, Zh. Exp. Theor. Phys. **7**, 203
- [154] Landau, L.D. 1946, J. Phys. U.S.S.R., **10**, 25.
- [155] Landau, L.D., & Lifshitz, E.M. 1959, *Fluid Mechanics*, (Pergamon Press: New York), chap. 2.
- [156] Lasota J.-P., Abramowicz M.A., Chen X., Krolik J., Narayan R., Yi I. 1996, ApJ, **462**, 142
- [157] Lesch, H. 1991, A&A, **245**, 48.
- [158] Levinson A. 1998, ApJ, **507**, 145.
- [159] Li, H., Colgate, S.A., Wendroff, B., & Liska, R. 2001, ApJ, **551**, 874.
- [160] Li, H., Lovelace, R.V.E., Finn, J.M., & Colgate, S.A. 2000, ApJ, 533, 1023.
- [161] Li, H., Lovelace, R.V.E., Finn, J.M., & Colgate, S.A. 2001b, “Magnetic Helix Formation Driven by Keplerian Disk Rotation,” ApJ, in press.
- [162] Li, J., & Wickramasinghe, D.T. 1997, in *Accretion Phenomena and Related Outflows*, IAU Colloquium 163, ASP Conf. Ser., **121**, 241.
- [163] Liang E.P.T., Thompson K.A. 1980, ApJ, **240**, 271
- [164] Lipunov V.M. 1987, Astron. Zh., **64**, 321
- [165] Lipunov, V.M. 1993, *Astrophysics of Neutron Stars*, (Berlin: Springer-Verlag) chaps. 6,7.
- [166] Livio M., Ogilvie G.I., & Pringle J.E. 1999, ApJ, **512**, 100.
- [167] Lovelace R.V.E. 1976, Nature, **262**, 649.

- [168] Lovelace, R.V.E., Berk, H.L., & Contopoulos, J. 1991, ApJ, **379**, 696.
- [169] Lovelace, R. V. E., Li, H., Colgate, S. A., & Nelson, A. F. 1999, ApJ, **513**, 805.
- [170] Lovelace R.V.E., Li, H., Koldoba, A.V., Ustyugova, G.S., & Romanova, M.M. 2001, "Poynting Jets from Accretion Disks," ApJ, submitted.
- [171] Lovelace R.V.E., Li H., Finn J.M., & Colgate S.A. 2001, submitted to ApJ.
- [172] Lovelace, R.V.E., Mehanian, C., Mobarry, C.M., & Sulkanen, M.E. 1986, ApJS, **62**, 1.
- [173] Lovelace R.V.E., Mobarry C.M., & Contopoulos J. 1989, in *Accretion Disks and Magnetic Fields in Astrophysics*, ed. G. Belvedere (Dordrecht: Kluwer), 71.
- [174] Lovelace R.V.E., Newman W.I., & Romanova M.M., 1997, ApJ, **424**, 628.
- [175] Lovelace, R.V.E., Romanova, M.M., & Contopoulos, J. 1993, ApJ, **403**, 158.
- [176] Lovelace, R.V.E., Romanova, M.M., & Newman, W.I. 1994, ApJ, **437**, 136.
- [177] Lovelace, R.V.E., Romanova, M.M., & Bisnovaty-Kogan, G. 1995, MNRAS, **275**, 244.
- [178] Lovelace, R.V.E., Romanova, M.M., & Bisnovaty-Kogan, G. 1999, ApJ, **514**, 368.
- [179] Lovelace, R.V.E., Ustyugova, G.S., & Koldoba, A.V. 1999, in *Active Galactic Nuclei and Related Phenomena*, IAU Symposium 194, eds. Y. Terzian, D. Weedman, & E. Khachikian (Astron. Soc. of Pacific: San Francisco), p. 208.
- [180] Lovelace, R.V.E., Koldoba, A.V., Ustyugova, G.V., & Romanova, M.M. 2001, "Poynting Jets from Accretion Disks," submitted to ApJ.
- [181] Lovelace R.V.E., Wang J.C.L., & Sulkanen M.E. 1987, ApJ, **315**, 504.
- [182] Lynden-Bell D. 1969, Nature, **223**, 690
- [183] Lynden-Bell, D. 1996, MNRAS, **279**, 389.
- [184] Lynden-Bell, D., & Boily, C. 1994, MNRAS, **267**, 146.
- [185] Lynden-Bell, D., & Pringle, J.E. 1974, MNRAS, **168**, 603.

- [186] Matsumoto R., Kato Sh., Fukue J., Okazaki A.T. 1984, Publ. Astron. Soc. Japan, **36**, 71
- [187] McConnell M.L., Ryan J.M., Collmar N. et al. 2000, ApJ, **543**, 928.
- [188] McCray R.A., Shull J.M., Boynton P.E., et al. 1982, Ap.J., **262**, 301
- [189] Meier D.L., Edgington S., Godon P., Payne D.G., & Lind K.R. 1997, Nature, **388**, 350.
- [190] Meier, D.L., Koide, S., & Uchida, Y. 2001, Science, **291**, 84.
- [191] Menon K., Quataert E., Narayan R. 1999, Proc. MG8 (Jerusalem, 1997). World Scientific, p.204
- [192] Merritt, D., & Ferrarese, L. 2001, ApJ, **547**, 140.
- [193] Mestel, L. 1968, MNRAS, **138**, 359.
- [194] Meszáros P. 1975 A&A, **44**, 59
- [195] Middleditch, J., & Nelson, J. 1976, ApJ, **208**, 567.
- [196] Middleditch, J., Puetter, R.C., & Pennypacker, C.R. 1985, ApJ, **292**, 267.
- [197] Mihara T., Makishima K., Ohashi T. et al. 1990, Nature, **346**, 250
- [198] Mihara T., Makishima K., Nagase F. 1997, Proceedings of an international Workshop "All-sky X-ray Observations in the Next Decade", March 3-5, 135
- [199] Miller, K., & Stone, J. 1997, ApJ, **489**, 890.
- [200] Mirabel I.F., & Rodriguez L.F. 1994 Nature, **371**, 46.
- [201] Morfill, G.E., Atmanspacher, H., Demmel, V., Scheingraber, H., & Voges, W. 1989, in *Timing Neutrons Stars*, H. Ögelman & E.P.J. van den Heuvel, eds. (Kluwer Acad. Pub.), p. 71
- [202] Muchotrzeb B., & Paczyński B. 1982, Acta Astr., **32**, 1
- [203] Mundt R. 1985, in *Protostars and Planets II*, D.C. Black and M.S. Mathews, eds. Univ. of Arizona Press, Tucson, 414.
- [204] Nagase, F. 1981, Space Sci. Rev., **30**, 395
- [205] Nagase, F., et al. 1984, ApJ, **280**, 259
- [206] Nagase, F. 1989, Publ. Astron. Soc. Japan, **41**, 1.
- [207] Narayan R., Barret D., McClintock J.E. 1996, A&A Suppl., **120**, 187

- [208] Narayan R., Garcia M.R., McClintock J.E. 1997, ApJ Lett. **478**, L79
- [209] Narayan R., Yu I. 1995, ApJ, **452**, 710
- [210] Nayfeh A., 1973, Perturbation methods. John Wiley & Sons, New York
- [211] Nayfeh A., 1981, Introduction into Perturbation Techniques. John Wiley & Sons, New York
- [212] Newman, W.I., Newman, A.L., & Lovelace, R.V.E. 1992, ApJ, **392**, 622.
- [213] Novikov I.D. & Thorne K.S. 1973, in Black Holes eds. C.DeWitt & B.DeWitt (New York: Gordon & Breach), p.345
- [214] Ostriker E.C. 1997, ApJ, **486**, 291.
- [215] Ouyed R. & Pudritz R.E. 1997, ApJ, **482**, 712.
- [216] Paczynski B., 1991, Ap.J., **370**, 597
- [217] Paczyński B., Bisnovatyi-Kogan G.S. 1981, Acta Astron., **31**, 283
- [218] Paczyński B., Wiita P.J. 1980, A&A, **88**, 23
- [219] Papaloizou J.C.B., Stanley G.Q.G., 1986, Mon.Not.R.A.S., **220**, 593
- [220] Parail, V.V., & Pogutse, O.P. 1965, in *Reviews of Plasma Physics*, V. 11, ed. M.A. Leontovich (New York: Consultants Bureau), 1.
- [221] Pariev V., Finn J.M., & Colgate S.A. 2001, ApJ, submitted
- [222] Parker, E.N. 1955, ApJ, **121**, 491.
- [223] Parker, E.N. 1979, *Cosmical Magnetic Fields* (Oxford: Clarendon Press), Chap. 17.
- [224] Parker, E.N. 1990, in *Mechanisms of Chromospheric and Coronal Heating*, eds. P. Ulmschneider, E.R. Priest, & R. Rosner (Berlin: Springer-Verlag), 615.
- [225] Pelletier G., & Pudritz R.E. 1992, ApJ, **394**, 117.
- [226] Phinney E.S. 1987, in *Superluminal Radio Sources*, J.A. Zensus, & T.J. Pearson, Cambridge: Cambridge Univ. Press, 301.
- [227] Popham R., Narayan R., 1991, Ap. J., **370**, 604
- [228] Popham P. & Narayan R. 1995, ApJ, **442**, 337
- [229] Popham P., Kenyon S., Hartmann L. & Narayan R. 1996, ApJ, **473**, 422
- [230] Porter, L.A., Klimchuk, J.A., & Sturrock, P.A. 1992, ApJ, **385**, 738.

- [231] Potter D. 1973, *Computational Physics*, (John Wiley & Sons: New York), 108.
- [232] Poutanen J., Krolik J.H. & Ryde F. 1997, MNRAS **292**, L21.
- [233] Prandtl L., 1905, Proc. Third Int. Math. Kongr., Heidelberg, pp. 484-491
- [234] Price R.H. & Liang E.P. 1977, ApJ, **218**, 247.
- [235] Pringle J.E., 1989, Month. Not. R.A.S., **236**, 107.
- [236] Pringle J.E. & Rees M.J. 1972, A&A, **21**, 1
- [237] Pringle J. E., Rees M. J. & Pacholczyk, A. G. 1973, A&A, **29**, 179
- [238] Pudritz R.E., & Norman C.A. 1986, ApJ, **301**, 571.
- [239] Quataert E. 1998, ApJ, **500**, 978
- [240] Rappaport, S.A., & Joss, P.C. 1977, Nature, **266**, 683.
- [241] Rappaport, S.A., & Joss, P.C. 1983, in *Accretion-Driven Stellar X-Ray Sources*, ed. W.H.G. Lewin and E.P.J. van den Heuvel (Cambridge University Press, Cambridge), p.1.
- [242] Rastätter, L. & Schindler, K. 1999, ApJ, **524**, 361.
- [243] Richstone, D., Ajhar, E. A., Bender, R., Bower, G., Dressler, A., Faber, S. M., Filippenko, A. V., Gebhardt, K., Green, R., Ho, L. C., Kormendy, J., Lauer, T. R., Magorrian, J., & Tremaine, S. 1998, Nature, **395A**, **14**.
- [244] Reames, D.V., Barbier, L.M., Von Rosenvinge, T.T., Mason, G.M., Mazur, J.E., & Dwyer, J.R. 1997, ApJ, **483**, 515.
- [245] Regev O. 1983, Astron. Ap., **126**, 146
- [246] Regev O., Bertout C. 1995, MNRAS, **272**, 71
- [247] Regev O. & Hougerat A.A. 1988, Mon.Not.R.A.S., **232**, 81
- [248] Riffert H., Herold H. 1995, ApJ, **450**, 508
- [249] Romanova M.M. 1999, in *Active Galactic Nuclei and Related Phenomena*, IAU Symposium 194, eds. Y. Terzian, D. Weedman, & E. Khachikian (Astron. Soc. of Pacific: San Francisco), p. 256.
- [250] Romanova, M.M., & Lovelace, R.V.E. 1992, A&A, **262**, 26.
- [251] Romanova M.M., & Lovelace R.V.E. 1997, ApJ, **475**, 97.
- [252] Romanova M.M. Ustyugova G.V., Koldoba A.V., Chechetkin V.M., & Lovelace R.V.E. 1997, ApJ, **482**, 708.

- [253] Romanova M.M., Ustyugova G.V., Koldoba A.V., Chechetkin V.M., & Lovelace R.V.E. 1998, ApJ, **500**, 703.
- [254] Sakurai T. 1987, PASJ, **39**, 821.
- [255] Santangelo A. et al. 1999, ApJ Lett, **523**, L85
- [256] Schade H. 1970, Kontinuumstheorie strömender Medien. Springer-Verlag
- [257] Schlichting H. 1964, Grenzschicht-Theorie. Verlag G. Braun. Karlsruhe
- [258] Schmidt M. 1963, ApJ, **136**, 164
- [259] Schreier, E., Levinson, R., Gursky, H., Kellogg, E., Tananbaum, H., & Giacconi, R. 1972, ApJ, **172**, L79.
- [260] Schreier, E.J., & Fabbiano, G. 1976, in *X-Ray Binaries*, NASA SP-389 (National Technical Information Service, Springfield, Virginia), p. 197.
- [261] Schwartsman V.F. 1971, Soviet Astron., **15**, 377
- [262] Scott D.M. et al. 2000, astro-ph/0002327
- [263] Shakura N.I. 1972, Astron. Zh., **49**, 921 (1973, Sov. Astron., **16**, 756)
- [264] Shakura N.I. & Sunyaev R.A. 1973, A&A, **24**, 337
- [265] Shakura N.I. & Sunyaev R.A. 1988, Adv. Space Res., **8**, (2)135
- [266] Shapiro S.L., Lightman A.P., Eardley D.M. 1976, ApJ, **204**, 187
- [267] Shapiro, S.L., & Teukolsky S.A. 1983, *Black Holes, White Dwarfs, and Neutron Stars*, (Wiley & Sons: New York).
- [268] Sheepmaker T., Jansen F.A., Deerenberg A.J.M., et al. 1981, Space Sci. Rev., **30**, 325
- [269] Sheffer, E.K., Kopaeva, I.F., Averintsev, M.B., Bisnovatyi-Kogan, G.S., Golynskaya, I.M., Gurin, L.S., D'yachkov, A.V., Zenchenko, V.M., Kurt, V.G., Mizyakina, T.A., Mironova, E.N., Sklyankin, V.A., Smirnov, A.S., Titarchuk, L.G., Shamolin, V.M., Shafer, E.Yu., Shmel'kin, A.A., & Giovannelli, F. 1992, Sov. Astron.-AJ, **36**, 41.
- [270] Shibata K., & Uchida Y. 1986, Publ. Astron. Soc. Jap., **38**, 631.
- [271] Shorokhov O.V. 2000, Diploma Thesis. MPhTI, Moscow
- [272] Shu F.H., Lizano S., Ruden S.P., & Najita J. 1988, ApJ Lett., **328**, L19.
- [273] Shu, F., Najita, J., Ostriker, E., & Wilkin, F. 1994, ApJ, **429**, 781. (?)

- [274] Spitzer L. 1940, MNRAS, **100**, 396
- [275] Spruit, H.C., Taam, R.E., 1990. A&A 229, 475
- [276] Stone J.M., & Norman M.L. 1994, ApJ, **433**, 746.
- [277] Sturrock, P.A. 1991, ApJ, **380**, 655.
- [278] Sunyaev R.A., Titarchuk L.G. 1980, Astron.Ap., **86**, 121
- [279] Tananbaum, H., Gursky, H., Kellogg, E.M., Levinson, R., Schreier, E., & Giacconi, R. 1972, ApJ, **174**, L143.
- [280] Tassoul J.-L. 1978, Theory of Rotating Stars, Princeton Univ. Press.
- [281] Tjemkes, S.A., Ziuderwijk, E.J., & Van Paradijs, J. 1986, Astron. & Astrophys., **154**, 77.
- [282] Toropin, Yu.M., Toropina, O.D., Savelyev, V.V., Romanova, M.M., Chechetkin, V.M., & Lovelace, R.V.E. 1999, ApJ, **517**, 906.
- [283] Trubnikov, B.A. 1958, *Magnetic Emission of High Temperature Plasma*, Dissertation, Moscow, USAEC Tech. Information Service, AEC-tr-4073 (1960)
- [284] Trubnikov, B.A. 1973, Voprosy Teorii Plasmy, **7**, 274.
- [285] Trümper J., Pietsch W., Reppin C., et al. 1978, Ap.J., **219**, 105
- [286] Tsuneta S. 1996, ApJ, **456**, 840
- [287] Tueller J., Cline T.L., Teegarden B.J. et al. 1984, Ap.J., **279**, 177-183
- [288] Turolla R., & Dullemond C. P. 2000, ApJ, **531**, L49
- [289] Ubertini P., Bazzano A., LaPadula C.D., et al. 1980, Proc. 17th Int. Cosmic-Ray Conf., Paris, **1**, 99
- [290] Uchida Y, & Shibata K. 1985, Publ. Astron. Soc. Jap., **37**, 515.
- [291] Ustyugova G.V., Koldoba A.V., Romanova M.M., Chechetkin V.M., & Lovelace R.V.E. 1995, ApJ Lett., **439**, L39.
- [292] Ustyugova G.V., Koldoba A.V., Romanova M.M., Chechetkin V.M., & Lovelace R.V.E. 1999 ApJ, **516**, 221.
- [293] Ustyugova G.V., Koldoba A.V., Romanova M.M., Chechetkin V.M., & Lovelace R.V.E. 2000 ApJ, **541**, L21.
- [294] Vasil'eva A.V., 1959, Math. Sbornik, **48**, 311

- [295] Velikhov E.P. 1959, J. Exper. Theor. Phys., **36**, 1398
- [296] Voges W., Pietsch W., Reppin C. et al. 1982, Ap.J., **263**, 803
- [297] Voges, W., Atmanspacher, H., & Scheingraber, H. 1987, Ap.J, **320**, 794
- [298] Wang, Y.-M. 1979, A&A, **74**, 253.
- [299] Wang, J.C.L., Wasserman, I.M., & Salpeter, E.E. 1988, ApJ Suppl., **68**, 735.
- [300] Weber E.J., & Davis L. 1967, ApJ, **148**, 217.
- [301] Woltjer, L. 1959, ApJ, **130**, 405.
- [302] Wrobel J.M., Herrnshtein J.R., 2000, ApJ Lett., **533**, L11
- [303] Zeldovich Ya.B. 1981, Proc. R. Soc. Lond., A **374** , 299
- [304] Zel'dovich Ya.B., Shakura N.I. 1969, AZh, **46**, 225;
- [305] Zwillinger D., 1992, Handbook of Differential Equations. Academic Press, Boston

Figure captions

Fig.1

Geometry of a thin accretion disk from Shapiro and Teukolsky (1983). Here, \dot{M} is the accretion rate, j is the total angular momentum flux, and $f_\phi = (1/r^2)\partial(r^2 t_{r\phi})$ is the viscous force with $t_{r\phi} = \eta\partial\Omega/\partial r$ the main component of the viscous stress tensor and η the dynamic viscosity coefficient.

Fig.2

The dependences of the optical depth τ_0 on radius, $r_* = r/r_g$, for the case $M_{BH} = 10^8 M_\odot$, $\alpha = 1.0$ and different values of \dot{m} . The thin solid, dot-triple dash, long dashed, heavy solid, short dashed, dotted and dot-dashed curves correspond to $\dot{m} = 1.0, 3.0, 8.0, 9.35, 10.0, 11.0, 15.0$, respectively. The upper curves correspond to the optically thick family, lower curves correspond to the optically thin family.

Fig.3

The specific angular momentum $j_{in} \equiv \ell_{in}$ as a function of the mass accretion rate \dot{M} for different viscosity parameters $\alpha = 0.01$ (squares), 0.1 (circles) and 0.5 (triangles), corresponding to viscosity prescription (73). The solid dots represent models with the saddle-type inner singular points, whereas the empty dots correspond to the nodal-type ones, from Artemova et al. (2001).

Fig.4

The specific angular momentum $j_{in} \equiv \ell_{in}$ as a function of the mass accretion rate \dot{M} for different viscosity parameters $\alpha = 0.01$ (squares), 0.1 (circles) and 0.5 (triangles), corresponding to viscosity prescription (119). The solid dots represent models with the saddle-type inner singular points, whereas the empty dots correspond to the nodal-type ones, from Artemova et al. (2001).

Fig.5

The position of the inner singular points as a function of the mass accretion rate \dot{M} for different viscosity parameters $\alpha = 0.01$ (squares), 0.1 (circles) and 0.5 (triangles), corresponding to viscosity prescription (73). The solid dots represent models with the saddle-type inner singular points, whereas the empty dots correspond to the nodal-type ones, from Artemova et al. (2001).

Fig.6

The position of the inner singular points as a function of the mass accretion rate \dot{M} for different viscosity parameters $\alpha = 0.01$ (squares), 0.1 (circles) and 0.5 (triangles), corresponding to viscosity prescription (119). The solid dots represent models with the saddle-type inner singular points, whereas the empty dots correspond to the nodal-type ones, from Artemova et al. (2001).

Fig.7

Poloidal projection of the instantaneous magnetic field in an accretion flow.

Fig.8

Equatorial projection of the magnetic field given by equation (265) for an infinitely conducting accretion flow.

Fig.9

Schematic drawing of the magnetic field configuration considered by LRBK95. The magnetosphere consists of an inner part, where the magnetic field lines are closed and an outer part where the field lines are open. The outer region where open field lines thread the disk gives rise to a MHD wind from the disk.

Fig.10

This shows two poloidal field lines used in the derivation of equation (300).

Fig.11

The figure shows the dependence of F_∞ and $F_K = (GM r_{cr})^{1/2}$ on the pulsar period P assuming $r_{cr} = r_{to}$ for $\dot{M} = 10^{17}$ g/s and 4×10^{17} g/s. The other parameters have been taken to be $\alpha = 0.1$, $D = 1$, $\tau_{max} = 5$, and $M = M_\odot$. Thus, each $\dot{M} = const.$ curve corresponds to different magnetic moments as $\mu \propto P^{1.17}$. F_∞ and F_K are measured in units of $(GM r_o)^{1/2}$ with $r_o = 10^8$ cm. This plot allows a comparison of the angular momentum influx to the star ($\dot{M} F_K$) in the case of outflows and spin-up ($r_{to} < r_{cr}$) with the case of magnetic braking where the influx is $\dot{M} F_\infty (r_{to} > r_{rc})$.

Fig.12

Geometry of disk accretion on to a rapidly rotating star with an aligned dipole magnetic field considered by LRBK99. Here, r_1 and r_2 are the boundaries of the region; R_A is the effective radius where the outflow begins; ω_* is the star's rotation rate; ω_K is the Keplerian rotation rate of the accretion disk; and $r_{cr} \equiv (GM/\omega_*^2)^{1/3}$ is the corotation radius. The magnetic field in the vicinity of r_1 has an essential time-dependence owing to the continual processes of stellar flux leaking outward into the disk, the resulting field loops being inflated by the differential rotation (LRBK95), and the reconnection between the open disk field and the closed stellar field loops. The dashed lines marked by the letters 'n' indicate neutral surfaces along which reconnection occurs.

Fig.13

Effective Alfvén radius R_A (normalized by the *nominal* Alfvén radius r_A) as a function of the normalized corotation radius r_{cr}/r_A for $\bar{\alpha} = 0.2$ obtained from equation (330). We have neglected the $\delta^{3/2} = (R_A/r_2)^{3/2}$ terms compared with

unity and taken the value $\mathcal{F}_0 = 0.234$ from LBC. Only the part of the solid curve above the dashed line $R_A = r_{cr}$ is consistent with our assumptions. The dashed horizontal line r_{to} indicates the “turnover radius” of the disk rotation curve or effective Alfvén radius in the regime discussed by LRBK95 where \dot{M}_{accr} falls onto the star and the star spins-up. For this line the turbulent magnetic diffusivity of the disk is taken to be $\alpha D = 0.1$. The points $a b c d$ and the associated vertical lines represent possible transitions between spin-down and spin-up of the pulsar as discussed in the text.

Fig. 14

Comparison of the observational and computational spectra of the cyclotron line. The solid curve is the observational results taken from Mihara et al. (1990), the dot curve is the approximation by the comptonized spectrum, and feature (17) with $a = 7 \cdot 10^{-4} \frac{eV \cdot s}{cm}$, $\sigma = 2 \cdot 10^{-4} \frac{eV \cdot s}{cm}$; from Baushev and Bisnovatyi-Kogan (1999).

Fig.15

Comparison of the observational and computational X-ray spectra of Her X-1. The solid curve is the observational results taken from McCray et al. (1982), the dot curve is the approximation by the comptonized spectrum, and the cyclotron feature (350) with $T_s = 0.9$ KeV, $T_e = 8$ KeV, $\tau_e = 14$, $a = 7 \cdot 10^{-4} \frac{eV \cdot s}{cm}$, $\sigma = 10^{-4} \frac{eV \cdot s}{cm}$, $B = 4 \times 10^{10}$ Gs; from Baushev and Bisnovatyi-Kogan (1999).

Fig.16

Schematic structure of the accretion column near the magnetic pole of the neutron star (top), and its radiation spectrum (bottom); from Bisnovatyi-Kogan (1999a).

Fig.17

Sketch of the magnetic field threading an accretion disk shown increase of the field owing to flux freezing in the accreting disk matter from Bisnovatyi-Kogan and Ruzmaikin (1976).

Fig.18

Sketch of the electromagnetic outflows from the two sides of the disk owing to the Faraday unipolar dynamo action of a rotating magnetized disk (Lovelace 1976).

Fig.19

Sketch of an accretion disk threaded by a magnetic field for conditions which may lead to hydromagnetic jet formation.

Fig.20

Simulations results for stationary MHD outflow obtained in a spherical coordinate system (Ustyugova et al. 1999). The solid lines represent the poloidal magnetic field, and the arrows the velocity vectors. The dashed lines in the left-hand plot represent the slow magnetosonic surface (the lowest dashed line), the Alfvén surface (the middle line), and the fast magnetosonic surface (the top line). In the right-hand panel, the dashed lines are surfaces of constant toroidal current density, while the lines on the outer boundary are the projections of the fast magnetosonic Mach cones.

Fig.21

Dependences of different velocities on distance s measured in units of r_i from the disk along the second magnetic field line away from the axis in Figure 20 (Ustyugova et al. 1999). This field line “starts” from the disk at $r \approx 6r_i$ where it has an angle $\theta \approx 28^\circ$ relative to the z -axis. The velocities are measured in units of $\sqrt{GM/r_i}$. Here, v_p is the poloidal velocity along the field line and v_\perp is the poloidal velocity perpendicular to the field line. Also, v_{Ap} is the poloidal Alfvén velocity, c_{fm} is the fast magnetosonic velocity, and v_{esc} is the local escape velocity.

Fig.22

“Initial” dipole-like vacuum magnetic field. In this and subsequent plots, r and z are measured in units of the radius r_0 of the O -point in the disk plane. The solid lines are the magnetic field lines for the case where the flux function on the disk surface is $\Psi(r, z = 0) = a^3 r^2 K / (a^2 + r^2)^{3/2}$ with $a = r_0 / \sqrt{2}$. In this and subsequent plots Ψ is measured in units of $\Psi_0 = r_0^2 K / 3^{3/2}$. Note that $B_z(0) = 6\sqrt{3}\Psi_0 / r_0^2 \approx 10.4\Psi_0 / r_0^2$. The dashed lines are the field lines for the case where the outer boundaries ($R_{max} = 10$, $Z_{max} = 10$) are perfectly conducting; for this case $\Psi(r, z = 0) \rightarrow \Psi(r, 0)[1 - (r/r_0 - 1)^2 / 81]$ so that the O -point is still at r_0 and Ψ_0 is unchanged. Because of axisymmetry and reflection symmetry about the $z = 0$ plane, the field need be shown in only one quadrant.

Fig.23

Poloidal field lines for Poynting jet case for twist $T = 1.84$ rad. and $(-H)_{max} = 1.13\Psi_0 / r_0$ with $\Psi = \text{const}$ contours measured in units of Ψ_0 which is the maximum value of Ψ . The outer boundaries at $r = R_{max}$ and $z = Z_{max}$ are perfectly conducting and correspond to an external plasma. This external plasma will expand in response to the magnetic pressure of the jet so that R_{max} and Z_{max} will increase with time. The initial poloidal magnetic field is shown by the dashed lines in Figure 22. The dashed contour is the separatrix with the X-point indicated. Note that the radial width of the upgoing field lines along the axis is about one-half the width of downgoing field lines at the outer wall as required for equilibrium.

Fig.24

Three dimensional view of two field lines originating from the disk at $x = \pm 0.32 r_0$ ($\Psi = 0.4\Psi_0$) for the Poynting jet of Figure 23. Each field line has a twist of ≈ 8.22 rad. or about 1.31 rotations about the z -axis from its beginning at r_1 and end at r_2 . The z -axis is tilted towards the viewer by 30° .

Fig.25

Time evolution of dipole-like field threading the disk from the initial configuration $t = 0$ (bottom panels) to the final quasi-stationary state $t = 1.2t_{out}$, where t_{out} is the rotation period of the disk at the outer radius R_{max} of the simulation region. The left-hand panels show the poloidal field lines which are the same as $\Psi(r, z) = \text{const}$ lines; Ψ is normalized by Ψ_{max} and the spacing between lines is 0.1. The middle panels show the poloidal velocity vectors \mathbf{v}_p . The right-hand panels show the constant lines of $-rB_\phi(r, z) > 0$ in units of Ψ_{max}/r_0 and the spacing between lines is 0.1.

This figure "GRFIG0.jpg" is available in "jpg" format from:

<http://arxiv.org/ps/astro-ph/0207625v1>

This figure "ADAFFIG1.jpg" is available in "jpg" format from:

<http://arxiv.org/ps/astro-ph/0207625v1>

This figure "FAD1.jpg" is available in "jpg" format from:

<http://arxiv.org/ps/astro-ph/0207625v1>

This figure "FCYC1.jpg" is available in "jpg" format from:

<http://arxiv.org/ps/astro-ph/0207625v1>

This figure "GBKL1.jpg" is available in "jpg" format from:

<http://arxiv.org/ps/astro-ph/0207625v1>

This figure "LRBK95_1.jpg" is available in "jpg" format from:

<http://arxiv.org/ps/astro-ph/0207625v1>

This figure "ADAFFI2B.jpg" is available in "jpg" format from:

<http://arxiv.org/ps/astro-ph/0207625v1>

This figure "FAD2.jpg" is available in "jpg" format from:

<http://arxiv.org/ps/astro-ph/0207625v1>

This figure "FCYC2.jpg" is available in "jpg" format from:

<http://arxiv.org/ps/astro-ph/0207625v1>

This figure "GBKL2.jpg" is available in "jpg" format from:

<http://arxiv.org/ps/astro-ph/0207625v1>

This figure "LRBK95_2.jpg" is available in "jpg" format from:

<http://arxiv.org/ps/astro-ph/0207625v1>

This figure "FAD3.jpg" is available in "jpg" format from:

<http://arxiv.org/ps/astro-ph/0207625v1>

This figure "FCYC3.jpg" is available in "jpg" format from:

<http://arxiv.org/ps/astro-ph/0207625v1>

This figure "GBKL3.jpg" is available in "jpg" format from:

<http://arxiv.org/ps/astro-ph/0207625v1>

This figure "FAD4.jpg" is available in "jpg" format from:

<http://arxiv.org/ps/astro-ph/0207625v1>

This figure "GBKL4.jpg" is available in "jpg" format from:

<http://arxiv.org/ps/astro-ph/0207625v1>

This figure "GBKL5.jpg" is available in "jpg" format from:

<http://arxiv.org/ps/astro-ph/0207625v1>

This figure "GBKL6.jpg" is available in "jpg" format from:

<http://arxiv.org/ps/astro-ph/0207625v1>

This figure "GBKL7.jpg" is available in "jpg" format from:

<http://arxiv.org/ps/astro-ph/0207625v1>

This figure "GRFIG9B.jpg" is available in "jpg" format from:

<http://arxiv.org/ps/astro-ph/0207625v1>

This figure "GRFIG10B.jpg" is available in "jpg" format from:

<http://arxiv.org/ps/astro-ph/0207625v1>

This figure "LRBK99.jpg" is available in "jpg" format from:

<http://arxiv.org/ps/astro-ph/0207625v1>

This figure "bkr.jpg" is available in "jpg" format from:

<http://arxiv.org/ps/astro-ph/0207625v1>

This figure "rvel.jpg" is available in "jpg" format from:

<http://arxiv.org/ps/astro-ph/0207625v1>